Democratic and Popular Republic of Algeria

Ministry of Higher Education and Scientific Research

University Mohamed Kheider of Biskra

Faculty of Exact Sciences and Science of Nature and Life

Department of Material Sciences

Thesis

Presented to obtain the degree of

Doctorate of Sciences

Speciality: Applied Physics

Elaboration and characterization of SnO_2:In thin films deposited by spray pyrolysis technique

Presented by:

BENNACEUR KHEIRA

Publicly defended on: / / 2020

In front of the board examiners:

M^{me}. H. Saidi	Professor	University of Biskra	President
M^{r}. A. Attaf	Professor	University of Biskra	Supervisor
M^{r}. A.Gueddim	Professor	University of Djelfa	Examiner
M^{r}. M. Maache	M.C.A	University of Djelfa	Examiner

Acadymic year 2019-2020

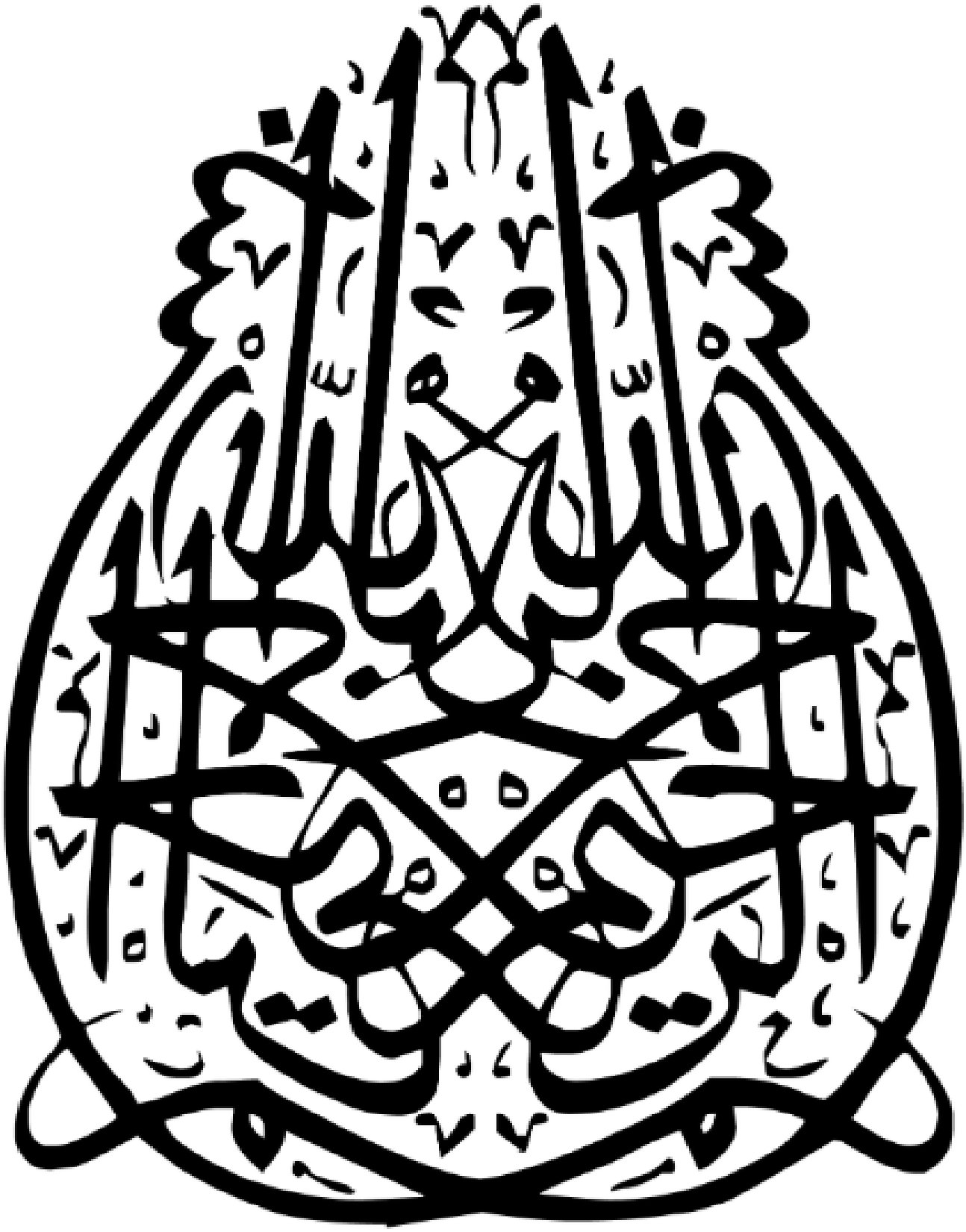

Table of contents

Acknowledgment

In the name of Allah the most glorious and merciful who gave me the power to work hard and confident to finish this modest work.

I am delighted to acknowledge my debt of gratitude my supervisor professor **Ab. Attaf** for his endurance, patience and encouragement. It has been a privilege to have his support and help. I hope the result will be as he wishes and wants.

It is a great honor for me that Mme. **H. Saidi**, Professor at Mohamed Khider University of Biskra, is the head of jury of my thesis. It is also my pleasant duty to thank Mr. **A.Gueddim**, professor at Ziane Achour University of Djelfa, and Mr. **M. Maache**, professor at Ziane Achour University of Djelfa, because they agreed to discuss my dissertation.

Great thanks to all my teachers, especially Pr. **S. Rahmane** and Dr. **T. Tibermacine** for their valuable suggestion to fulfill my research successfully.

I would like to thank all those who helped me here and there especially Mme. **Almi Kenza**, assistant Professor at Mohamed Khider University of Biskra, and Mr. **Gasmi Brahim** may God bless you wherever you are near or far.

Dedication

I dedicate this thesis to the special people who deserve much respect and great love:

To my family and my husband for their support, encouragement, understanding, and love and may God bless them.

To my friends and colleagues

To all those who helped me without hesitation

Thank you a lot, indeed

General Introduction

Tin dioxide (SnO_2) is a part of a family of binary transparent conducting oxides (TCO), their earth abundance and non-toxicity make it an ideal candidate for several applications [1]. Tin dioxide films besides have a high transparency and a good electrical conductivity, various other beneficial properties like high reflectivity for infrared light, high mechanical hardness and good environmental stability [2]. Due to its properties we can find it in several applications such as gas sensors [3], solar cell [4], anti reflective coatings [5], transparent electrodes in electroluminescent lamps and displays [6].

SnO_2 has n-type conductivity owing to the intrinsic defects. It can be readily doped with diverse ions to fulfill the demands of several application fields. SnO_2 can display n-type and p-type conductivity behavior according to type of dopants.SnO_2 either doped or undoped can be synthesised by numerous techniques such as spray pyrolysis [7], chemical vapor deposition [8], reactive evaporation [9] sputtering, sol–gel [10,11] and pulsed laser ablation[12]. Among the various deposition techniques the spray pyrolysis is the most suitable for the preparation of tin dioxide thin films because it is simple, low cost and easy to add doping materials and promising for high rate and mass production capability of uniform large area coatings in industrial application.

In this context, we chose tin dioxide as the basic material. Indeed, it is an available materiel and easy to deposit as thin films [13]. The aim of this work was to prepare undoped and doped SnO_2 thin films by ultrasonic spray pyrolysis under a vast range of deposition conditions, in order to find the optimum growth conditions to obtain a high thin film quality.

We can summarize the goals of this thesis as follows:

• The elaboration of $Sn0_2$ thin films on glass substrates using ultrasonic spray pyrolysis technique.

• Optimizing the quality of $Sn0_2$ thin films by studying the influence of the deposition parameters on the physical properties of the layers (molarity, substrate temperature, deposition time).

• The improvement of these layers quality by studying the influence of the dopant on the structural, optical and electrical properties in order to obtain transparent and conductor films.

Our thesis is divided into 5 chapters. In the first chapter, we make a brief summary of the physical properties (optical, electrical...) of SnO_2 material with its applications. Then, we explain various depositions techniques used to deposit SnO_2 films. The second chapter is about the USP (ultrasonic spray pyrolysis) experimental setup and experimental conditions used in this work. In addition, we explain the methods which are used in this thesis for the characterization of the SnO_2 films.

The third chapter is about the optimum conditions to prepare SnO_2 thin films. For this, we study the influence of the molarity, substrate temperature and deposition time on the films.

In the fourth chapter, we present the results of the structural, optical and electrical properties of indium-doped SnO_2 thin films and we are going to discuss their evolution according to the deposition parameters adopted during the preparation of films.

The last chapter presents the comparison of structural, optical and electrical characteristics of SnO_2.In films deposited by different precursors. In addition, the effect of annealing temperature on SnO_2 doped films properties is examined in this chapter.

Finally, we give a general conclusion summarize of the main obtained results in this thesis.

Reference

[1] Y. Feng, X. Jiang, E. Ghafari, B. Kucukgok, C. Zhang, I. Ferguson, Na Lu, Adv Compos Hybrid Mater, 1 (2018) 114–126.

[2] D. Mark. Allendorf, A. M. B. Van.Mol, Top Organomet Chem, 9 (2005) 1-48.

[3] Xi-Tao Yin, sensor and Actuators B: Chemical, (200) (2014) 213-218

[4] A. Goetzbergera, C. Heblinga, H. Schockb, Mater. Sci. Eng, (R 40) (2003) 1-46.

[5] C. Chukwuemeka Uhuegbu, Growth and characterization of ternary chalcogenide thin films for efficient solar cells and possible industrial applications, PhD thesis (2007).

[6] A. M. Bernardus van. Chemical vapour deposition of tin oxide thin films, PhD thesis, Technische Universiteit Eindhoven, 2000.

[7] H. Bendjedidi, A. Attaf, H. Saidi, M. S. Aida, S. Semmari, A. Bouhdjar, and Y. Benkhetta, Journal of Semiconductors, 36 (12) (2015)

[8] J.J. Berry, D.S. Ginley, P.E. Burrows, Appl. Phys. Lett. 92 (2008) 193304.

[9] K. Omura, P. Veluchamy, M. Tsuji, T. Nishio, M. Murozono, J. Electrochem. Soc. 146 (1999) 2113.

[10] B.D. Ann, S.H. Oh, D.U. Hong, D.H. Shin, A. Moujoud, H.J. Kim, Cryst. Growth 310 (2008) 3303.

[11] M.-M. Bagheri-Mohagheghi, M. Shokooh-Saremi, J. Phys. D Appl. Phys. 37 (2004) 1248.

[12] A.N. Banerjee, R. Maity, P.K. Ghosh, K.K. Chattopadyay, Thin Solid Films, 474 (2005) 261.

[13] S. Abbas, A. Ben Haoua, B. Ben Haoua, A. Rahal, Journal of New Technology and Materials JNTM, 04 (01) (2014)106-111.

CHAPTER I

SnO_2: a review on material and deposition process

In this chapter we will summarize the fundamental physical properties of tin dioxide thin film and their applications. Then, the depositions techniques that are used to develop SnO_2 thin films and which are going to be described later on.

I.1. Transparent conducting oxides

Visible light, which is made up of wavelengths of the electromagnetic spectrum in the range of 380-740 nm or energies in the range of 1.7-3.3 eV, may pass easily through the material with a band gap larger than 3,3 eV. So making it optically transparent, because interband transitions do not take place in the visible light range.

Thus, one could think that high optical transparency and high electrical conductivity don`t fit with each other because the optical transparency of a semiconductor material requires minimum band gap energy of about 3.3 eV which is too large to transfer electrons into the conduction band at room temperature [1].

Transparent conducting oxides (TCO) constitutes of a specific group of materials that contain high transparent and conductivity. TCOs come from different materials. In addition, they are typically normal semiconductors, doped with one or more sorts of impurities. The dopants and native defects have important role in these systems which are to control the conductivity. As a result, defects take part to conductivity in a semiconductor, which is optically transparent. A desired TCO material would have more than 80% optical transmission in the visible light range, a carrier concentration of the order of 10^{20} cm^{-3} and a resistivity of the order of 10^{-3} Ω cm.[2]

In 1907, Badeker [3] reported that the initial TCO films were prepared by thermal oxidation of cadmium. Researchers were not interested in CdO because of its toxic nature, although the films were electrically conducting and optically transparent.

The important TCO semiconductors are impurity-doped SnO2, In_2O_3, ZnO and CdO, as well as the ternary compounds Zn_2SnO_4, $ZnSnO_3$, $Zn_2In_2O_5$, $Zn_3In_2O_6$, In_2SnO_4, $CdSnO_3$, and multi-component oxides contain the combinations of ZnO, In_2O_3 and SnO_2.

I.1.1. Tin dioxide (SnO2)

Tin (IV) dioxide (SnO2) is an n type wide-band-gap semiconductor in the older notation called stannic oxide. Its mineral form is named cassiterite, which is the major ore of tin.

I.1.1.1. Crystal structure

SnO_2 is cassiterite with a tetragonal rutile structure under ambient conditions [4]. Tin has the electronic configuration $[Kr]4d^{10}5s^25p^2$. The unit cell of SnO_2, as shown schematically in Fig.I.1, (a=b=0.4738 nm, c=0.3187 nm [5]) contains six atoms, two tin and four oxygen. Oxygen atoms are joined to form octahedral network and the metal atoms regularly occupy the interstitial sites of the oxygen octahedral. Thus, each Sn atom has six closest oxygen neighbors which form a distorted octahedron. Sn atoms are located at the center of the oxygen octahedron. The distance between Sn and O atoms within one octahedron is 2.057 Å. [6]

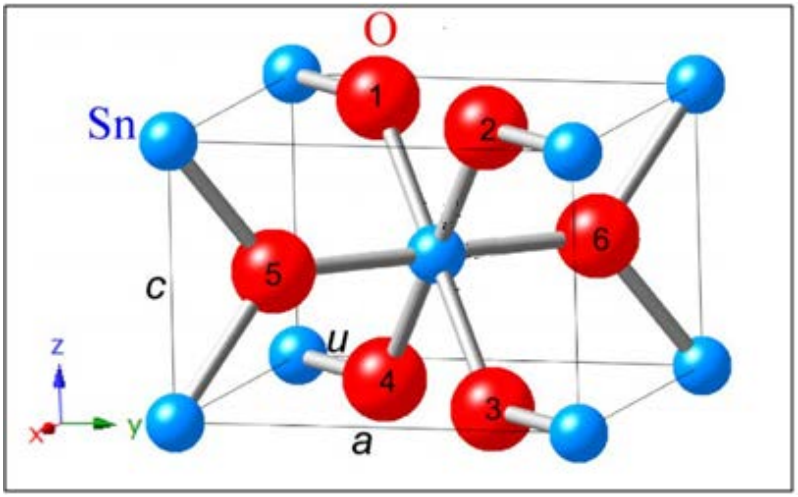

Fig.I.1. Unit cell of the crystal structure of SnO_2.

I.1.1.2.Electrical properties

Due to oxygen vacancies and tin interstitials, tin dioxide is an n-type semiconductor. Experimental data suggests that the cause of the non stoichiometry in SnO_2 is oxygen vacancies rather than tin interstitials [7].

An oxygen vacancy is formed when an oxygen atom is removed in a normal site. It can be created under the impact of temperature. The oxygen vacancies exist in three different charge states: V_o^0, V_o^+ and V_o^{2+}in the oxide [8].

In this process, the two negative actual charges, i.e. two electrons, of the oxygen ion are left in the crystal. The oxygen vacancy has two negative actual charges if these two electrons are placed at the oxygen vacancy. In this situation, the oxygen vacancy has zero effective charge. These vacancies are neutral (V_o^0). The oxygen vacancy is singly (V_o^+) or doubly ionized (V_o^{2+}), respectively if one or both of the localized electrons are excited and moved away from the neighborhood of the oxygen vacancy. The ionized oxygen vacancies will have an effective positive charge as far as the electrons are removed. Shallow donor

levels for V_o^+ and V_o^{2+} have been identified 0.03 and 0.15 eV below the conduction band minimum (CBM), respectively [9]. All these cases are close to the CBM so that they will not cause a loss of transparency, but will enhance the conductivity by introducing carrier electrons into the conduction band. This occurs even at room temperature and gives undoped layers fairly low resistivity: $\rho_{SnO2} \approx 10^{-2}\Omega$.cm.

I.1.1.3. Optical properties

Tin dioxide (SnO_2) has a direct wide band gap (3.6- 4.2 eV).The interest in SnO_2 coatings is because of the coexistence of good electrical conductivity and a high transparency in the visible range of the electromagnetic spectrum. The model SnO_2 transmission spectra are represented in Fig I.2. At short wavelengths (high energies), electron-interband transitions from the valence band to the conduction band quell the transmission. However, long wavelengths (infrared light) light are reflected due to the plasma edge. The visible spectrum is between about 1.7 eV to 3.3 eV (380 to 740 nm wavelength). The band gap of the material is higher than the maximum energy of visible spectrum, so none of the light is absorbed and just passes through the material. Thus it appears transparent. [10].

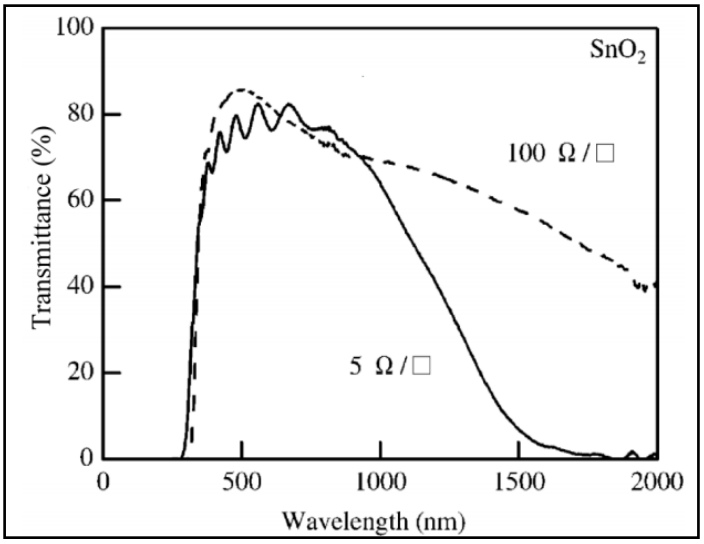

Fig.I.2. Optical transmittance of SnO_2 films for different conductivity of the films. (From Ref. [11]).

I.1.2. Influence of the doping on the properties of tin dioxide

It is possible to modify the physico-chemical characteristics of tin dioxide by resorting to doping. We can distinguish two types of doping:

Unintentional doping is related to the incorporation of elements from the substrate into the matrix influenced by high temperatures. We take the example of CVD process [12] or other processes in which the deposits are carried out cold but require an annealing at given temperatures according to the fixed objective. Typically in this case, Na^+ ions which have

weak atomic rays can easily goes in the matrix of the thin layer obtained where sodium ions diffuse from the soda-lime glass substrate.

The second type of doping is controlled one which consists in introducing into the matrix an element having a valence different that of the elements composing the oxide. For this, it is necessary that the atomic radius of the "incoming" ion is weaker (near) than the ion "host" one in order to be able to generate a substitution. This type of doping can be done either by substitution of tin or by substitution of oxygen.

$$Sn^{4+}+Sb \rightarrow Sn+Sb^{5+}+e^{-}$$

$$O^{2-}+F \rightarrow O+F^{-}+e^{-}$$

In both cases, we will have a free electron in the conduction band. So, the conductivity of the films rises with the number of charge carriers [12].

I.1.2.1. Crystallographic modifications

Several studies treated the effect of the doping element introduction on crystallographic modifications.

Most of the works carried out on this type of oxide showed that the increase in the rate of any doping element can generate modifications in the crystallographic orientation and affects the crystals size.

According to the doping element (Antimony [13], Fluorine [14], chrome [15], manganese [16] and Indium [17]) and the content introduced into the matrix of tin dioxide, doping is accompanied by a reduction in grains size. These atoms increase the internal stresses and reduce the growth of crystallites. This has a direct relation with the decrease of grain size and the rise of grain boundaries, which mainly affects the electrical properties [18].

We noticed that the indium content incorporated in the SnO_2 matrix plays a very important role in the crystallographic modification. Tin dioxide obtained from the pyrolysis spray method did not keep the same crystallographic orientations when the indium-doping rate was high [19].

The introduction of indium up to In / Sn >5 at% changes the preferential orientation and the crystalline structure tends to deteriorate due to the indium substitution (Fig.I.3).

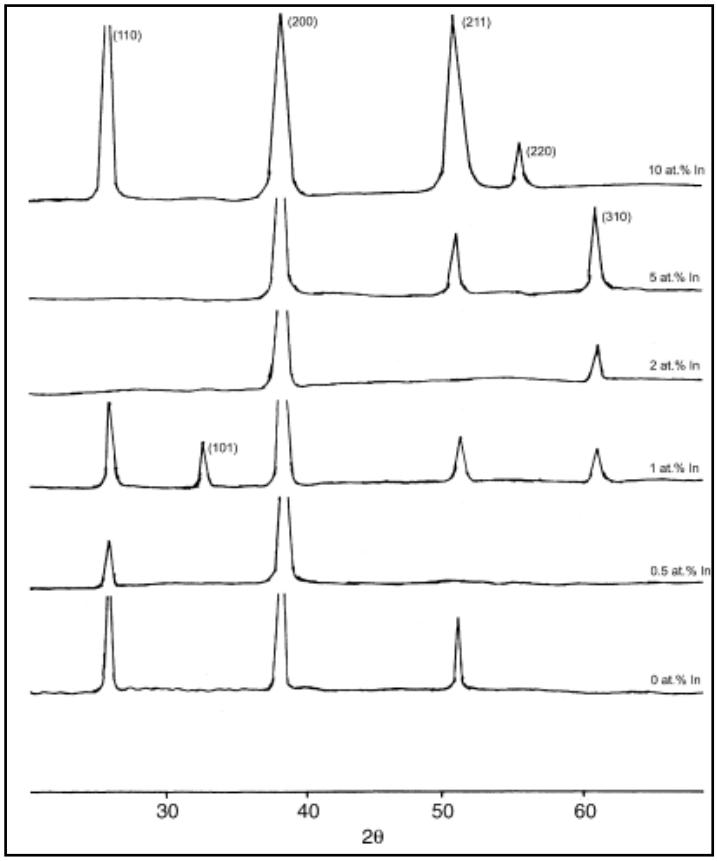

Fig.I.3. XRD patterns of indium-doped tin dioxide films with different indium concentration [19].

I.1.2.2. Modifications of the optical properties of SnO_2

The authors [20] reported that the differences observed in the transmission spectra are caused by the increase of the doping concentration. In addition, there is change in the values of the gap. The transmission in the UV-Vis domain is influenced by the doping rate; see Fig.I.4.[19].

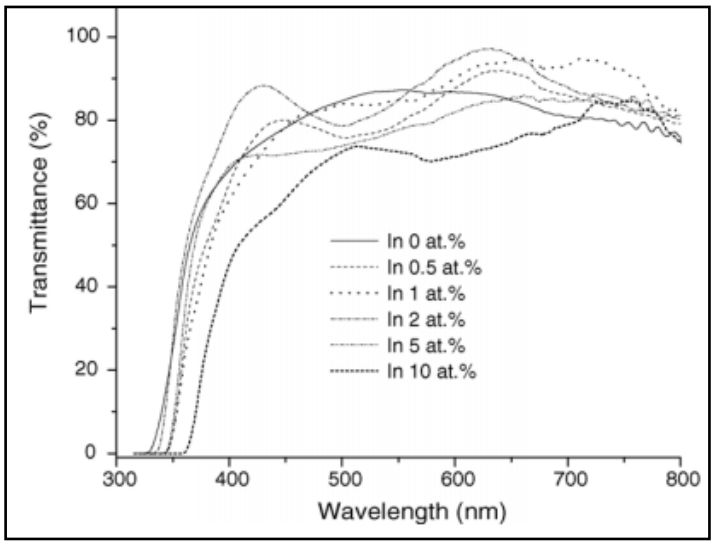

Fig.I.4. UV–Visible transmission spectra of SnO2:In films with different indium concentrations[19].

In the literature we find that doping has influence on gap energy [19, 21]. According to Caglar et al. [21], the gap energy values of the doped SnO_2 films with indium are dependent of the doping rate (see Table I.1).

Table I.1: Influence of the indium level on the gap energy values of the films SnO_2 [21].

In doping rate (at%)	Gap energy (e V)
0	**3.88**
0.1	**3.87**
5	**3.74**
10	**3.66**

I.1.2.3. Modifications of the electrical properties of SnO_2

As we said before, the introduction of dopants may lead to an increase in the number of charge carriers within the matrix. Thus, it may modify more or less the material conductivity values, depending on the dopant and the doping rate.

Depending on the valence of the dopants, acceptors or donors, the doping will induce n-type or p-type conductivity. Substitution doping can be done on the cation (the metal) or the anion (oxygen).

Doping may cause an increase or decrease in the grain size. This structural variation causes changes in the electrical properties. The decrease in the number of grain boundaries results in an increase in the mobility of the charge carriers [22].

I.1.3. Influence of post-deposition annealing

The annealing temperature has an influence on the crystallinity, resistivity and transmission rate of SnO_2 layers. The increase in the annealing temperature may lead to the increase of the crystallization rate of the SnO_2 thin films (Fig 1.5) [17] and decreases their resistivity (Fig I.6) [23].

In the following table Patil et al. [24] summarize the effect of annealing on various parameters: thickness, grain size and transmission. Increasing the annealing temperature decreases film thickness, increases grain size and transmission rate.

Table I.2: Effect of the annealing temperature on the properties of the thin films of undoped tin dioxide prepared by the spray pyrolysis technique on the crystallographic and optical properties [24].

Annealing temperature	Thickness (µm)	Grain size (Å)	Transmission rate (%) at 650 nm
300 °C	**0,95**	**39**	**73**
350 °C	**0,90**	**42**	**78**
400 °C	**0,78**	**55**	**79**
450 °C	**0,59**	**59**	**82**
500 °C	**0,40**	**65**	**85**

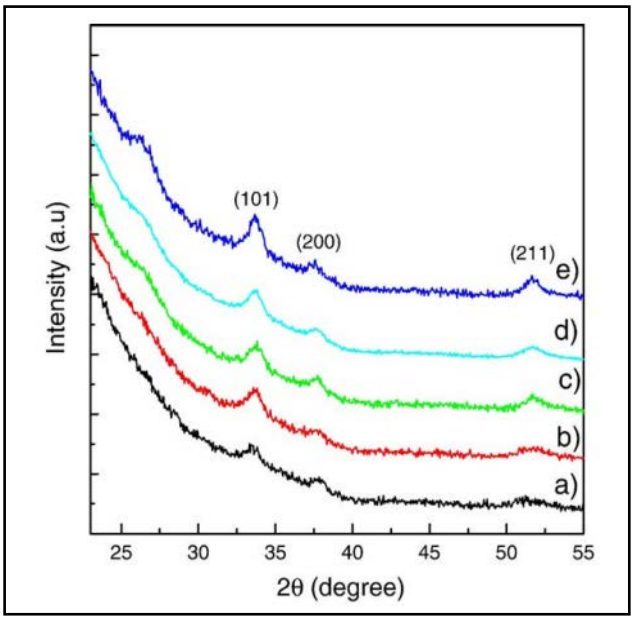

Fig.I.5. XRD of the films with In /Sn ratio of 0.2 post annealed at different temperatures. a) = 400 °C, b) = 500 °C, c) = 600 °C, d) = 700 °C, e) =800 °C[17].

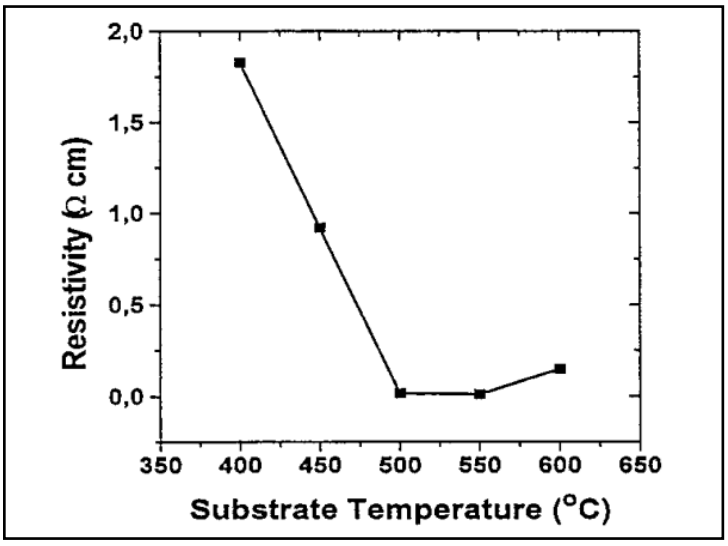

Fig.I.6. Variation of the resistivity of SnO_2 films prepared by the method of chemical vapor deposition (CVD) of $SnCl_2$ as a function of annealing temperature [23].

I.1.4. Applications of SnO_2 thin films

I.1.4.1. Lithium-Ion Batteries (LIBs)

Similar to other batteries, a rechargeable lithium-ion battery is made of one or more power-generating compartments called cells. Each cell has mainly three constituents: a positive electrode, a negative electrode and a chemical known as electrolyte in between them. The positive electrode is made of typically from a chemical compound which is lithium-cobalt oxide ($LiCoO_2$) or, in latest batteries, from lithium iron phosphate ($LiFePO_4$). The negative electrode is commonly made of carbon (graphite (LiC_6)) and the electrolyte is different according to the type of the battery.

While the battery is charging up, the lithium-cobalt oxide, positive electrode free up some of its lithium ions that shift across the electrolyte to the negative, graphite electrode and stay there. The battery takes in and stores energy during this operation. As the battery is discharging, the lithium ions withdraw through the electrolyte to the positive electrode, generating the energy that powers the battery. In both cases, electrons roll in the opposite direction to the ions around the outer circuit (Fig I.7).

LIBs have been the focus of many because of their high energy density, high power, smooth discharge and lightweight. In addition, it is ecologically harmless [25]. The electrode's material is one of the essential constituents for perfecting LIBs. It has a very important contribution in establishing battery. In comparison with the graphite used commercially, SnO_2 has been confirmed to be one of the most favorable anode materials for high efficiency LIBs [26, 27–29].

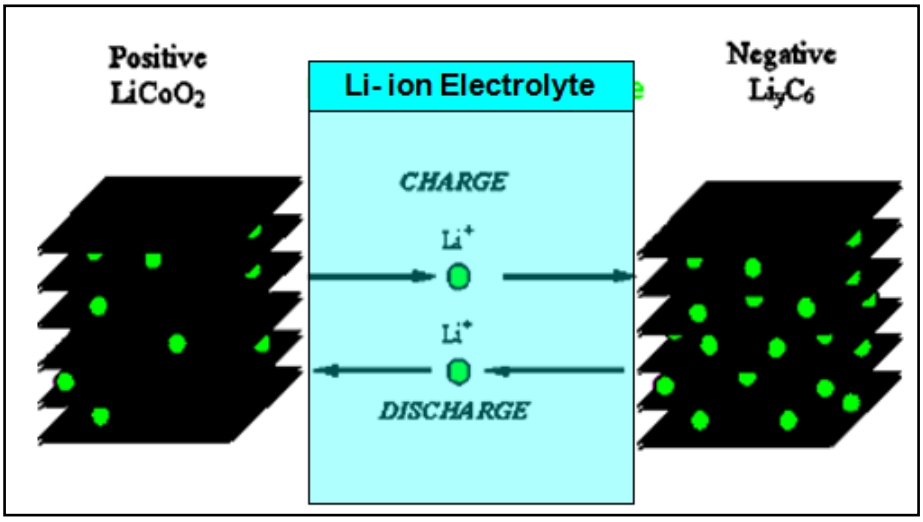

Fig.I.7. Li-ion battery Principle

I.1.4.2. Gas Sensors

The activity of an electrical semiconducting gas sensor depends on the variation in electrical conductivity that semiconductor materials face it while exposed to a gaseous atmosphere of different components. Thus, an electrical circuit assesses this response and the producing change in resistance is employed as the output signal for the instrument.

The sensor is generally made up of an oxide semiconductor film on an insulating substrate with two linked metal electrodes. Tin dioxide is one of the most employed oxides for this application. A model of a SnO_2 gas sensor is displayed in Fig I.8 to detect carbon monoxide CO. The reaction of CO with surface adsorbed oxygen ions leads to the formation of CO_2 and free electrons which augment the electrical conductivity in order to fulfill the aim of CO detection [30].

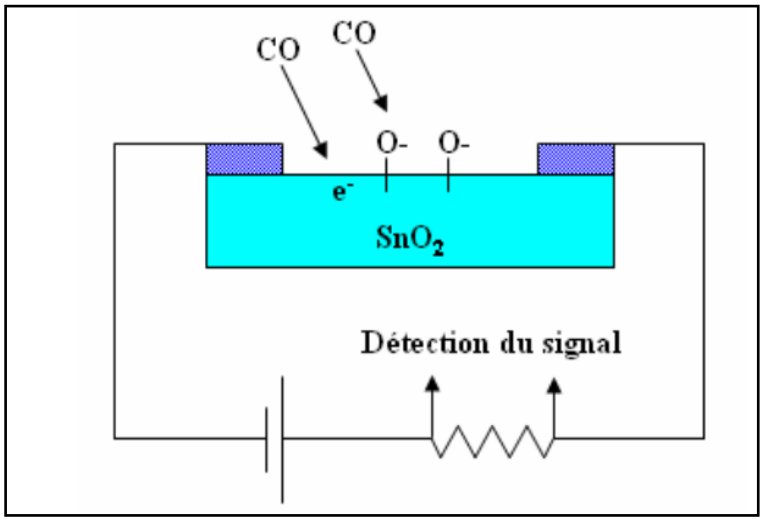

Fig I.8. Example of CO detector based in SnO2 thin film [31].

Park made tin dioxide films on glass substrate that were examined as sensors for CH_2Cl_2 in oxygen [32]. SnO_2 thin films with high certain area for NO_2 sensors have been prepared adopting the spray pyrolysis procedure [33].

The proportion between the resistivity before and after exposure with the gas is known as sensor sensitivity. Salehi et al prove that doping is very crucial in rising sensitivity by optimizing dopant concentration like SnO_2 layer indium doping to detect CO [34].

I.1.4.3. Solar cells

Tin dioxide coatings is widely used in thin film solar cells prepared from hydrogenated amorphous silicon (a-Si:H). This kind of solar cells is composed of a glass plate, coated with a transparent conducting oxide for example tin dioxide, a p-i-n structure prepared from a-Si: H and a metal electrode, as displayed in Fig I.9.The amorphous silicon layer is deposited on the upper side of the TCO layer. Moreover, the tin dioxide layer is

important to have a high transparency in the visible region, a high conductivity and optimal light scattering for an optimal process of the solar cell. By scattering the light at a rough surface, the light can be trapped in the a-Si: H layer for rising light absorption as represented in Fig I.10 [35].

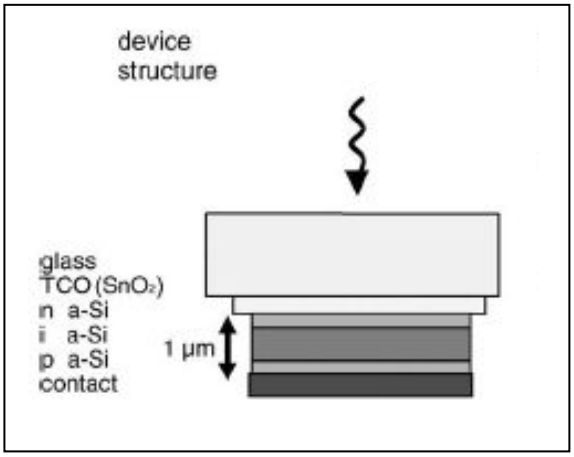

Fig.I.9. Structure of a pin amorphous silicon solar cell.

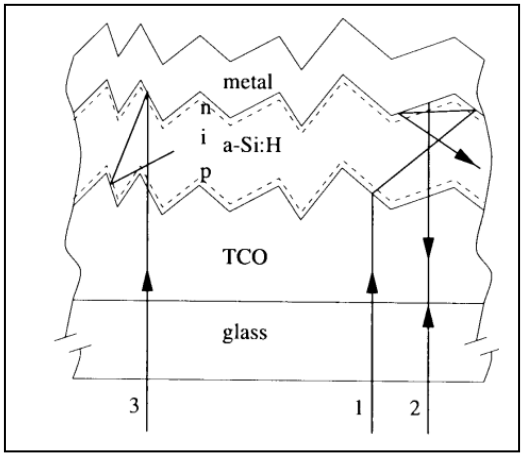

Fig.I.10. Schematic representation of the light trapping effect.

I.1.4.4. Low-Emissivity coatings

Low-Emissivity glass (low-E glass) is employed to reflect the heat transmitted by infrared radiation with long wavelength, generally about 10µm. This can be realized by coating the glass with fluorine doped tin oxide (FTO). The required characteristics of this coating are a high visible transmission and a high infrared reflectivity. Therefore, the thickness of the layers has an essential role since a higher thickness leads to a higher infrared reflectivity but a lower visible transmission. In general, the FTO layer is 300-400nm thick [36].

I.2. Thin film deposition methods

The thin film deposition methods may be divided into two categories: (i): physical methods (PVD) and (ii) chemical methods. In physical methods (Physical Vapor Deposition), the pure source material is gasified via evaporation that relies on physical processes like thermal evaporation or by bombardment from an energetic beam of electrons, photons or ions. The gasified material will then condense on the substrate surface to form a solid layer. There are no chemical reactions that occur in the entire process. In chemical methods, the source material is not pure as it is mixed with a volatile precursor. A chemical reaction of mixture on a substrate surface produces a film of desired composition while the byproduct is then eliminated. The following schema shows the different thin film deposition techniques Fig I.11.

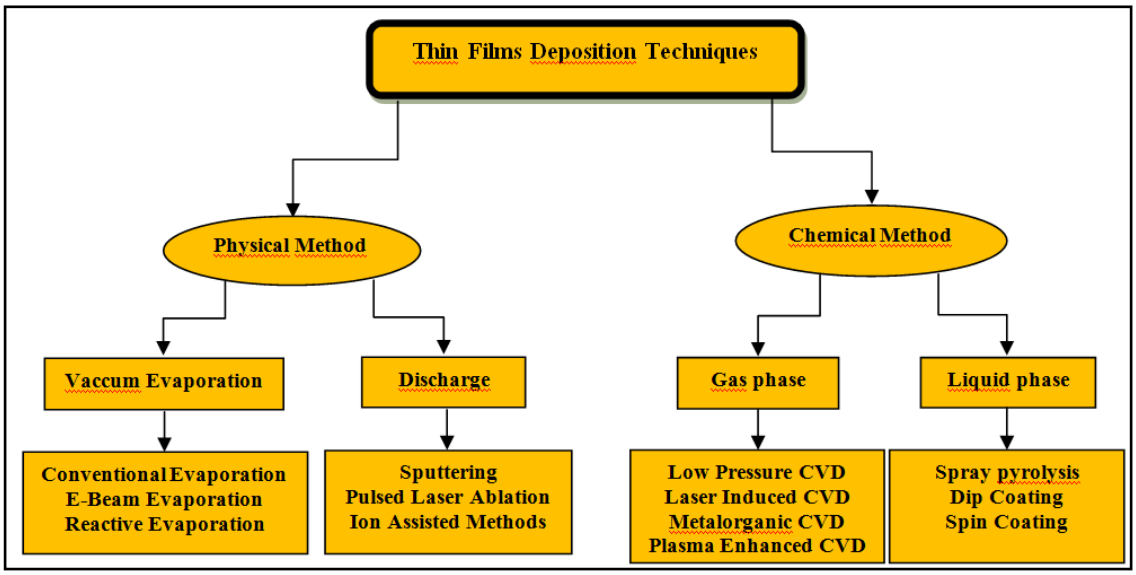

Fig.I.11. Classification of different thin film deposition methods.

Each of the previous methods has advantages and disadvantages. Nevertheless, it can be exploited these coatings in the commercial field only if they can be produced in a large area at low cost. Therefore, the most common methods to be frequently used are spray pyrolysis and sputtering because of their simplicity, reproducible results and the ability to coat on large area substrates. The next sections include all details about thin film deposition methods.

I.2.1 Physical Methods

Some of the physical deposition methods are discussed in the following sections.

I.2.1.1.Vacuum Evaporation

The vacuum evaporation process is very easy, suitable and commonly used technique. Evaporation of the material, in this method, happens in a vacuum chamber. It is required to provide an enough amount of heat to the evaporator to obtain the needed vapor pressure and the evaporated material is permitted to condense on the substrate maintained at a desired temperature [37]. Vacuum evaporation is available for many materials especially metals, but not for the refractory metals which have low pressures of vapor. By heating the materials, the vapor pressure is increased to a standard where the evaporation and sublimation take place. The major parameters of the process are the substrate material, source and substrate temperatures, source-substrate distance and pressure. This technique opens the door to different source designs, which involve resistance-heated filaments, electron beams, crucibles heated by radio frequency induction, etc.

I.2.1.2. Pulsed Laser Deposition (PLD)

PLD is an amended thermal process utilized for the deposition alloys and/or compounds with controlled chemical substances. A high-power pulsed laser, in laser deposition, is irradiated into the target of source materials through a quartz window. To raise the energy intensity of the laser power on the target source, a quartz lens is required. The ablated or evaporated atoms from the surface are gathered on close substrate surfaces to form thin films (Fig I.12) [38].The target material is topically heated to the melting point, melted and vaporized in a vacuum. The laser pulsed can supply photo-emitted electrons from the target to form a plasma plume and the evaporation process would be complicated because of the thermal and plasma operations including together. The best use of different parameters like ablation energy, base vacuum level, setting oxygen pressure, distance between target and substrate and the temperature of substrates may lead to the required deposition rate and structural quality.

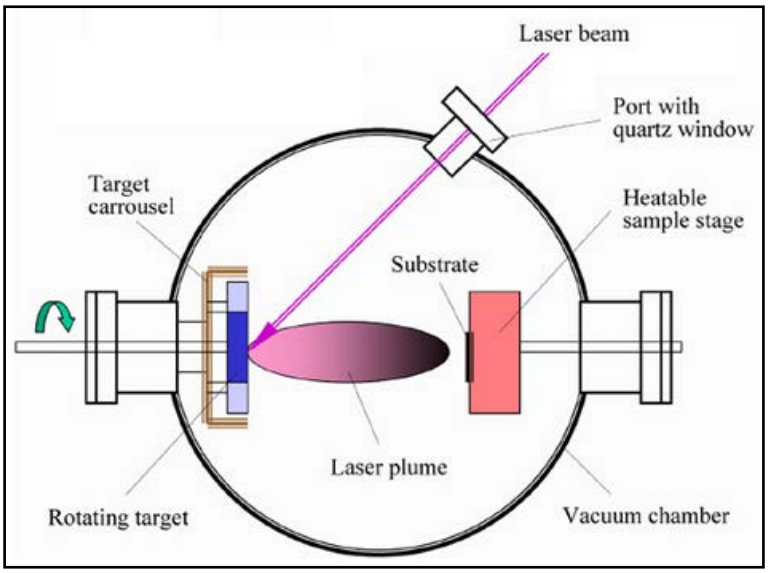

Fig.I.12. General schema of PLD[38].

I.2.1.3. Sputtering Process

Sputtering is one of the most versatile techniques used for the deposition of transparent conductors when device quality films are required. Sputtering process produces films with better controlled composition, provides films with greater adhesion and homogeneity and permits better control of film thickness. The sputtering process involves the creation of gas plasma usually an inert gas such as argon by applying voltage between a cathode and an anode.

The target holder is used as a cathode and the anode is the substrate holder. Source material is subjected to intense bombardment by ions. By momentum transfer, particles are ejected from the surface of the cathode and they diffuse away from it, depositing a thin film onto the substrate. Sputtering is normally performed at a pressure of 10^{-2}–10^{-3}Torr.

Normally there are two modes of powering the sputtering system; direct current (DC) and radio frequency (RF) biasing (Fig.I.13). Concerning DC sputtering system, the direct voltage is applied between the cathode and the anode. This method is limited for conducting materials only. Whereas RF sputtering system is convenient for both conducting and non-conducting materials; a high frequency generator (13.56 MHz) is linked between the electrodes of the system. When sputtering source uses magnetic field at the sputtering target surface, this process is called Magnetron sputtering [39].

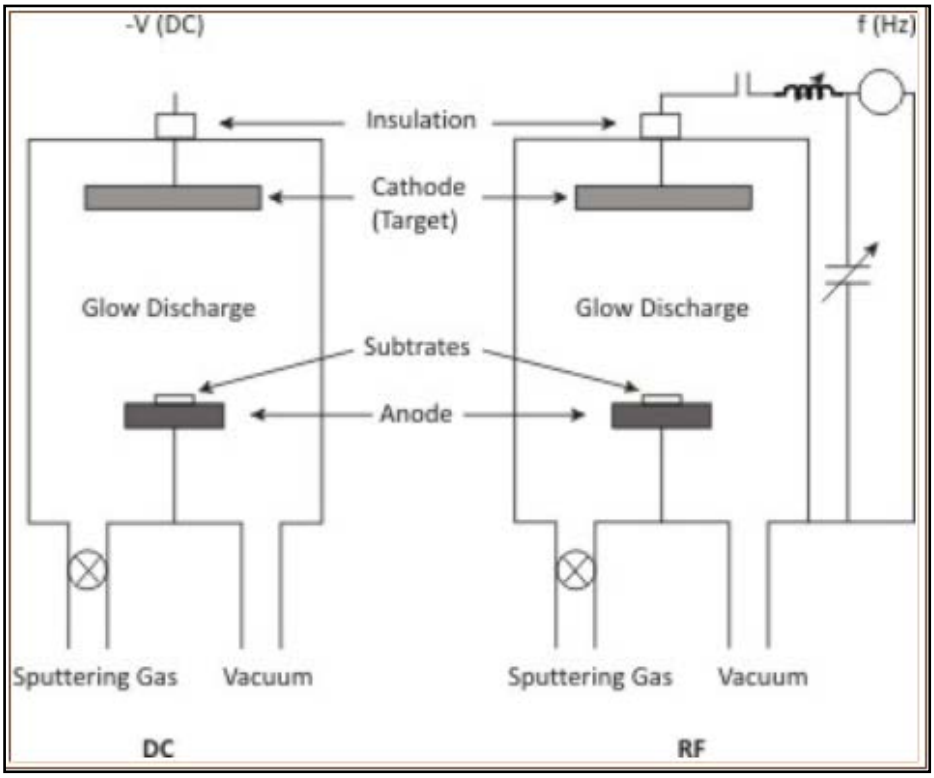

Fig.I.13. Schematic of DC and RF sputtering process [39].

I.2.2.Chemical Processes

I.2.2.1.Laser-Induced Chemical Vapor Deposition (LCVD)

LCVD [40] utilizes a laser beam for highly localized heating on the substrate that induces film deposition by CVD surface reactions (Fig.I.14).

Another mode of utilizing laser (or electron radiation) is to activate gaseous reactant atoms or molecules by their absorption of the specific wavelength of the photonic energy supplied. The resulting chemical gas phase reactions are very specific, leading to highly pure

film deposits. On the other hand, the activation matching of the spectral properties with the reactant species limits the choice of reactions and hence the film deposits that can be obtained.

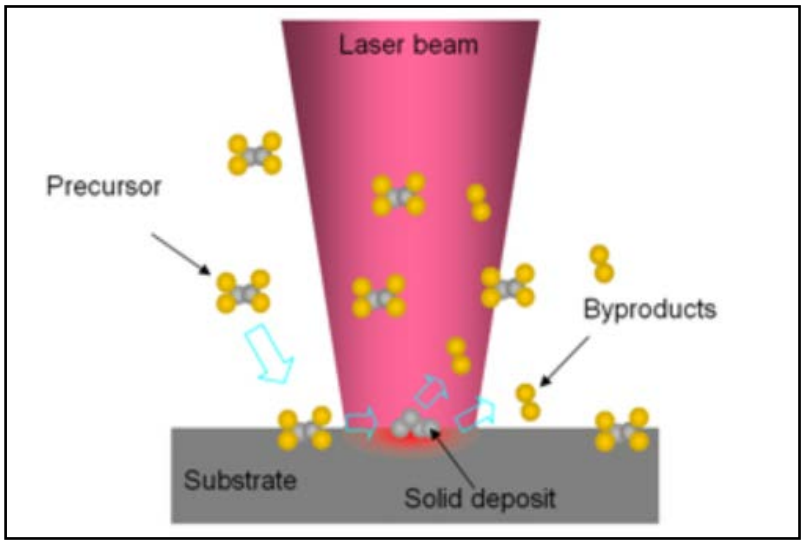

Fig.I.14. Principle of LCVD

I.2.2.2. Spin coating

Spin coating is a technique that is commonly used to deposit thin films on wafer surfaces. In this process an extra amount of a solution is put on a substrate, this latter is revolved fast around a vertical axis to the coating zone. The liquid equally diffuses on the substrate surface and form thin films because of the centrifugal power [41]. The technique includes fluid flow and evaporation behaviors that generally permit the construction of uniform coatings (Fig I.15).

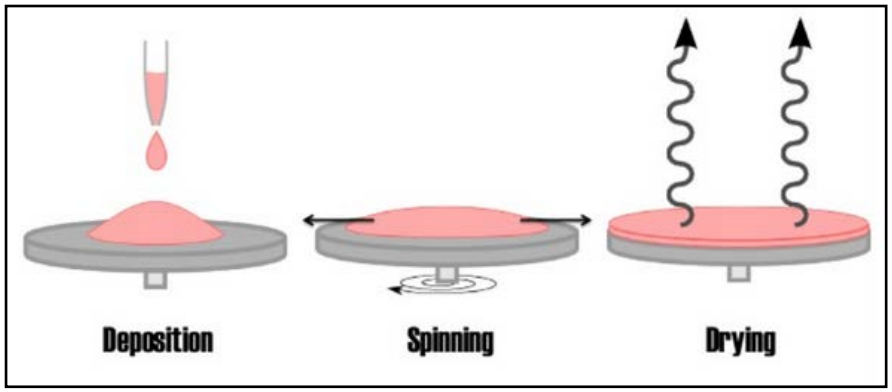

Fig.I.15.schematic illustration of the spin coating process [42]

I.2.2.3.Dip coating

This technique is based on dipping the substrate into a solution, which has hydrolysable metal components and withdrawal it at a stable speed, at controlled temperature and atmospheric conditions (Fig I.16). The operations of hydrolysis and condensation occur in

these conditions. The pulling speed, the solid content and the viscosity of the liquid are the important factors influencing the thickness of coating. The films, in this technique, are hardened by high temperature treatments. The average of heating should be checked in order not to crack the films. This method is exploited in the commercial field to deposit coatings on both sides of a glass substrate on wide area coatings.

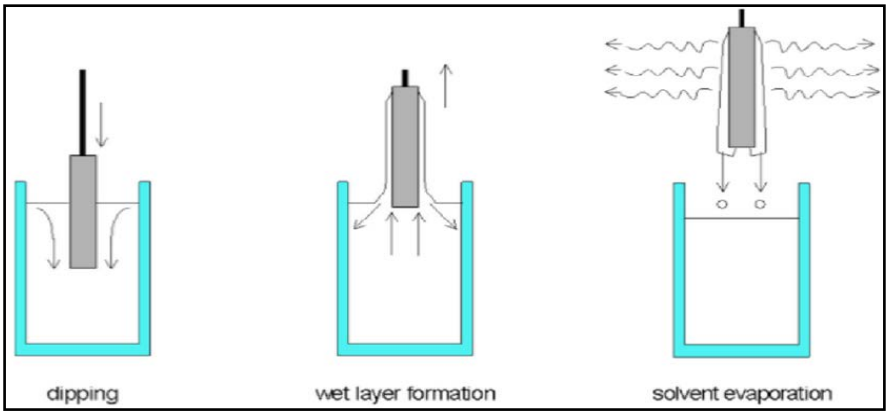

Fig.I.16. schematic illustration of the dip coating technique [43].

I.2.2.4. Spray pyrolysis

The spray pyrolysis technique includes spraying of a solution (usually aqueous, containing soluble salts of the constituent atoms of the desired compound) on a substrate maintained at high temperatures. The sprayed droplets react with the hot substrate surface and undergo pyrolytic (endothermic) decomposition and form cluster of crystallites of the sprayed materials. Thin film deposition using spray pyrolysis can be divided into three main steps: atomization of the precursor solution, transportation of the resultant aerosol and decomposition of the precursor on the substrate.

- **Atomization of the precursor solution**

The film quality and the droplet size of the aerosol are typically set by the atomization technique. The most commonly used techniques for generating droplets are:

1) The pneumatic method (PS): a relatively pressurized air flow carry the solution that contains precursors, the atomization into droplets is composed at the nozzle orifice.

2) Ultrasonic spray method (USP): an ultrasonic wave generator atomizes the solution. The droplet size is more regular and thinner in ultrasonic spray nozzle than in pneumatic spray. In addition, comparing with the droplet speed in PS, it is low in USP; hence, this may affect the films growth in both methods [44].

- **Transportation of the resultant aerosol**

The droplets have to be moved to the substrate, when aerosol is transported, without composing powder or salt particles. The mechanism of SnO_2 film growth was investigated by

Sears et al [45]. They discussed the effect of forces that determine the path of the droplets and the evaporation. Also, they suggested a model of a film growth taking into consideration the gravitational, electric thermophoretic and Stokes forces (Fig.I.17).

- **Decomposition of the precursor on the substrate**

During decomposition of the precursor, several operations take place simultaneously (evaporation of residual solvent, spreading of the droplet, and salt decomposition). They are identified in Fig.I.18.

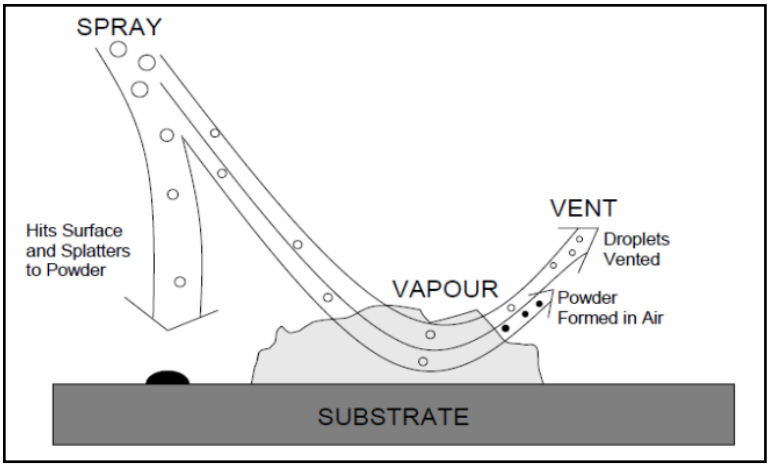

Fig.I.17. Schematic of aerosol transport by Sears et al. [45]

As shown in Fig.I.18, the four processes (A-D) explain the four potential states that the droplets may undergo during spray pyrolysis deposition as it is moved to the substrate.

In process (A): when the droplets are near a heated substrate with insufficient high temperature to entirely evaporate the solution, the droplets will influence the substrate and decompose. When the droplets are in contact with the substrate, they will fully vaporize and a dry precipitate is let behind. Because droplet vaporization needs some heat, the substrate temperature is slightly reduced at the impact point, adversely affecting the reaction kinetics. This process has a weak sticking probability.

In process (B): the droplet dries up completely before it arrives onto the substrate surface and hits it, which is characteristic of this process. Some particles evaporate and condense in the gaps between the particles where the surface reaction begins. The vaporization of the particle topically eliminates out much heat, but not to the same extent as in process (A). This process has a medium sticking probability.

In process (C): a precipitate will form as soon the processing environment causes droplets evaporate prior to reach the substrate vicinity. The precipitate is converted into a vapor state when it reaches the immediate vicinity of the substrate. There is enough time for it

to warm up at ambient temperature. This is a classical CVD reaction which results in a high quality film deposition and a high sticking probability.

In process (D): the droplet quickly forms a precipitate mainly if the temperature is sufficiently elevated. The precipitate is vaporized when it is close to the substrate and then a chemical reaction takes place in the vapor phase. All reactant and product molecules are in the vapor phases which make the reaction homogeneous. The latter causes the condensation of molecules into crystallites in the form of a powder precipitate. This powder affects the composition of the layer. Moreover, the homogeneous reaction reduces the deposition efficiency of this process.

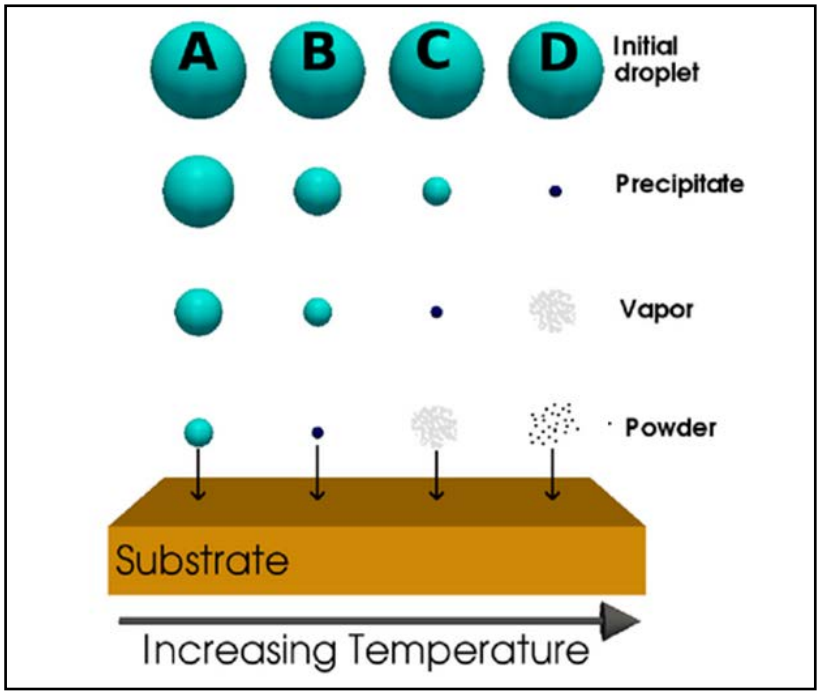

Fig. I.18. Schematic describing different deposition processes that occur as the deposition temperature change. [46]

References

[1] H. Hosono. Thin Solid Films, 515 (2007) 6000 – 6014.

[2] T. Minami. Semicond. Sci. Technol., 20 (2005) 35–44.

[3] K. B¨adeker. Ann. Phys. (Leipzig), 22:749 (1907).

[4] Q. Zhang, P. Liu, C. Miao, Z. Chen, C. M. Lawrence Wub and C-Hung Shek, RSC Advances, 5 (49) (2015) 39285-39290.

[5] Y.hi. Zhai, Y.J.Yin, Q.Zhao, J.J.Zhao , Journal of Synthetic Crystals, 44(8) (2015) 2150-2157.

[6] X.Q. Pan, L. Fu, J. Appl. Phys, 89 (2001) 6048-6055.

[7] K. G. Godinho, A. Walsh, G. W. Watson, J. Phys. Chem. C113 (2009) 439–448.

[8] R. Hasunuma, C. Tamura, T. Nomura, Y. Kikuchi, K. Ohmori, M. Sato, A. Uedono, T. Chikyow, K. Shiraishi, K. Yamada and K. Yamabe, ECS Transactions, 28(2) (2010) 263-272.

[9] J.D. Prades, J. Arbiol, A. Cirera, J.R. Morante, M. Avella, L. Zanotti, E. Comini, G. Faglia and G. Sberveglieri, G.Sensor Actuat. B 126,(2007) 6–12.

[10] H. Hosono, D.C. Paine, Handbook of Transparent Conductors, Springer, New York Heidelberg Dordrecht London, (2010).

[11] D.S. Ginley, C. Bright, MRS Bulletin, 25 (2000) 15-18.

[12] F. Arefi-Khonsari, F. Hellegouarc'h and J. Amouroux, Journal of Vacuum Science and Technology, A 16(4) (1998) 2240.

[13] A. Rahal, A. Benhaoua, C. Bouzidi, B. Benhaoua, B. Gasmi, Superlattice. Microstruct. 76 (2014) 105-114.

[14] P.V. Bhuvaneswari, P. Velusamy, R. RameshBabu, S. Moorthy Babu, K. Ramamurthi, M. Arivanandhan, Mater. Sci. Semicond. Process. 16 (2013) 1964–1970.

[15] F.H. Aragón, J.A.H. Coaquira, D.S. Candela, E. Baggio Saitovitch, P. Hidalgo, D. Gouvêa, and P.C. Morais, J. Phys.: Conference Series, 217, 012079 (2010).

[16] A. Azam, A.S. Ahmed, M. Chaman, and A.H. Naqvi, J. Appl. Phys, 108, 094329 (2010).

[17] Z. Ji, Z. He, Y. Song, K. Liu and Z.Ye, Journal of Crystal Growth, 259 (2003) 282–285.

[18] C. Terrier, J.P. Chatelon, R. Berjoan and J.A. Rojer, Journal of sol-gel Siences and Technology, 10 (1997) 75-81.

[19] P.K.Manoj, B. Joseph, V.K. Vaidyan,D. Sumangala Devi Amma, Ceram.Int. 33(2007) 273–278.

[20] C. Terrier, J.P. Chatelon and J.A. Roger, Thin Solid Films, 295(1997) 95-100.

[21] M. Caglar, K. Cemil Atar,Spectrochimica Acta Part A: Molecular and Biomolecular Spectroscopy, 96 (2012) 882–888.

[22] Z. Ji, J. Xi, L. Huo and Y. Zhao, Phys. Stat. Sol, (c) 5 (10) (2008) 3364– 3367.

[23] Y.P.Yavada, G.Denicolò, A.C. Aias, L.S. Roman and L.S. Hümmelgen, Materials Chemistry and Physics, 48 (1997) 263-267.

[24] P.S. Patila, R.K. Kawar, T. Seth, D.P. Amalnerkar and Chigare, Ceramics International 29 (2003) 34.

[25] Y.N.Zhou,M.Z.Xue,and Z.W.Fu, Journal of Power Sources, 234 (2013)310–332.

[26] Y.Wang,H.C.Zeng, and J.Y.Lee, Advanced Materials,18 (5) (2006) 645–649.

[27] D. Deng and J. Y. Lee, Chemistry of Materials, 20 (5) (2008)1841–1846.

[28] C.Wang,Y.Zhou,M.Ge,X.Xu,Z.Zhang,andJ.Z.Jiang, Journal of the American Chemical Society, 132 (1) (2010) 46–47.

[29] Z.Wang, D.Luan, F.Y.C.Boey, and X.W.Lou, Journal of the American Chemical Society, 133 (13) (2011) 4738–4741.

[30] Xi-Tao Yin, sensor and Actuators B: Chemical, (200) (2014) 213-218

[31] F.Ynineb, « Contribution à l'élaboration de couches minces d'Oxydes Transparents Conducteurs (TCO) », magister thesis, Mentouri University, Constantine, (2010).

[32] S.H. Park, Y.C. Son, W.S. Willis, S.L. Suib and K.E. Creasy, Chemistry of Materials, 10(9) (1998) 2389-2398.

[33] G. Leo, R. Rella, P.Siciliano, S. Capone, J.C. Alonso, V. Pankov and A. Ortiz, Sensors and Actuators B, 58(1-3) (1999) 370-374.

[34] A. Salehi, M. Gholizade, Sensors and Actuators B, 89 (2003) 173-179.

[35] A. Goetzbergera, C. Heblinga, H. Schockb, Mater. Sci. Eng, (R 40) (2003) 1-46.

[36] A. M. B. van Mol, Chemical vapour deposition of tin oxide thin films, Eindhoven University of Technology, (2003)

[37] O. Daranfad, "Elaboration et caractérisation des couches minces de Sulfure de Zinc préparées par spray ultrasonique", magister thesis, Mentouri University, Constantine, 2013.

[38] K. Wang; Laser Based Fabrication of Graphene; INTECH;(2013).

[39] M. Ohring, "Materials Science of Thin Films Deposition and Structure", Second Edition, Academic Press, (2002).

[40] J. L. Hixson, C. S. Cassidy, R. L. Stewart, R. M. Taylor, L. R. Matthews, K. H. Church, R. Mamazza and C. S. Ferekides, the Materials Research Society Symposium Proceedings Series, 668 (2011).

[41] N. V. Varun, Albert Y. Tong, V. Ramanuj, “Numerical Studies on Spin Coating of Metals”, University of Texas, Arlington, The 3rd USA International Conference on Surfaces, Coatings and Nanostructured Materials (NANOSMAT-USA), 18-20 May, 2016

[42] S. L. Hellstrom, "Basic models of spin coating," (Submitted as coursework for Physics 210, Stanford University, 2007).

[43] S. Bashir Khan, H.Wu, C. Pan and Z. Zhang, Journal of Material sciences, 05 (2017) 06.

[44] A. Hafdallah, F. Yanineb, M.S. Aida, N. Attaf, Journal of Alloys and Compounds, 509 (2011) 7267–7270.

[45] W.M. Sears and M.A. Gee, Thin Solid Films, 165(1) (1988) 265.

[46] J.C. Viguie and J. Spitz, J. Electrochem. Soc.,122 (4) (1975) 585.

CHAPTER II

Preparation of SnO_2 Thin Films and Characterization Techniques

As indicate in the previous chapter, different techniques have been used to grow SnO_2 films like sol gel, PLD, MBE, sputter deposition, CVD etc. However, many of them have disadvantages for example lengthy post processing (annealing) time, or costly targets, precursors and apparatus. Ultrasonic spray pyrolysis (USP) is low cost technique, thus, it is the most adequate in commercial exploitation because of its ability to offer high-quality films. Many groups employ USP technique to produce SnO_2 thin films using $SnCl_4.5H_2O$ or $SnCl_2.2H_2O$ as a source of Sn [1-4]. In this study, we employ $SnCl_4.5H_2O$ and $SnCl_2.2H_2O$ to get SnO_2. In this chapter, at the very beginning, we briefly present the basis of USP and the certain setup is employed in this study. After that, we characterize the model experimental parameters for the deposition of SnO_2 and SnO_2:In films. Finally, we describe the different methods chosen for characterizations of the structural, optical and electrical properties.

II.1.Deposition Process

II.1.1 The used deposition system

This work was fulfilled in thin films laboratory (LPCMA) at the University of Biskra. The technique employed to deposit SnO_2 thin film is ultrasonic spray pyrolysis (USP). Fig.II.1 shows the diagram of USP which set up to prepare thin films.

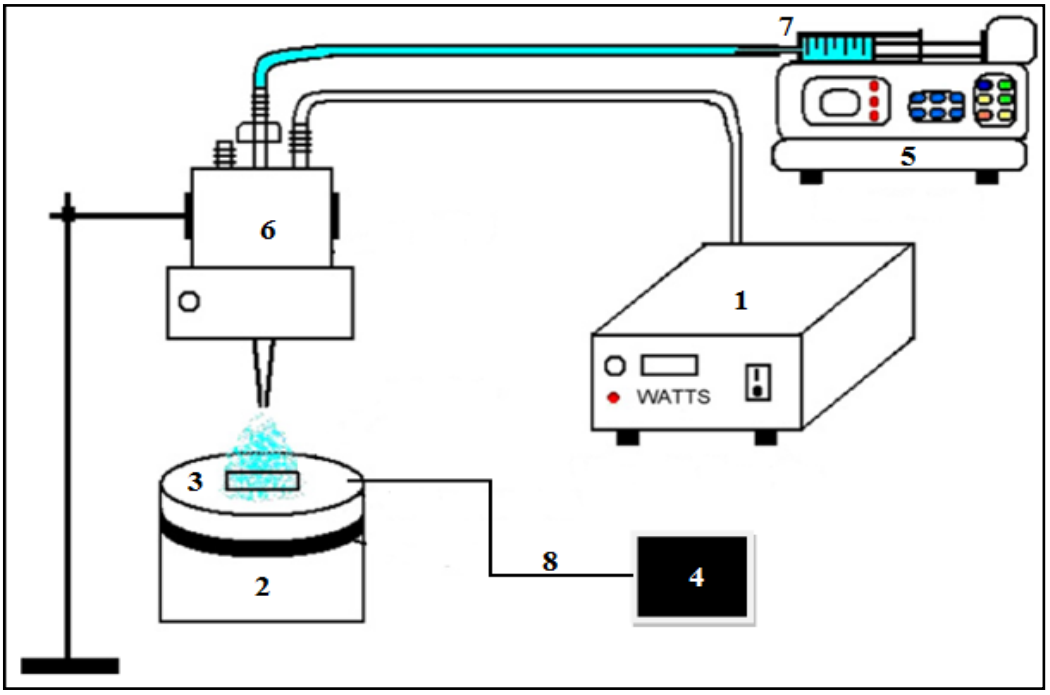

Fig.II.1. Schematic diagram of ultrasonic spray pyrolysis [5]. Modified

1: Ultrasonic generator with 40 kHz frequency allows to generate the ultrasonic waves and send them to the atomizer.

2: Resistance to heat up the substrate

3: substrate holder.

4: Temperature regulator connected with a thermocouple to check the temperature.

5: Syringe pump Model PHOENIX D-CP (GF-FOURES) to control the flow rate

6: Atomizer to decay the solution to fine droplets.

7: Syringe contains the solution.

8: Thermocouple.

II.1.2. Preparation of substrates

II.1.2.1. Choice of the substrate

The substrate is an essential element in any structure involving a film. It plays a crucial role as a principal material in thin film growth. In this work, we chose the glass slides ($25\times25mm^2$) as substrates. The reasons behind this choice are:

- ✓ The compatibility between the coefficient of dilation of the glass and tin dioxide which reduce the stress in the interface film/substrate.
- ✓ Economic reasons.
- ✓ High transparency.

II.1.2.2. Cleaning of the substrate

The purity and the surface state are the main responsible of the adherence and the quality of the thin films. Therefore, the way of cleaning the substrates surface is as follows:

- ✓ The use of pen with diamond point for cutting the substrates.
- ✓ The process of cleaning should be done with soap solution.
- ✓ Rinsing with the distilled water
- ✓ Rinsing with acetone during 5 min.
- ✓ Rinsing with distilled water.
- ✓ Rising with ethanol during 5 min.
- ✓ Cleaning in distilled water bath.
- ✓ Drying using a drier.

III.1.3. Preparation of the solution

The precursors used are: ($SnCl_2$:$2H_2O$), ($SnCl_4$: $5H_2O$), and the doping source is indium chloride ($InCl_3$). Both precursor and doping compound are dissolved in methanol at room temperature. A little HCl is added to the solutions. Three initial types of solutions were prepared:

- ✓ Tin (IV) chloride pentahydrate ($SnCl_4$: $5H_2O$) was diluted in methanol.
- ✓ a fixed molarity (0.1 mol/l) of $SnCl_4$: $5H_2O$ was diluted with different concentrations of $InCl_3$ varying from 0 to 20 % in methanol.
- ✓ a fixed molarity (0.1 mol/l) of $SnCl_2$: $2H_2O$ was diluted with different concentrations of $InCl_3$ varying from 0 to 4 % in methanol.

The experimental conditions for SnO2 thin films elaboration are shown below in Table. II.1

Table. II.1. Summary of the experimental conditions of the SnO2 thin films

Precursor	Substrate Temperature (˚C)	Concentration of solution (mol/l)	Deposition time (min)	Doping concentration (In wt%)	Solution flow rate (ml/h)	Distance spray nozzle-substrate (cm)	Annealing temperature (°C)
$SnCl_4.5H_2O$	450	0.05	5	0	50	5	/
		0.1					
		0.15					
		0.2					
	350	0.1					
	400						
	450						
	500						
	475	0.15	2				
			3				
			4				
			5				
$SnCl_4.5H_2O$	450	0.1	5	0	50	5	/
				1			
				2			
				4			
				6			
				8			
$SnCl_4.5H_2O$	450	0.1	5	0	50	5	600
				10			
				20			
$SnCl_4.5H_2O$	400	0.1	5	1	50	5	600
				2			
				4			
				6			
				8			
$SnCl_2.2H_2O$	450	0.1	5	0	50	5	/
				1			
				2			
				3			
				4			

II.1.4. Deposition of thin films

We put the substrate on an electric resistance linked to a temperature controller. The temperature is gradually increased from the room temperature to a chosen one. We put the amplitude of the sound wave at 40% when the temperature amounts to the wanted, and the solution sprayed on the heated substrate is fixed by the Syringe pump PHOENIX D-CP. Hence, the solutions were sprayed over the hot substrate in the form of fine droplets. Upon reaching the heated surface, these droplets subject pyrolytic decomposition to form a film on the substrate surface, which provides the thermal energy to the decomposition and subsequent recombination.

II.1.5. Properties of the used elements

❖ Tin (IV) chloride pentahydrate

-Chemical Names: Tin (IV) chloride pentahydrate; Tetrachlorostannane pentahydrate; Tin chloride pentahydrate; Stannic chloride pentahydratee

- Appearance: White to yellow powder or chunks

-Molecular Formula: $SnCl_4.5H_2O$

-Molecular Weight: 350.585 g/mol

- Density: 2.04 g/cm3.

- Melting point: 56 °C

- Reference [C.A.S]: 10026-06-9

Fig. II.2. Tin (IV) chloride Pentahydrate

❖ Tin (II) chloride dihydrate

-Chemical Names: Stannous chloride; Stannous chloride dihydrate; Dihydrated stannous chloride; Tin dichloride dihydrate; Stannochlor

-Appearance: White crystalline solid

-Molecular Formula: $SnCl_2.2H_2O$

-Molecular Weight: 225.63 g/mol

- Density: 2.71 g/cm3.

- Melting point: 38 °C

- Boiling point: 652°C

- Reference [C.A.S] : 10025-69-1

Fig. II.3. Tin (II) chloride dihydrate

❖ **Methanol**

-Chemical Names: Methanol; Methyl alcohol; Wood alcohol; Carbinol;

-Molecular Formula: CH_4O or CH_3OH

- Aspect: Colorless liquid

-Molecular Weight: 32.042 g/mol

- Density: 0.16 g/cm3 at 20°C.

- Melting point: -97.8 °C

- Boiling point: 65°C

- Reference [C.A.S] : 67-56-1

Fig. II.4. Methanol

❖ **Indium chloride:**

-Chemical Names: Indium chloride (InCl3); Indiclor; Indium (III) Chloride Anhydrous;

-Appearance: white crystal

-Molecular Formula: $InCl_3$

-Molecular Weight: 221.18 g/mol

- Density: 3.46 g/cm3.

- Melting point: 586 °C

- Boiling point: 800°C

- Reference [C.A.S]: 10025-82-8

Fig. II.5.Indium chloride

II.2. Characterization methods

In this part, we present the technical characterizations of thin films.

II.2.1. Structural Analysis

II.2.1.1. X- Ray Diffraction (XRD) Technique

Diffraction is a phenomenon by which X-rays are reflected from the atoms in a crystalline solid. The diffracted X-rays create a pattern that shows the structural orientation of each atom in a given compound.

Bragg's law is considered as the primary principle behind X-ray diffraction. When monochromatic X-rays affect upon the atoms in a crystal lattice, each atom acts like source of scattering. As shown in the schematic representation in Fig.II.6, the crystal lattice functions as group of parallel reflecting planes. The intensity of the reflected rays reaches the maximum at

particular angles (constructive interference) when the path difference between two reflected waves from two different planes in an integral multiple of the X-rays' wavelength λ. This is known as Bragg's law that is presented by the following relation:

$$2d\ sin\ \theta = n\lambda \qquad \text{(II.1)}$$

Where,

d: interplanar spacing

θ: diffraction angle

λ: wavelength of x-ray

n: order of diffraction

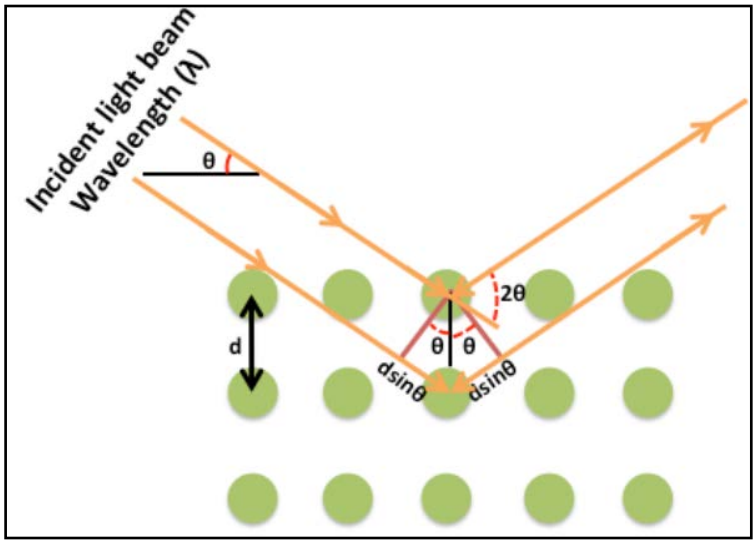

Fig. II.6.Schematic description of Bragg's Diffraction Law.

The X-rays diffraction provides a series of information about the crystal structure, orientation, average crystalline size and stress in the films. In this study, we measured the crystalline properties of the films with X-ray diffraction (XRD) using a D8 ADVANCE diffractometer (λ=1.5405 Å). The diffraction patterns experimentally achieved are compared with standard powder diffraction files published by the International Centre for Diffraction Data (ICDD) [6].

a. Determination of the crystallite size

The average crystallite size of the deposits is estimated from the full width at half maximum (FWHM) of the most intense diffraction line by Scherrer's formula as follows [7]

$$G = \frac{0.9\lambda}{\beta cos\theta} \qquad \text{(II.2)}$$

Where, G is crystallite size, λ is wavelength of X-ray used, β is full width at half maxima of the peak (FWHM) in radians, θ is Bragg's angle.

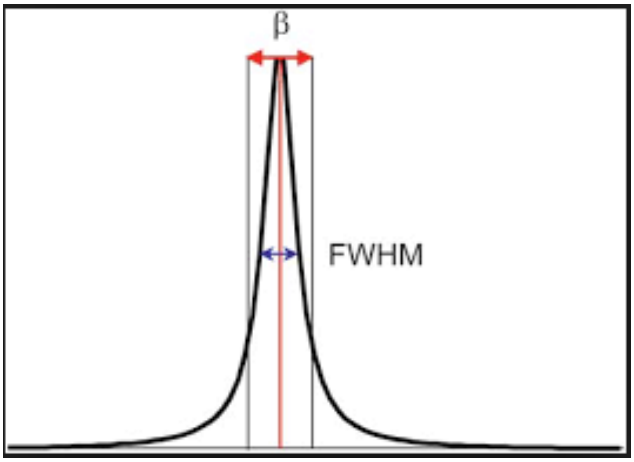

Fig. II.7.Illustration showing the definition of β from the diffraction curves of the X-rays.

b. Determination of the texture coefficient

The preferred orientation's degree can be assessed by comparing the remarkable intensities in a diffraction pattern to a bulk standard. Barret and Massalski [8] adapted a method to realize this which is called the texture coefficient:

$$TC(hkl) = \frac{I(hkl)/I_0(hkl)}{N^{-1}\sum I(hkl)/I_0(hkl)} \qquad \text{(II.3)}$$

TC: the texture coefficient of a given plane (hkl)

I: the measured intensity

I_0: the intensity of a bulk powder

N: the number of reflections noticed in the pattern

Any deviation of the texture coefficient from unity indicates a higher degree of preferred orientation of the crystallites.

c. Determination of the lattice parameters

The lattice parameters (a=b, c) have been determined by the equation below [9]:

$$d_{hkl} = \frac{a}{\sqrt{h^2+K^2+l^2\frac{a^2}{C^2}}} \quad \text{(II.4)}$$

and

$$\frac{c}{a} = 0{,}672 \quad \text{(II.5)}$$

a and c: the lattice parameters

h, k, l: the Miller indices of the planes

d_{hkl}: the interplanar spacing.

d. Strain Determination

To estimate the strain (Ɛ), the following relation is used [10]:

$$\varepsilon = \frac{\beta \cos \theta}{4} \quad \text{(II.6)}$$

B: full width at half of the peak maximum (FWHM)

θ: Bragg's angle.

e. Determination of the dislocation density (δ)

The dislocation density (δ) is defined as the length of dislocation lines per unit volume of the crystal, was estimated by using crystallite size values and the Williamson and Smallman's formula [11]:

$$\delta = \frac{1}{G^2} \quad \text{(II.7)}$$

G: crystallite size

II.2.1.2. Scanning Electron Microscopy (SEM)

The SEM uses a high energy electron ray by electron guns in order to get high resolution images of the sample surface. This ray is quickened towards the samples (with a positive electrical potential) while is concentrating using metal apertures and electromagnetic lenses. In the last lens, the SEM consists of groups of coils which permit to deflect the electron beam back and forth through the sample (Fig II.8). The formation of secondary electrons back scattered electrons, characteristic and continuum x-rays, Auger electrons and photons of various energies are a result of bombardment of the sample surface with high

energy electrons [12]. The main impacts on the electrons of a beam impinging the sample is elastic scattering (the loss of energy is negligible with change of direction) and inelastic scattering (energy loss with negligible change of direction). The major cause of elastic scattering is the interactions with the atoms' nuclei and lead to important deviations from the direction of the incident beam. Inelastic scattering results from two mechanisms, inelastic interaction with the atomic nucleus and inelastic interaction with the tied electrons. The moving electron frees energy in the Coulomb field of the nucleus and sends white or continuum x ray radiation when inelastic scattering happens through interaction with the atomic nucleus. Energy is transferred from the electron beam to the loosely bound electron which is emitted if inelastic scattering happens among a loosely bound electron on an outer shell of the atom and an electron of the incident ray. The electrons emitted through this process are called secondary electrons. Nevertheless, these electrons are generally recollected by ionized atoms in the sample [13].

In this study, we used a TESCAN VEGA3 scanning electron microscope to investigate the surface morphology of our films.

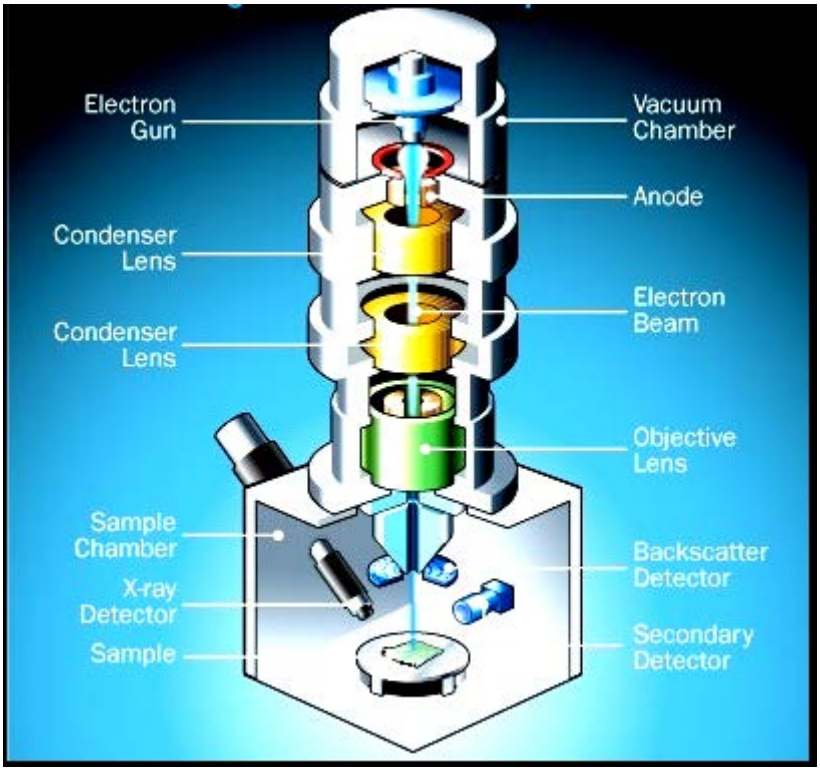

Fig. II.8. Schematic representation of scanning electronic microscopy.

II.2.1.3.Thickness Measurement Using Weight Difference Method

The film thickness is an important parameter in the study of the film properties. Among various techniques that evaluate the film thickness, one can write the weight difference technique. It is simple and useful .The thickness "t" can be calculated as follows [14]:

$$t = m/A\rho_b \qquad \text{(II.8)}$$

m: the mass of the film

A: the substrate area

ρ_b: the density of the material in the bulk form.

The mass of the film has been measured by using a single pan microbalance.

II.2.2.Optical Analysis

The spectrophotometry is the quantitative measurement of transmission or reflection properties by material as a function of wavelength of the incident radiation. We measured the sample transmittance spectra with a dual beam UV-VIS-NIR scanning spectrophotometer of type SHIMADZU UV-3101 PC. The principle of this process is shown in Fig II.9.

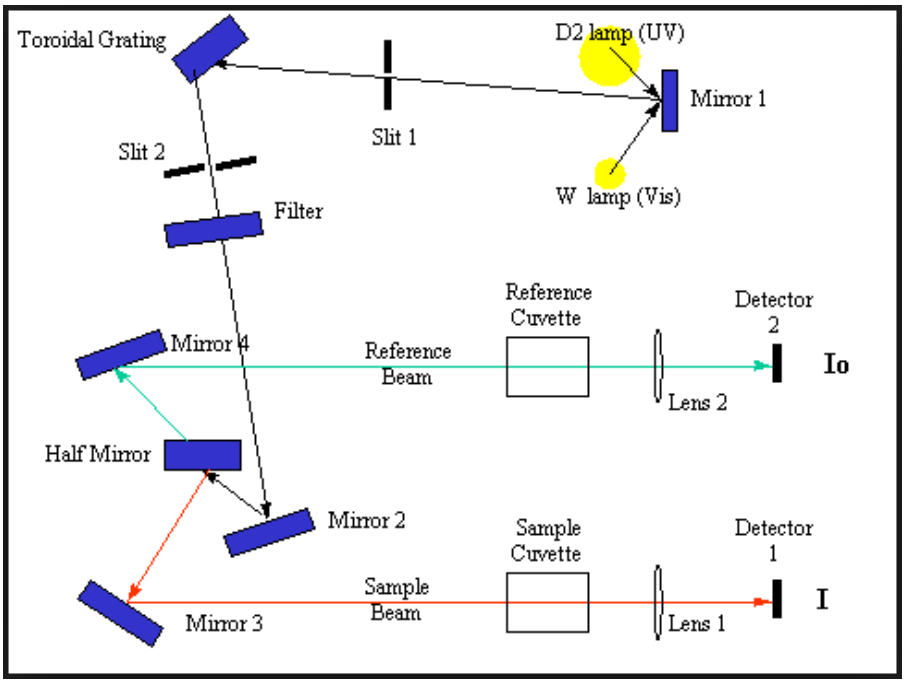

Fig. II.9. The principle of operation of UV-visible.

The light is moved from the source by optics in the instrument and hits the surface of the sample in which the light is distributed into three parts: Transmission (*T*), Reflection (*R*) and Absorption (*A*). The total of these three parts must be equal to the input light. As a result, if we esteem the sum of input light is1, one can write:

$$T + R + A = 1 \qquad \text{(II.9)}$$

The amount of light crossing a sample (*I*) comparing it with that of light before crossing the sample (I_0). The ratio (I/I_0) is known as the transmittance and generally expressed as a percentage (*T %*). The experimental data (the transmittance (*T*)) is used to calculate the absorbance (*A*), absorption coefficient (α), refractive index (*n*), band gap (*Eg*) and film thickness (*t*).

II.2.2.1. Absorption coefficient

In general the intensity of light I_0 effecting into the sample can be divided into a reflected part I_R, an absorbed part I_A and a transmitted part *I*. The absorption coefficient (α) of the films, presented by Beer-Lambert relation, hypothesizing that the reflected light is negligible [15]:

$$\frac{I}{I_0} = e^{-\alpha t} \qquad \text{(II.10)}$$

And

$$T(\%) = \frac{I}{I_0} \cdot (100) \qquad \text{(II.11)}$$

Then

$$\alpha = \frac{1}{t} \ln \frac{100}{T\%} \qquad \text{(II.12)}$$

α: the absorption coefficient

t: the thickness of the film

T: the transmittance.

II.2.2.2.Optical Gap

In the strong absorption region, the photons induce electronic transitions from the valence band to the empty energy states in the conduction band. By using Tauc relationship [16], we can evaluate in this area the value of the optical band gap:

$$(\alpha h\nu) = A\left(h\nu - E_g\right)^m \qquad \text{(II.13)}$$

α*:* absorption coefficient

hv: the photon energy

Eg: optical gap

m and *A*: constants,

m identifies the optical type of transition and takes the values 1/2, 2 (depending on whether the optical transitions are respectively direct allowed or indirect allowed).

It has been noticed that the plots of $(\alpha h\nu)^2$ versus $h\nu$ are linear over a wide range of photon energies showing the direct type of transitions. The extrapolation of the straight part of the scheme on the energy axis presents the band gap energy as it is represented in Fig II.10 [17].

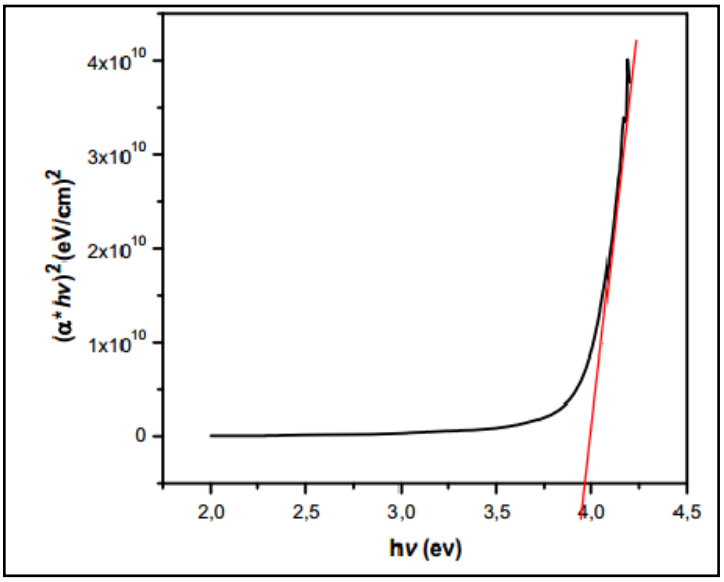

Fig. II.10. Determination of band gap Eg.

II.2.2.3. Disorder calculation of the Urbach Energy

Urbach energy is usually explained as the width of the band tail because of the localized states in the typical band gap that is associated with the disordered or low crystalline materials. The spectral dependence of the absorption coefficient (α) and photon energy (hν) is called "Urbach empirical rule" which can be expressed through the following relation:

$$\alpha = \alpha_0 \exp\left(\frac{h\nu}{E_{00}}\right) \qquad \text{(II.14)}$$

When we take the logarithm of both extremities of the previous equation, hereafter, one may obtain a straight line equation. It is presented as follows:

$$\ln \alpha = \ln \alpha_0 + \frac{h\nu}{E_{00}} \qquad \text{(II.15)}$$

By plotting *Lnα* as function of *hν*, we can determine E_{00} value as the reciprocal of the linear part slope [18]. (Fig. II.11.)

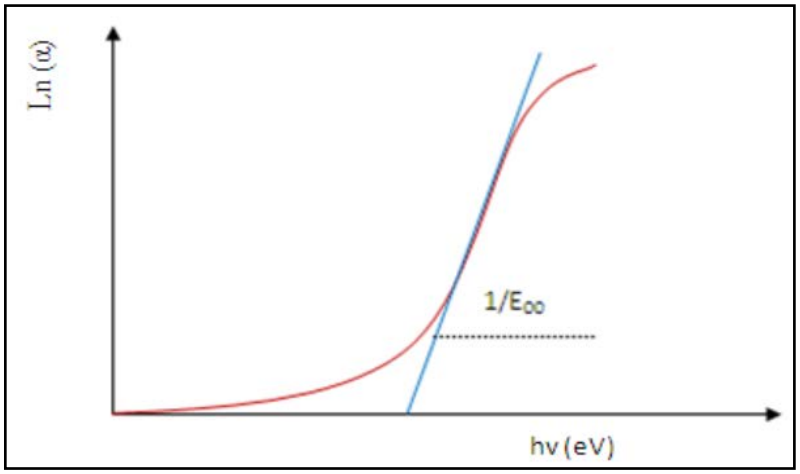

Fig. II.11. Determination of the disorder.

II.2.3. Electrical Analysis

II.2.3.1. Four-point probe

The purpose of the 4-point probe is to measure the resistivity of any semiconductor material. It can measure either bulk or thin film specimen, each of which consists of a different expression. Four-point probe technique is very simple, by passing a current through two outer probes and measuring the voltage through the inner probes to determine the sample resistivity. A model schematic setup is shown in Fig. II.12.

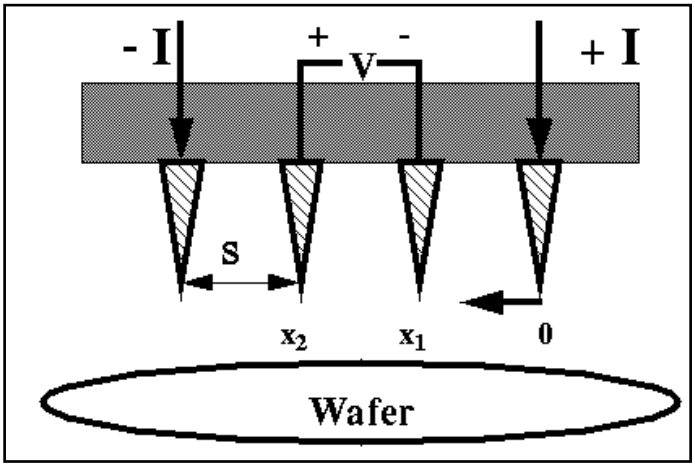

Fig. II.12.Schematic Diagram showing the four-point probe technique.

For a very thin layer where the sample thickness t << s, the probe spacing, we assume a cylindrical protrusion of current emanating from the outer probe tips [19]. The differential resistance is:

$$dR = \rho\left(\frac{dx}{A}\right) \quad \text{(II.16)}$$

The expression for the area A is:

$$A = 2\pi xt \quad \text{(II.17)}$$

We carry out the integration between the inner probes (where the voltage is measured):

$$R = \int_{x_1}^{x_2} \rho \frac{dx}{2\pi xt} = \int_{s}^{2s} \frac{\rho}{2\pi t}\frac{dx}{x} = \frac{\rho}{2\pi t}\ln 2 \quad \text{(II.18)}$$

Where probe spacing is uniformly s. Due to the superposition of current at the outer two tips, R = V/2I. Thus, we arrive at the expression for thin film resistivity:

$$\rho = \frac{\pi t}{ln\ 2}\left(\frac{V}{I}\right) \quad \text{(II.19)}$$

The sheet resistance $R_s = {}^{\rho}/_{t}$ can be expressed as:

$$R_S = 4.53\ V/I \quad \text{(II.20)}$$

II.2.4. Hall measurement

This measurement can be employed to determine the transport properties of a material like carrier concentration (n), type (n or p) and Hall mobility of the samples.

When an electron moves, under the effect of an electric field, along a direction perpendicular to an applied magnetic field $\vec{B}$, it undergoes a force $\vec{F}$ (called the Lorentz force) perpendicular to the plane formed by its trajectory and $\vec{B}$. As illustrated in a Fig.II.13, the electrons deviate to one side of the thin conductor which causes a potential between the two sides of the sample. This measurable transverse voltage is called the Hall Effect (V_H) after E. H. Hall who discovered it in 1879 [20].

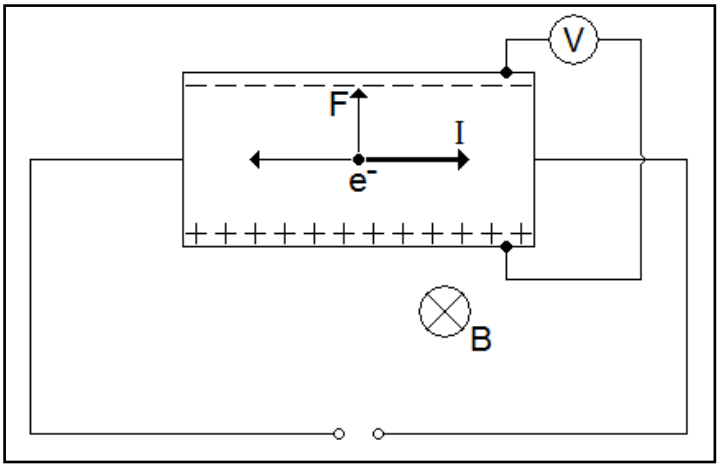

Fig. II.13. Descriptive diagram of Hall effect.

The Hall voltage is given by

$$\Delta V_H = \frac{IB}{N_H\, et} \qquad \text{(II.21)}$$

e = electron charge.

N_H = density of mobile charges

t = film thickness

By plotting ΔV_H as function of B, we can get the carrier concentration N_H (see Fig II.14)

$$\Delta V_H = \frac{I}{N_H\, et} B; \quad R_H = \frac{1}{N_H\, e} \qquad \text{(II.22)}$$

The slope = $R_H \frac{I}{t}$

R_H: Hall coefficient

As a result, the carrier concentration can be deduced:

$$N_H = \frac{1}{R_H\, e} \qquad \text{(II.23)}$$

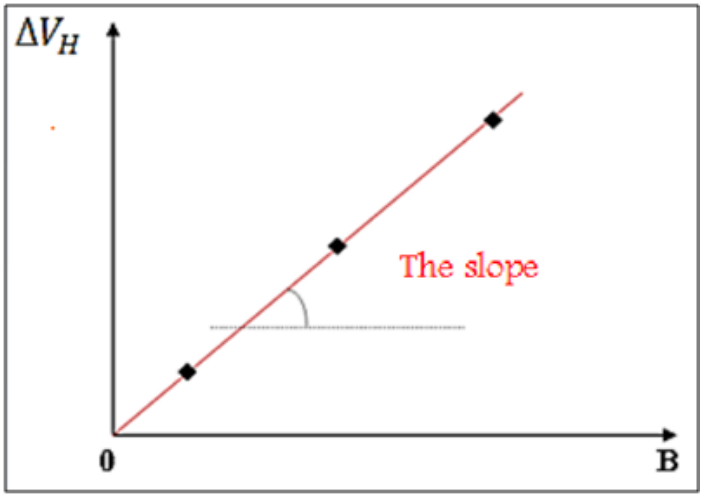

Fig. II.14. Determination of Hall coefficient.

We can also determine the type of semiconductor (n or p) by the sign of the product $B.RH$, where [21]:

$B.RH < 0$ for a n-type semiconductor

$B.RH > 0$ for a p-type semiconductor

a. Figure of merit

The optical transmittance and electrical conductivity are both important parameters by which we evaluate the quality of transparent conducting oxides. These two parameters are inversely proportional to each other. The method through which it is correlating the properties of TCO films by means of figure of merit (F) is presented by the following equation [22]:

$$F = -\frac{1}{(\rho \ln T)} \qquad \text{(II.24)}$$

ρ: the electrical resistivity

T: the average transmittance in the wavelength range of 400 – 800 nm.

References

[1] A. Benhaoua, A. Rahal, B. Benhaoua , M. Jlassi, Superlattices and Microstructures, 70 (2014) 61–69.

[2] A. Rahal, S. Benramache, B. Benhaoua, J. Semiconduct. 34 (2013) 083002.

[3] M. Thirumoorthi, J.T.J. Prakash, Superlattice Microstruct. 89 (2016) 378-389.

[4] K. Deva Arun Kumar, S. Valanarasu, K. Jeyadheepan, H. S. Kim, D. Vikraman, J. Mat. Sci, 29 (2018) 3648–3656.

[5] L.A. Patil, M.D. Shinde, A.R. Bari, V.V. Deo, Sensors and Actuators, B 143 (2009) 270–277.

[6] A. Aldrin, "Preparation and characterization of certain II-VI, I-III-VI2 semiconductor thin films and transparent conducting oxides", PhD thesis, Cochin University of Science and Technology, Kerala, India, 2004.

[7] M. Devika, K.T.R. Reddy, Appl.Phys.100 (2006) 023518.

[8] CS. Barrett, T. Massalski, Structure of Metals. McGraw Hill; (1980) 204.

[9] S.P. Choudhury and al, Materials Today: Proceedings 3 (2016) 1609–1619.

[10] A. Bouhdjer, Study of Thin Layers of Indium Oxide (In_2O_3) Elaborated by Chemical Means, PhD thesis, Med Khider University of Biskra, 2016.

[11] G.K. Williamson, R.E. Smallman III, Philos. Mag. 1 (1956) 34–45.

[12] J. Goldstein, D.E. Newbury, D.C. Joy, C.E. Lyman, P. Echlin, E. Llfshin, and al. Scanning Electron Microscopy and X-ray Microanalysis. 3rd ed. Springer.

[13] J.I. Goldstein: "Practical Scanning Electron Microscopy", in Chap. 3: "Electron Beam-Specimen Interaction", ed. J.I. Goldstein and H. Yakowitz, PlenumPress, New York, 1975.

[14] A. Bergauer, C. Eisenmenger-Sittner, Physics of Thin Films, LVA 130 032; (2006).

[15] A. Muthukumar, G. Giusti, M. Jouvert, V. Consonni, D. Bellet, Thin Solid Films 545 (2013) 302–309.

[16] K. Bennaceur, A. Attaf, H. Saidi, M.S. Aida, A. Bouhdjer, H. Ezzaouia, J Fundam Appl Sci,10(2) (2018) 84-96.

[17] A. Allag, S. Rahmane, N. Kouidri, H. Attouche, A. Ouahab, J Mater Sci: Mater Electron, 28 (2017) 4772-4779.

[18] F.Zhu, K.Zhang, E.Guenther, Ch.S. Jin, Institute of Materials Research & Engineering, Singapor, 2000.

[19] L. B.Valdes, Proc. IRE, 42(1954) 420.

[20] S. Faÿ, L'oxyde de zinc par dépôt chimique en phase vapeur comme contact électrique transparent et diffuseur de lumière pour les cellules solaires, PhD thesis, Federal Institute Of Technology, Lausanne, 2003.

[21] C.Y. Tsay, S.C. Liang, J. Alloys and Compounds, 622 (2015) 644-650.

[22] V. Senthilkumar, P. Vickraman, Curr. Appl. Phys. 10 (2010) 880.

CHAPTER III

Optimum Conditions for SnO_2 Thin Films Preparation

In this chapter, we have made a detailed research about the influence of the deposition parameters (molarity, deposition time and substrate temperature) on the optoelectronic properties of the SnO_2 films, in order to obtain the optimum conditions for preparing these films which can be used as transparent contact for thin film solar cells.

All the films considered in this chapter were grown under the same conditions (precursor $SnCl_4$: $5H_2O$, Solution flow rate 50 ml/h and distance spray nozzle-substrate 5 cm), but with different molarities (0.05, 0.1, 0.15 and 0.2 mol/l), different deposition times (2, 3, 4 and 5 min) and different substrate temperatures (350, 400, 450 and 500˚C).

III.1. Effect of molarities

III.1.1. Thickness of the film

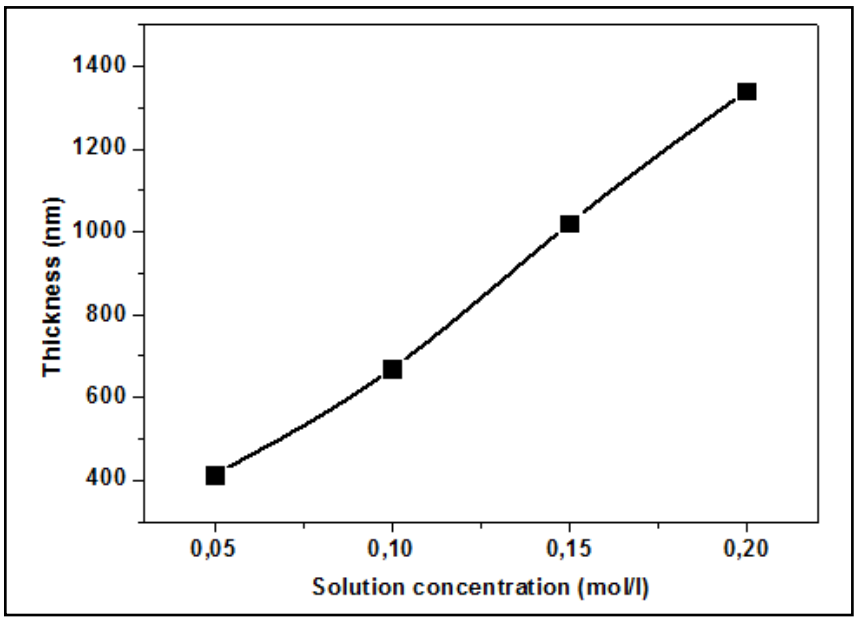

Fig. III.1. Variation of thickness versus solution concentration.

The thickness of the SnO_2 films prepared with different precursor solution concentrations were calculated using different weight method (see chapter II) (Fig. III.1).The rise of the molarity leads to an increase in the density of atoms in the solution and then increases the thickness of the deposited thin film. Therefore, by increasing of the precursor concentration, one can observe an almost linear increase of the film thickness.

III.1.2. Structural properties

The XRD spectra of SnO_2 films prepared with four different precursor solution concentrations are shown in Fig. III.2.

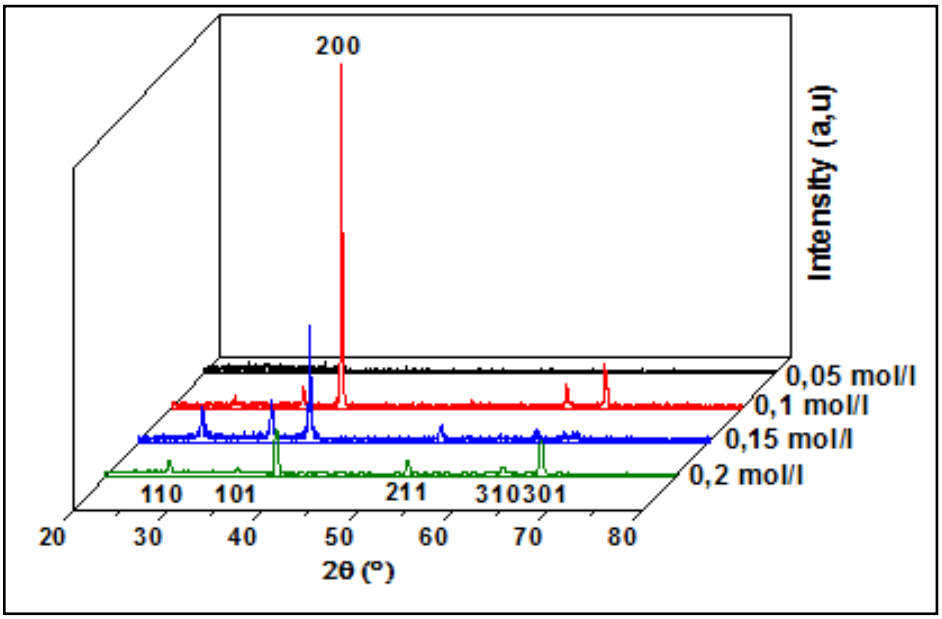

Fig. III.2. X-ray diffraction patterns of SnO_2 thin films, for different solution concentrations.

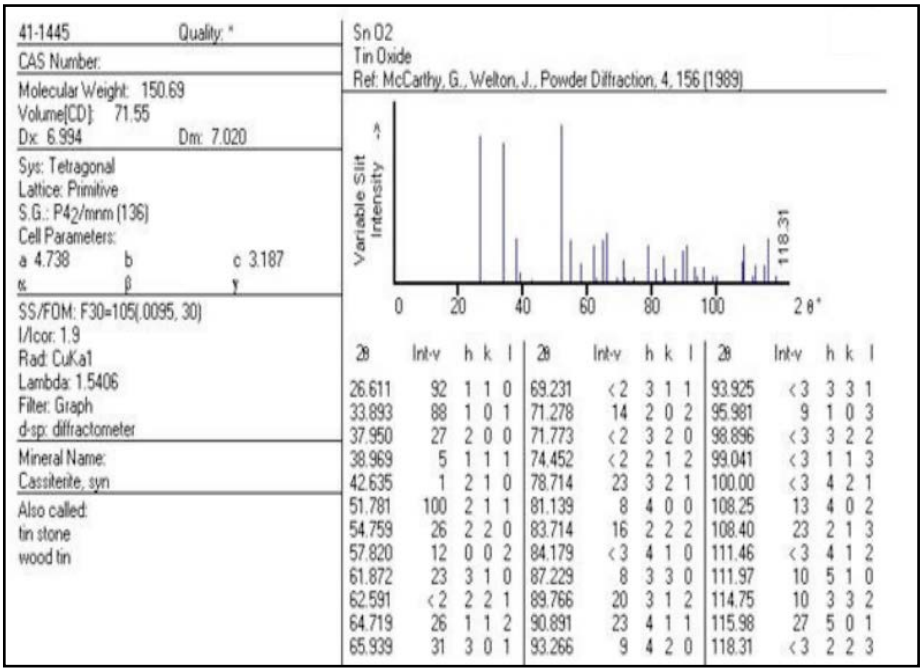

Fig. III.3.ASTM file of SnO_2

The sample with 0.05mol/l concentration is amorphous or composed of highly dispersed small crystallites. By increasing the molarity up to 0.1 M, the intensity of peaks and crystallite size have been increased and the crystallinity of the films is improved too. Six

peaks along (110), (101), (200), (211), (301) and (310) planes are clearly observed which indicate that the films are polycrystalline in nature. These peaks show that the films have a cassiterite tetragonal crystalline phase (JCPDS card No. 041-1445). The preferential orientation is (200) for films with molarities 0.1, 0.15 and 0.2 (Fig. III.2).The strong diffraction from (200) plane denote that the films have a sturdy crystallographic texture along (200) which has low formation energy. D.R. Deepu [1] has found the same peak (200) for film deposited by spray pyrolysis. Also, the crystallite of the SnO_2 films preferred the plane (200) for the films deposited [2].

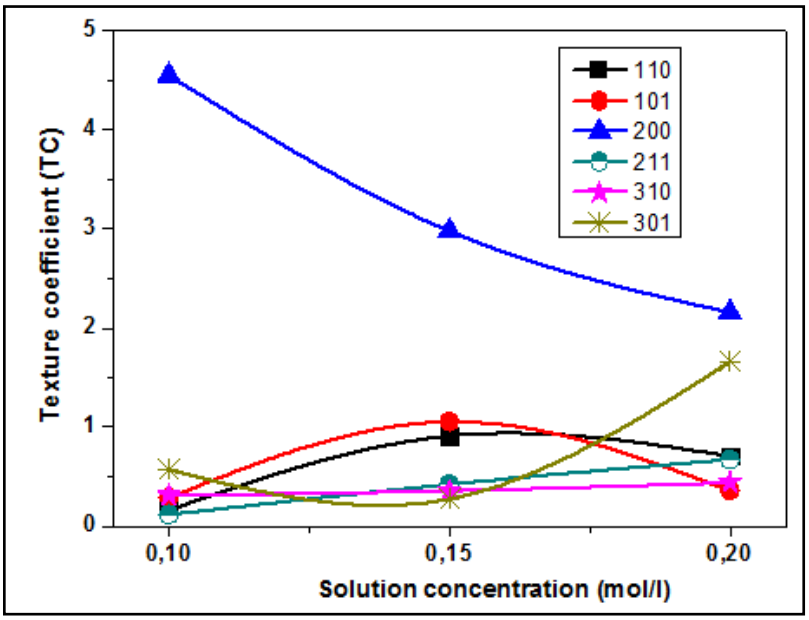

Fig. III.4. Variation of texture coefficient (TC) with solution concentration.

.

Fig. III.4. shows TC values of (200) peaks for all films that are larger than unity. In all samples, TC values for (200) are relatively higher than those of other planes and those values continuously decrease with an increase of the solution concentration. This affirms the reorientation with rising solution concentration. Also, Memarian and Rozati [3] mentioned that the intensity of (200) is decreased with increasing the thickness.

As the molarity increases, the intensity along (301) orientation decreases slightly then increases while the intensity of (110) orientation increases then decreases. But, we do not observe a significant change in (310) and (211) orientations. Agashe and al [4] have found that the (200) direction is predominant in the range 0.03-0.3 mol/l. They explained that the change in the preferred growth (in the range 0.01-0.03mol/l) is attributed to the gradual incorporation of Sn at interstitial sites in the SnO_2 lattice. Consonni and al [5] presented that if

the film thickness is increased, the (100) and (301) crystallographic orientations will be predominant.

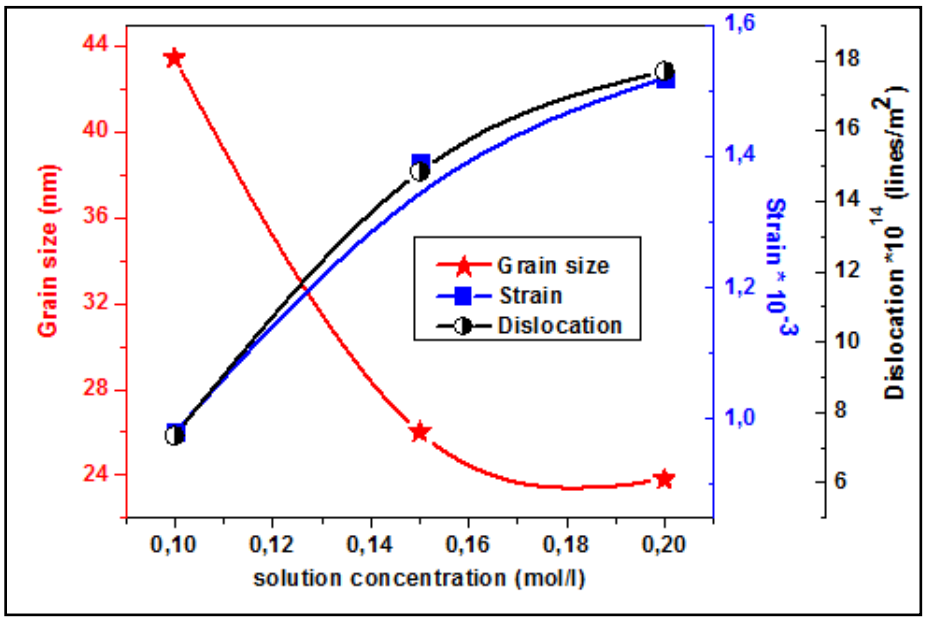

Fig. III.5. The variation of grain size, strain and dislocation density with solution concentration.

The crystallite size (G) of the films was calculated from preferential orientation (200) peak by using Scherrer formula. Fig.III.5 shows the plot of crystallite size, strain and dislocation density as a function of solution concentration. The average grain size decreases from 43.42 to 23.78 nm with the increase of solution concentration. It is observed that the crystallite size value reduces with the increase of solution concentration and this is maybe due to the increased nucleation centers. A similar behavior has been found by another research [6]. On the other hand, the strain and dislocation density increase along plane (200) with the increase of solution concentration as shown in Fig. III.5.The reduction in grain size in the films is attributed to the increase of the stress. The latter is the product of internal strains.

III.1.3. Optical properties

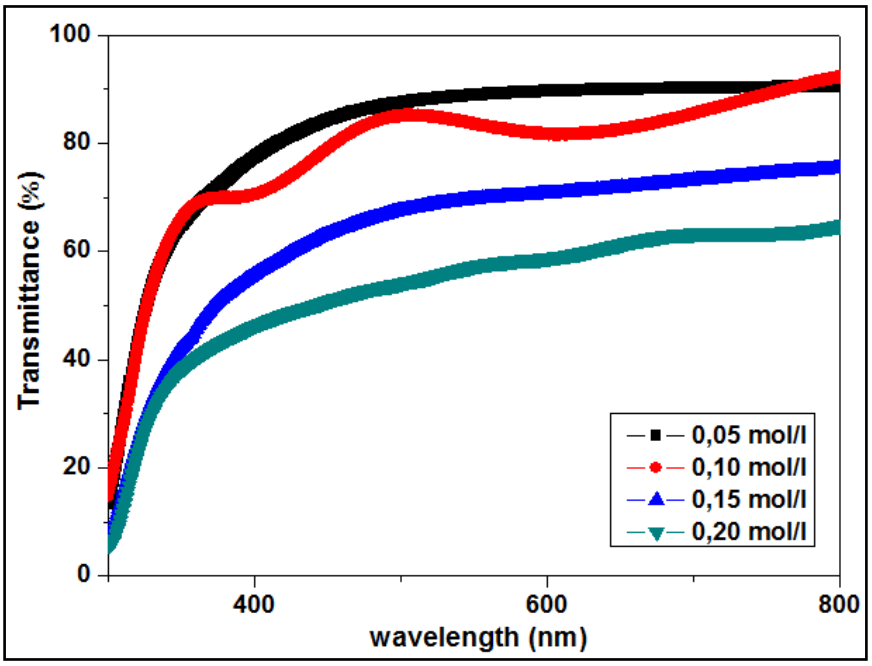

Fig. III.6. Optical transmittance of SnO_2 films as a function of wavelength for different solution concentrations.

Fig. III.6 shows the variation of transmittance with wavelength of SnO_2 thin films with different solution concentrations. It is clearly noticed that films are completely transparent in the visible region. Moreover, the absorption edges shift to longer wavelength region with increasing of molarity. The rise of the concentration of solution leads to an increase in number of particles. The latter produces an increase in thickness. As it is known the transmittance is depending on thickness of samples according to Beer-Lambert law (see chap.II). Therefore, the rise of the film thickness leads to a decrease in the optical transmittance. Similar observation has been found by Belhamri and al [7].

The film with 0.1 mol/l concentration has the most fringes and this could be due to its smooth surface. Moreover, the absence of interference fringes in the other films can be attributed to the roughness of the interface air/film in which the incident light is diffused rather than reflected in one direction.

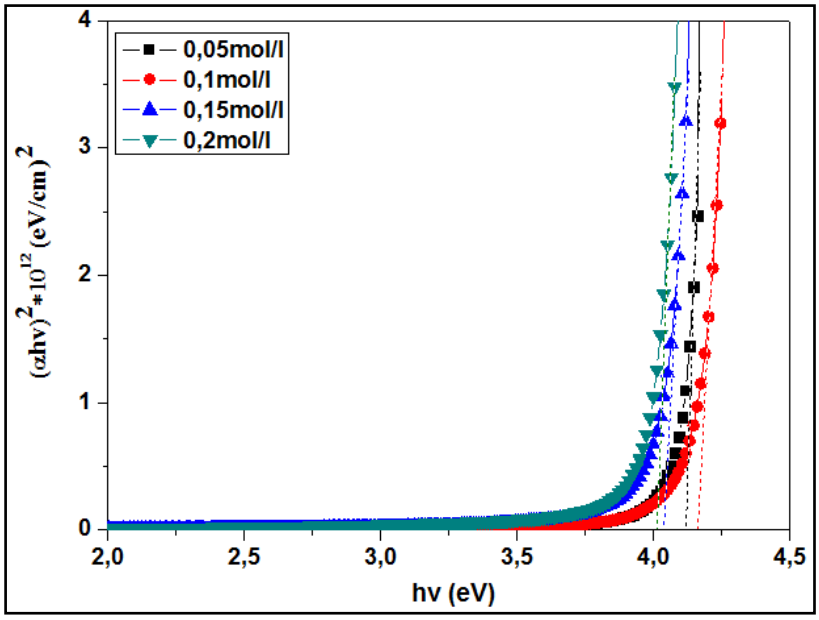

Fig. III.7. The plot $(\alpha h\nu)^2$ versus $(h\nu)$ for the calculation of the optical band gap energy Eg.

The optical band gap of SnO_2 films has been determined on the basis of UV–VIS transmission measurements by plotting $(\alpha h\nu)^2$ as function of $h\nu$ using the relation indicated in previous chapter as it is shown in Fig. III.7.

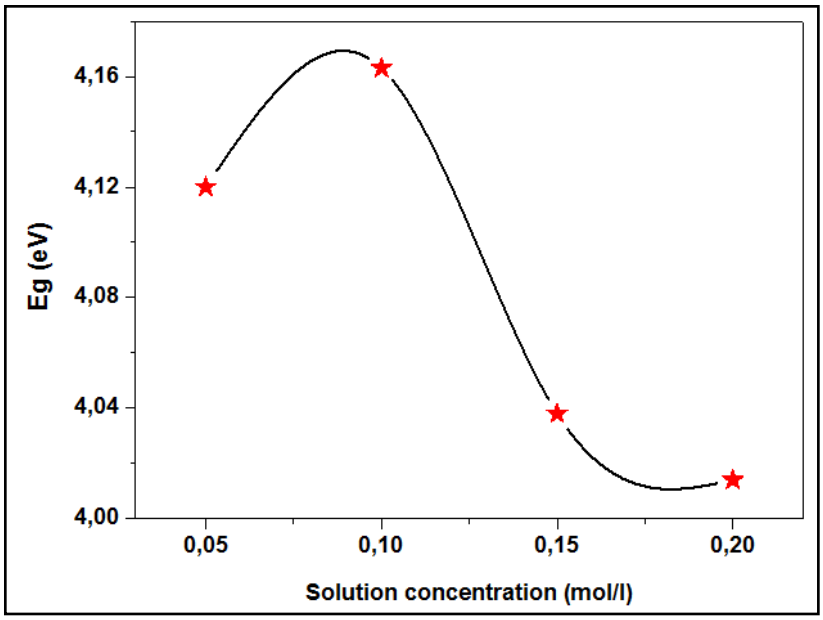

Fig. III.8. Variation of band gap with solution concentration.

The variation of band gap as function of solution concentration is shown in Fig. III.8. Energy band gap values is in the range of 4,014–4,163 eV, the same values have been found in previous research [8]. It can be seen that the band gap is inversely proportional to the dislocation. The change in the band gap is attributed to the variation of grain size or the

structural phase and carrier concentration [9]. It is clear that the band gap energy increases with the increasing of solution concentration from 0.05 to 0.1 M, then decreases. The band gap widening might be due to the Burstein–Moss effect [10, 11] (The Fermi level inside the conduction band goes up with raise in the carrier's concentration. Consequently, the value of the band gap increases and causes the shift of absorption edge to shorter wavelength (blue shift), as shown in Fig. III.6). This phenomenon is accompanied by an increase in the carriers concentration. However, the narrowing of band gap can be attributed to the deterioration of crystal structure of the film and increases the dislocation which can be seen from XRD analysis of our samples.

III.1.4. Electrical properties

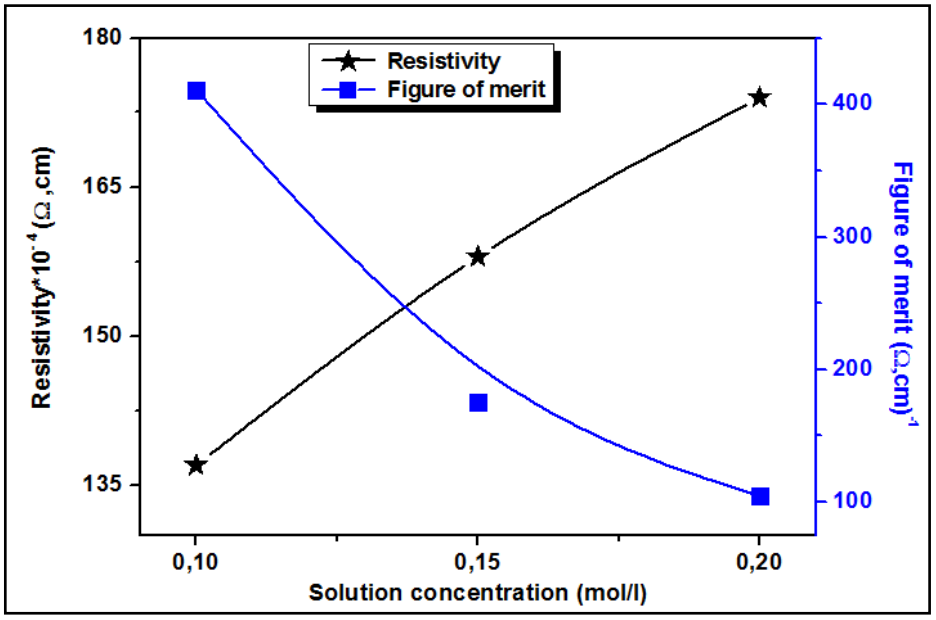

Fig.III.9. Variation of electrical resistivity and figure of merit with solution concentration.

Fig. III.9 shows the variation of electrical resistivity (ρ) and figure of merit (F) with solution concentration. ρ is increased with the increasing of solution concentration. It is well known that the increment in resistivity depends upon the decrease in grain size. When the grain sizes decrease, many grain boundaries are formed. The increase in grain boundary leads to the reduction of free electrons concentration through trapping them at grain boundaries because of the large number of defects. The trapping of electrons produces potential barriers at the grain boundaries which reduces the motion of electrons. Therefore, the grain boundaries act as scattering centers.

From Fig. III.9 it is obvious that the figure of merit is inversely proportional to the resistivity. The maximum value of figure of merit, ($4{,}105\times 10^2$ $(\Omega.cm)^{-1}$ at λ =550 nm), was obtained for the film deposited at the concentration solution of 0.1 mol/l. This may be due to the formation of a good quality film in terms of conductivity and transmittance.

III.2. Effect of deposition time

III.2.1.Thickness of the film

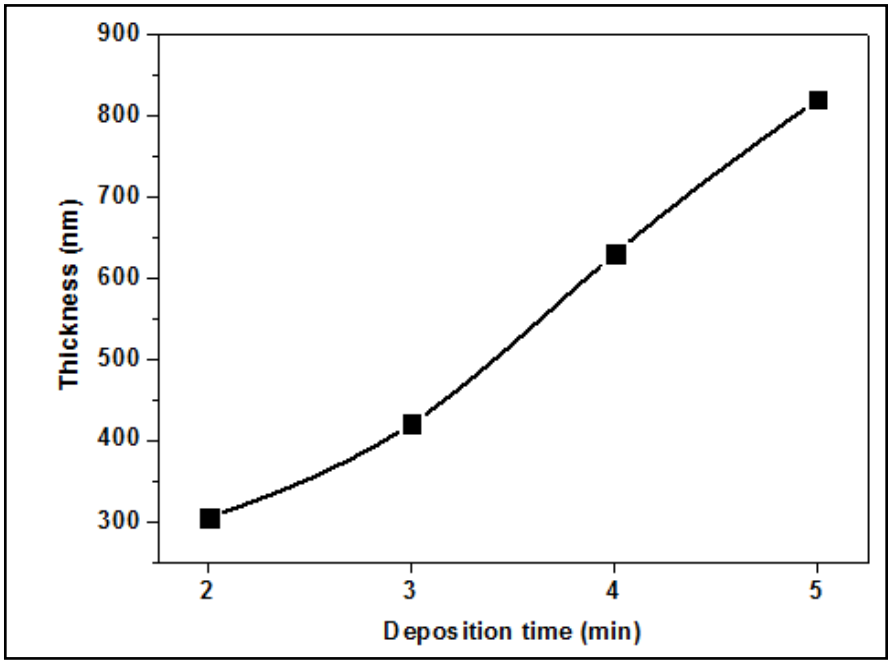

Fig. III.10. Variation of thickness versus deposition time.

Fig. III.10 gives the plot of films thickness versus deposition time. It is clear that, the spraying time is directly related with the thickness of the film in which the film thickness increases with the increasing of time. This attributed to the relative increase in the amount of tin sprayed.

III.2.2.Structural properties

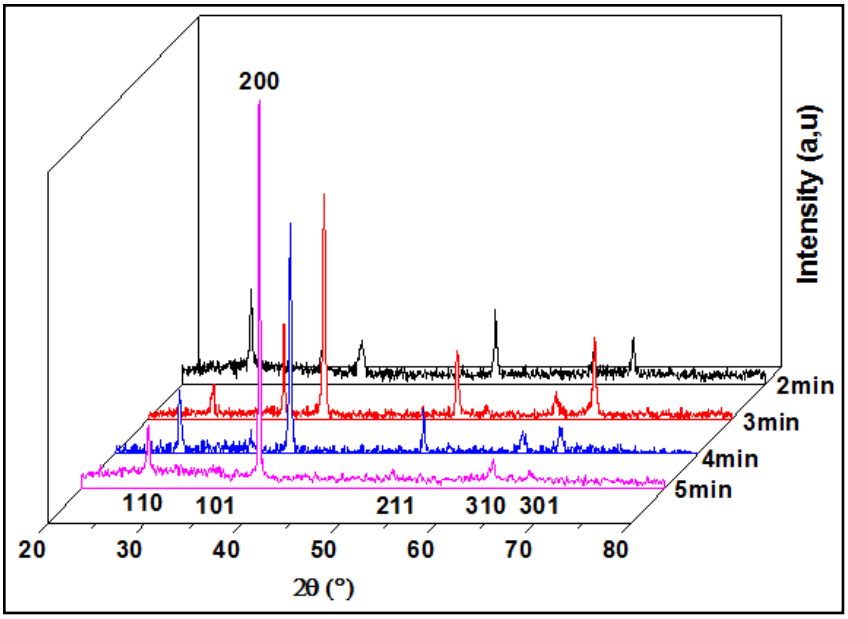

Fig. III.11. X-ray diffraction patterns of SnO_2 thin filmsas function of deposition time.

The crystalline quality of SnO_2 thin films was carried out by analyzing the X-ray diffraction which is shown in Fig. III.11.In the X-Ray Diffraction pattern (110), (101), (200), (211), (310) and (301) diffraction peaks are observed. It indicates that the films are polycrystalline and crystallize in a tetragonal structure (JCPDS card No. 041-1445). We found that the film deposited at 2 min grows along the (110) plane whereas the other films (3, 4 and 5 min) grow along the (200) plane. The (200) plane is dominant compared to other planes; this is consistent with the literature [12]. The intensity of the peak (200) increases with an increase in the deposition time (especially at 5 minutes), denote a rising of the amount of solute to form layers with an increase in the deposition time.

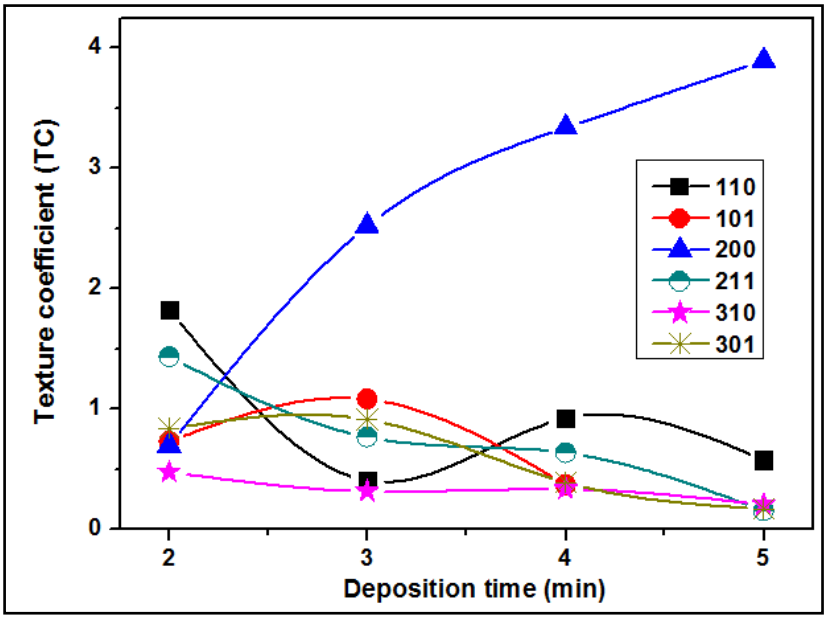

Fig. III.12. Variation of texture coefficient (TC)with deposition time.

Fig. III.12 shows the variation of the texture coefficient with the deposition time for each peak of SnO_2 thin films. In all samples, TC values of (110), (310) and (301) planes are smaller than unity whereas the TC (200) is larger than the unity. Generally, TC value of (200) peaks for all films is relatively higher than those of other planes, this value increases with the increasing of deposition time. This goes in harmony with the XRD analysis which confirms that the (200) plane has high texture growth.

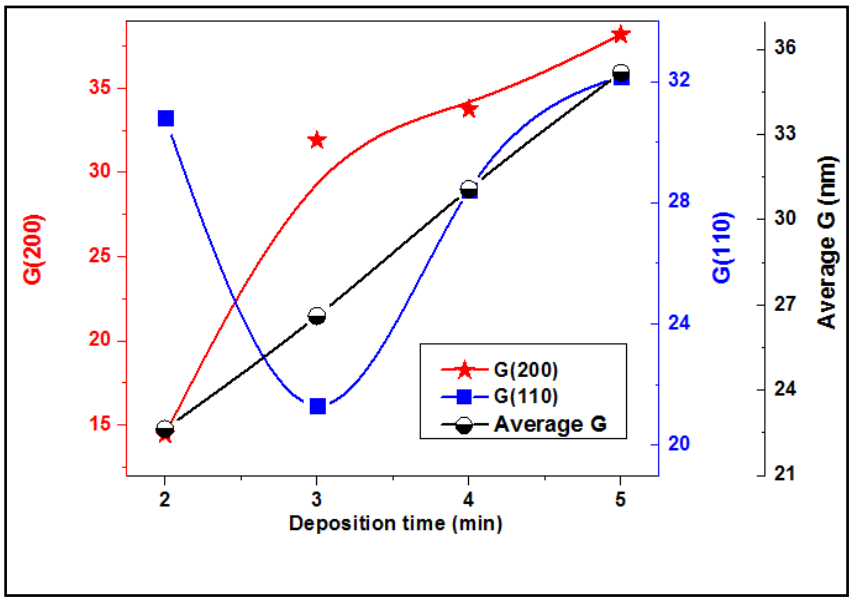

Fig. III.13. Average grain size of SnO_2thin film as a function of deposition time.

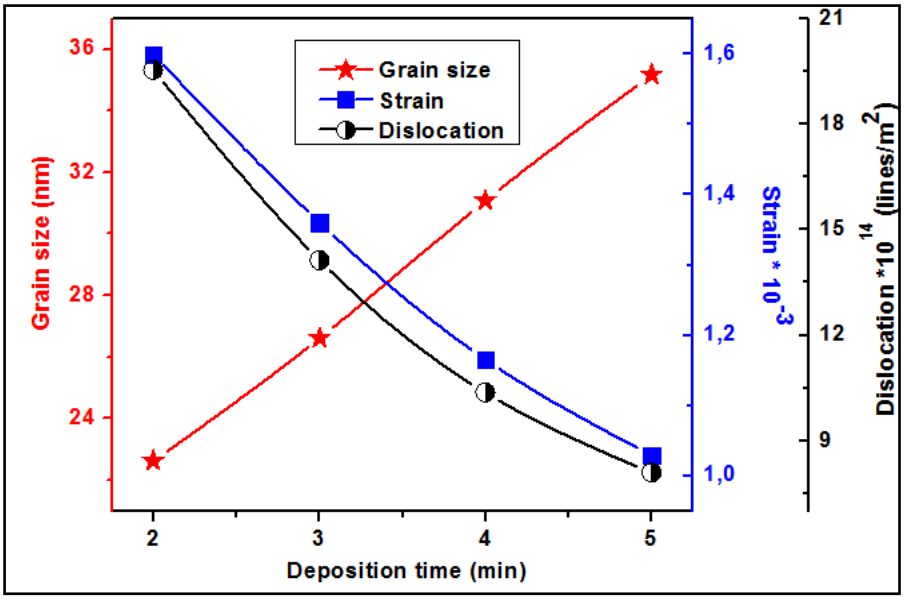

Fig. III.14. The variation of grain size, strain and dislocation density with deposition time.

The crystallite size (G) of the films was calculated from preferential orientation (200) and (110) peaks (Fig. III.13.).The variation of grain size, strain and dislocation density as function of the deposition time, are depicted in the same Fig. III.14. The G value increases as the deposition time and this indicates the improvement in crystallinity of the film. Also, Fig. III.12 presents crystallinity increment from 2min to 5min. This implies that the crystallinity becomes better in higher deposition time. The G values continuously increases from 14,436 nm to 38,174 nm as the deposition time increases too. As the deposition time increases, the quantity of solute arriving at the substrate increases to create layer, which increases the electrostatic interaction between solute particles and thereby raising the probability of more solute to be collected together to form a crystallite. Thus as the deposition time increases (thickness increases), grain size also increases. In the case where deposition time is not sufficient, the small crystallites on the substrate are unable to grow to become larger. So, the thinner films have smaller crystallites than the thicker ones. While the film grows thicker, the larger crystallites are formed via the gathering of more amount of solute [13].Therefore, the obtained results are in agreement with the literature data [14].Furthermore, the strain and dislocation density decrease with the increase of deposition time as shown in Fig. III.14. This reduction is attributed to the improvement of crystalline quality of the films with the increase of the deposition time.

III.2.3.Optical properties

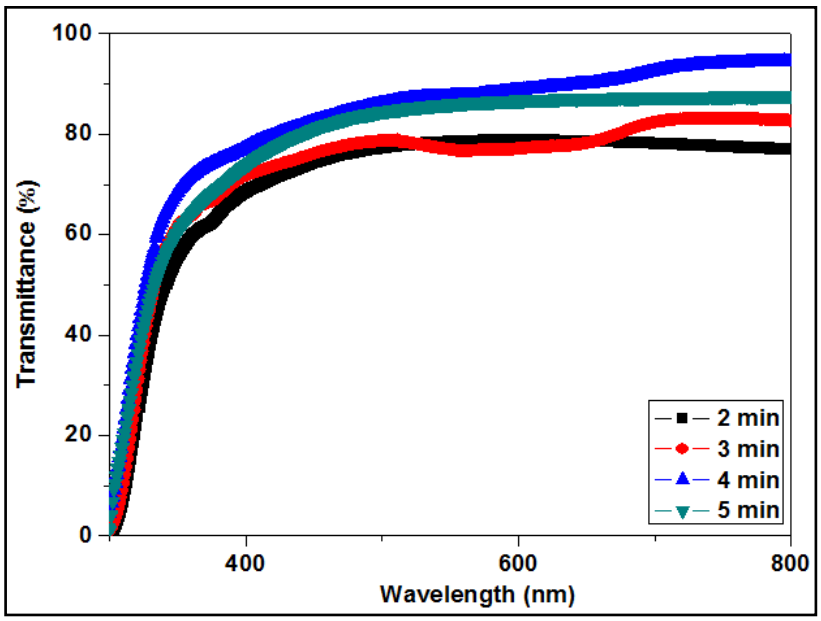

Fig. III.15. Optical transmittance spectra of SnO_2 thin films as a function of deposition time.

Fig. III.15 shows the optical transmittance of SnO_2 thin films with various time depositions in the wavelength range 300–800 nm. The variations in the thickness influence significantly the optical transmittance which means that the average transmittance of the film increases as the deposition time increases. The increase in transmittance may be attributed to the improvement of crystallinity, lowering of defect density and decreasing in scattering of light on the surface. Fig. III.15 exhibits that all films are fully transparent in the visible region, particularly the films prepared at 5 and 4 min, which show high optical transmittance. It was also seen that the absorption edge shifted towards a shorter wavelength, i.e., a blue shift, with the increasing of deposition time.

The band gap of the films can be concluded from a plot $(\alpha h\nu)^2$ vs photon energy ($h\nu$) and extrapolating the straight line portion of this plot to the energy axis (see Fig. III.16.).

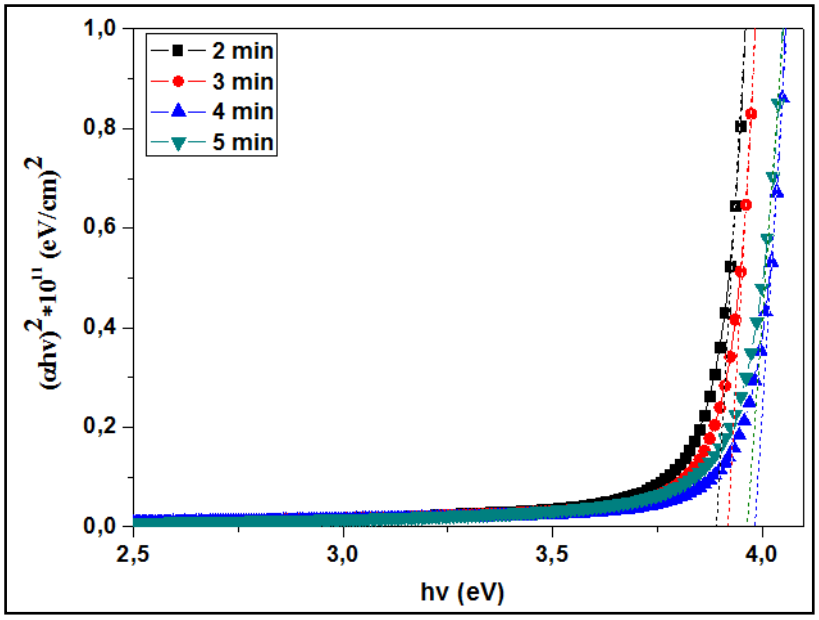

Fig. III.16. The plot $(\alpha hv)^2$ versus (hv) for the calculate the optical band gap energy Eg.

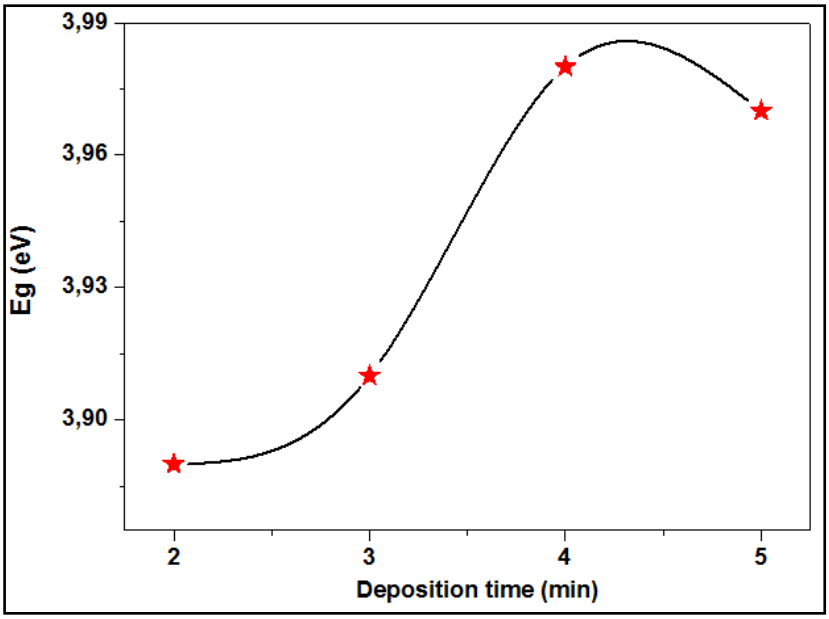

Fig. III.17. Variation of band gap with deposition times.

Fig. III.17 shows the variations of band gap as a function of deposition time. The band gap energy values are in the range of 3,889 -3,98eV. It can be observed that Eg increases as the deposition time increases. The broadening is attributed to the amelioration of crystalline quality of the films and the reduction of the dislocation. Therefore, there is an agreement with XRD analysis and the achieved results. On the other hand, the band gap widening might be due to the Burstein–Moss effect. It is well known that in a semiconductor the absorption edge shifts to shorter wavelength with increasing carrier concentration.

III.2.4.Electrical properties

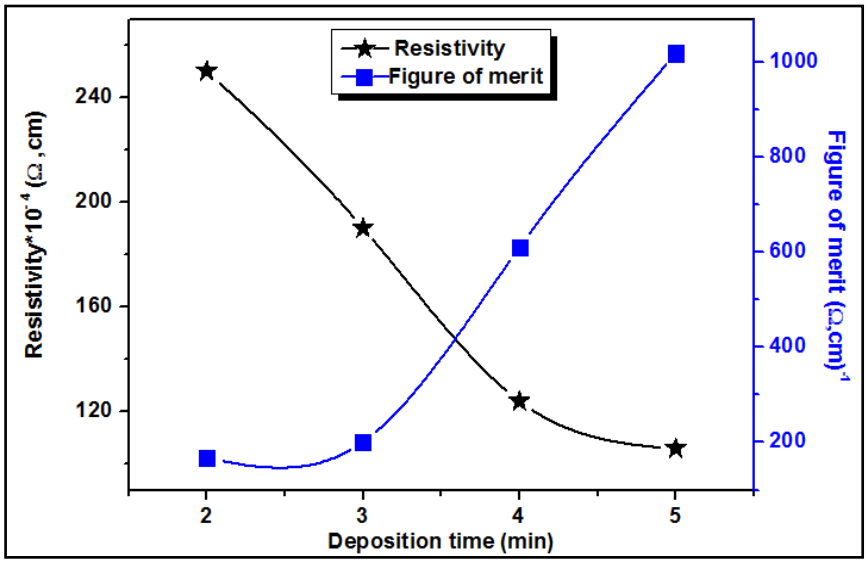

Fig. III.18. Variation of electrical resistivity and figure of merit with deposition time.

The electrical resistivity and figure of merit of the films that are formed at different deposition times are shown in Fig. III.18.It is observed that the resistivity decreases with the increasing the deposition time. The lowest resistivity which was obtained for the deposition time equals 5 min is attributed to the best crystallinity of the films prepared at this deposition time. This result is consistent with the result of the XRD characterization which denotes that the films grown at 5 min have a larger grain size than the other films. An increase in grain size of this film leads to reduction of grain boundary scattering, and then a decrease in electrical resistivity. On the other side, with the increasing of the films thickness, there is a possibility to create more impurity (Sn interstitial) which generates more free electrons. They observed that with the increasing of film thickness, the resistivity values of undoped and doped SnO_2 films are decreased too [15, 16]. Shihui Yu et al reported that the thicker film has less lattice defects, good crystalline structure and lower resistivity. When the film thickness decreases, the lattice defect increases, the crystalline structure deteriorates and the resistivity increases [17].

From Fig. III.18 it is clear that the figure of merit is inversely proportional to the electrical resistivity, whereas its variation and film thickness is proportionally. Thus, a thicker film will have a lower resistivity which in turn will have higher figure of merit. Therefore, for the sake of comparison between optical and electrical properties the figure of merit serves useful function [18]. It was found a maximum figure of merit for the film deposited at 5 min.

This is probably due to formation of good quality of the film in terms of conductivity and transmittance at this time.

III.3. Effect of substrate temperature

III.3.1.Thickness of the film

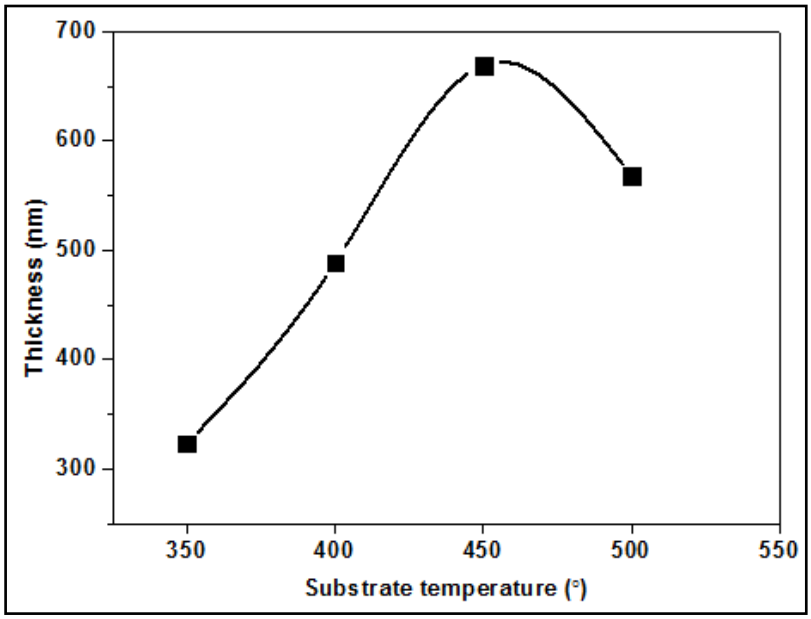

Fig. III.19. Variation of thickness versus substrate temperature.

The film thickness increases with increasing substrate temperature from 350°C to 450°C and then decreases at higher temperature (500°C) (Fig. III.19.).At 350°C, the substrate temperature is not enough to decompose drops of Sn^{+4} ions from the solution and then the thickness is low. At higher temperature (i.e., 500°C), the decline in film thickness may be attributed to a raised evaporation rate of the starting materials [19]. At a certain substrate temperature (i.e., 450°C), the decomposition happens at the optimum rate leading to final thickness (670 nm).

III.3.2. Structural properties

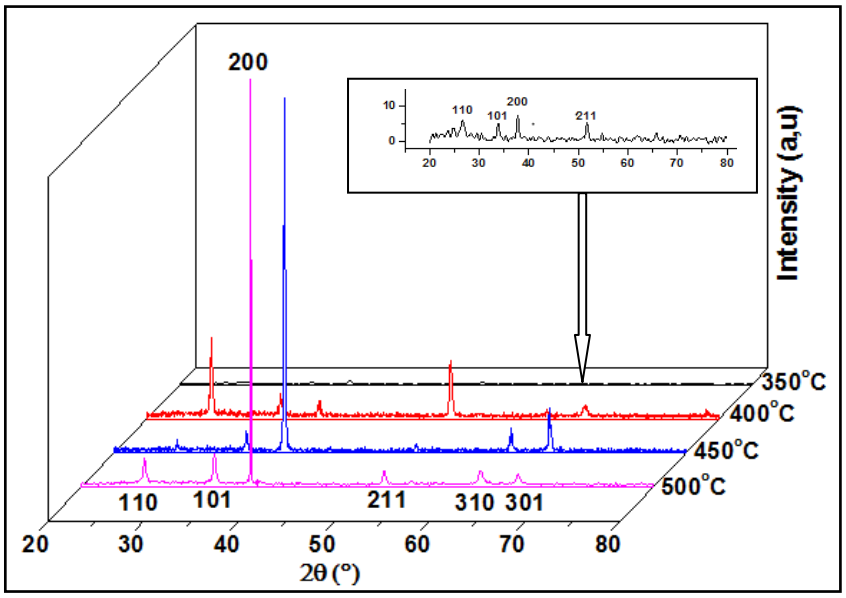

Fig. III.20.XDR patterns of SnO_2thin films with different substrate temperatures.

The XRD patterns of SnO_2 thin films are presented in Fig. III.20. The films deposited at 350°Cdisplay four peaks along (110), (101), (200) and (211) with very low intensity. Also, the substrate temperature is not sufficiently high for completing the chemical reaction of the solution and this will lead to remained initial components and unwished byproducts in the films [20]. The preferred orientation is along (110) plane for films deposited at 400ºC. Additional peaks along (101), (200), (211), (310) and (301) planes are also appeared. At 450°C, the preferred orientation has changed to (200), whereas (110) has decreased. It is clear that, by increasing the temperature, the crystallinity has enhanced and the intensity of the peak has increased. Chacko et al [21] have shown that at 375˚C the SnO_2 films produced by the pyrolysis spray method are amorphous and their crystallization starts at only 400°C and becomes good at 500° C. Also, they have found a similar tendency for (200) and (110) texture. It is observed that all the tin dioxide films are polycrystalline in nature and are of a cassiterite tetragonal (rutile) structure.

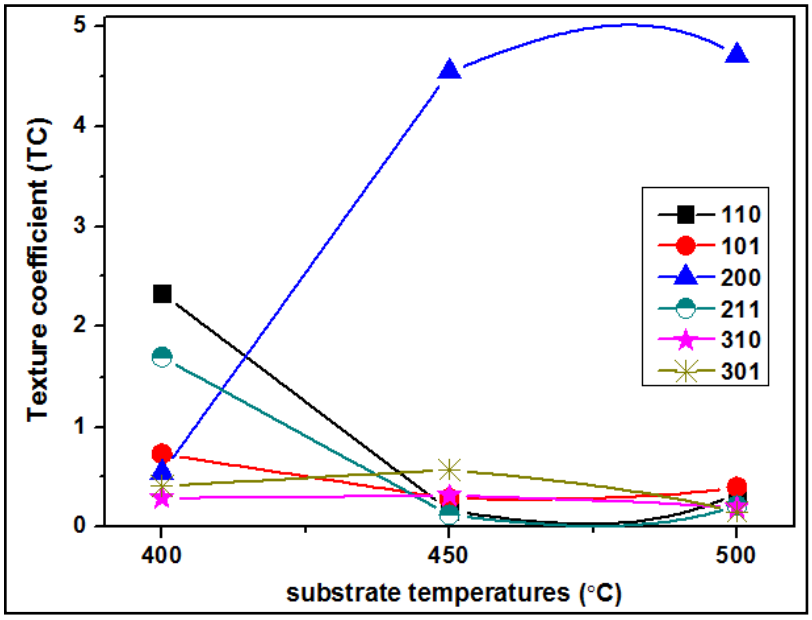

Fig. III.21. Variation of texture coefficient (TC)with substrate temperature.

The texture coefficients values of the samples for (110), (101), (200), (211), (310) and (301) planes are shown in Fig. III.21. TC value of (200) peak increases with the increasing of substrate temperature where TC (200) was larger than unity.

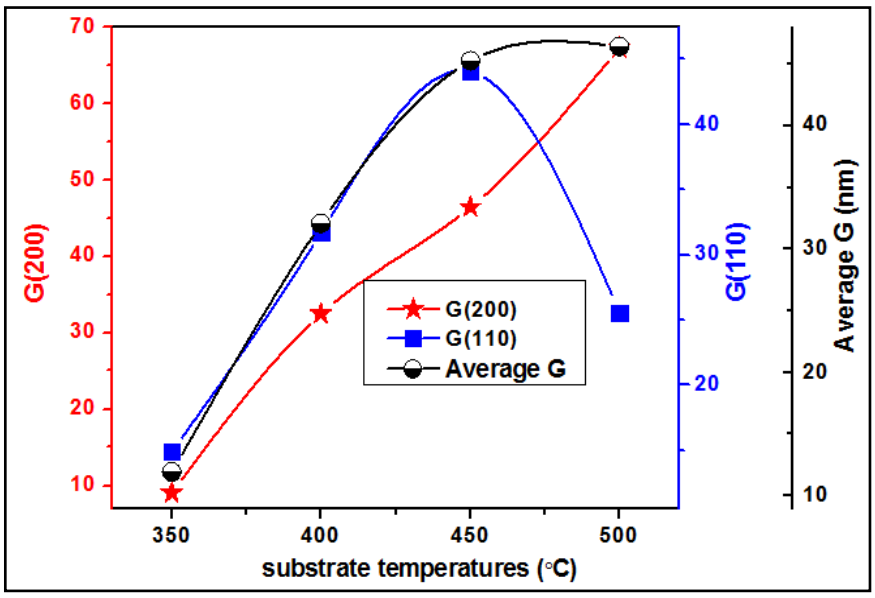

Fig. III.22. Average grain size of SnO_2thin film as a function of substrate temperature.

Fig.III.22 shows the variation of crystallite size as a function of substrate temperatures. When the substrate temperature goes up to 450 ˚C, the crystallites sizes for all planes will have the same tendency.

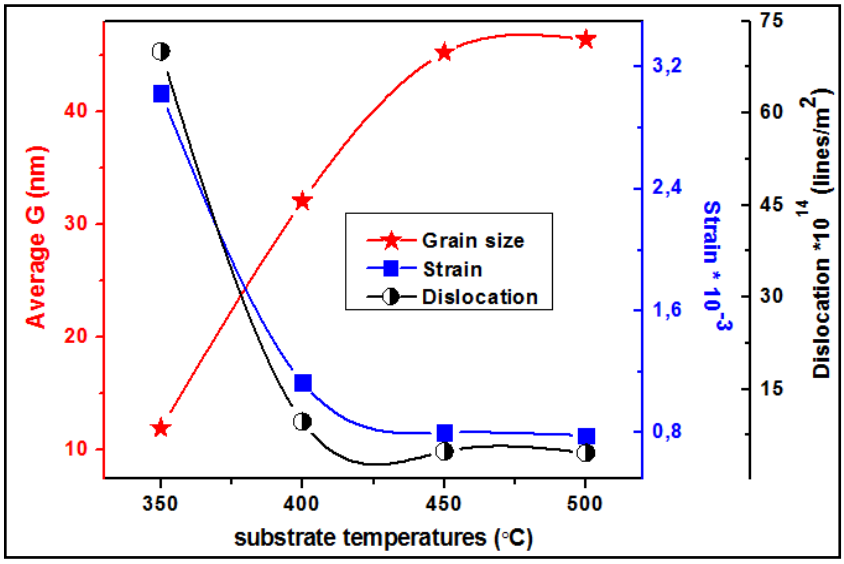

Fig. III.23. The variation of grain size, strain and dislocation density with substrate temperature.

Fig. III.23 shows the plot of crystallite size, strain and dislocation density as a function of substrate temperatures. As the substrate temperature increases up to 450˚C, the crystallite size 'G' varies linearly with the substrate temperature. However, above this value (450˚C) slowly increases. The crystallites sizes vary in the range of 9,038 to 67,23nm. Augmentation in crystallite size and crystallinity with substrate temperature is attributed to the optimum rate of supply of thermal energy for recrystallization with substrate temperature (this goes in accord with the XRD analysis) [22].On the other hand, it can be seen that strain and dislocation density decrease while grain size increases with an increase in the substrate temperature from 350 to 500˚C (Fig. III.23).

III.3.3.Optical properties

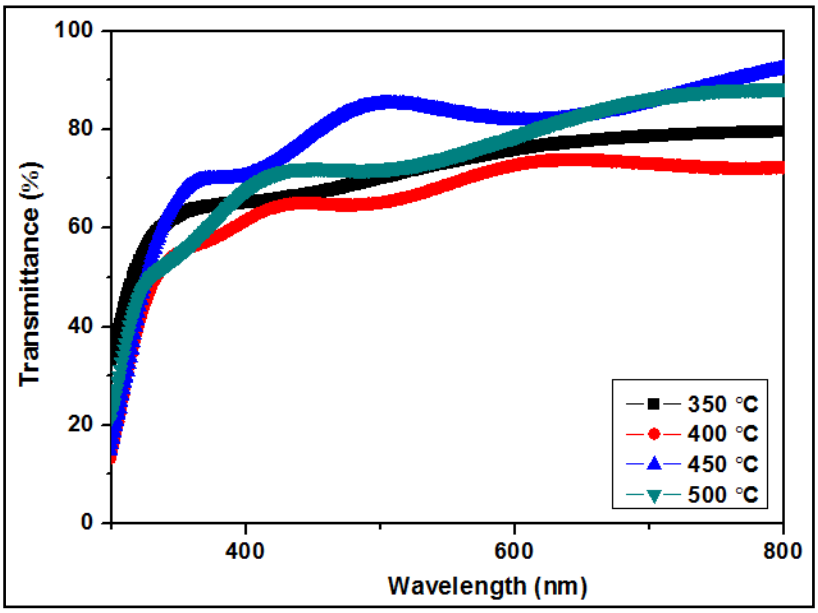

Fig. III.24. Optical transmittance spectra of SnO_2 thin films as a function of substrate temperature.

Fig. III.24 shows the variation of the transmittance measured as a function of the wavelength of SnO_2 thin films deposited at various substrate temperatures. The average transmission in the visible region vary in the range 63 to 93% depending upon the substrate temperature. With the increasing of substrate temperature, the optical transmission reaches a maximum value for a film at 450 °C. Although, the sample deposited at 500 °C has a high crystalline quality than the film prepared at 450 °C, the latter shows the high optical transmittance. This may be due to the oxygen deficiency in the film prepared at 500 °C [23].

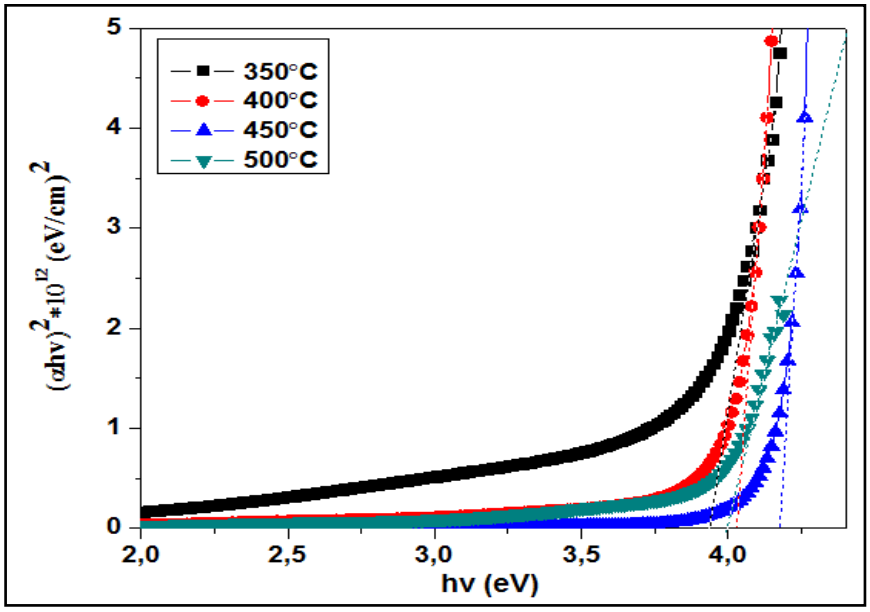

Fig. III.25. The plot of (αhv^2) vs (hv) for SnO_2 film

The values of the optical band gap are obtained by extrapolating the tangential line of the data to the abscissa axis in the plot of αhv^2 as a function of hv as shown in Fig. III.25.

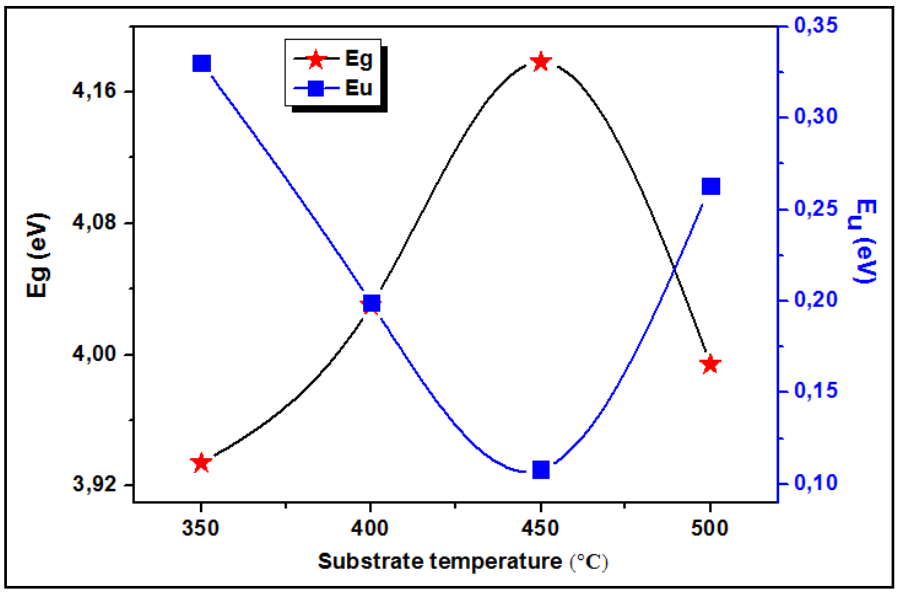

Fig. III.26. Variation of Urbach energy and band gap with substrate temperature.

The variation of band gap and Urbach energy as function of substrate temperature is shown in Fig. III.26.It is obvious that when the temperature is raised up to 450°C, the band gap energy is increased. This increment can be attributed to the improvement of crystallinity of these films. It can be seen that the band gap is inversely proportional to the Urbach energy (Eu). So, the diminution in the band gap might be attributed to the increase in the band tail width (Urbach tail).

It is observed that Urbach energy (Eu) decreases with the increasing of substrate temperature from 350°C to 450°C, then increases at higher temperature. It is known that Urbach tail energy depends on point, linear and surface defects. So the disordered materials produce localized states extended in the band gap, which lead to a reduction in the optical band gap energy [24]. However, the decrease in Urbach energy is attributed to the vanishing of localized states. Sample prepared at 500°C has a high band tail width despite the high crystalline quality of this film. This may be due to the non- stoichiometric of this film.

III.3.4.Electrical properties

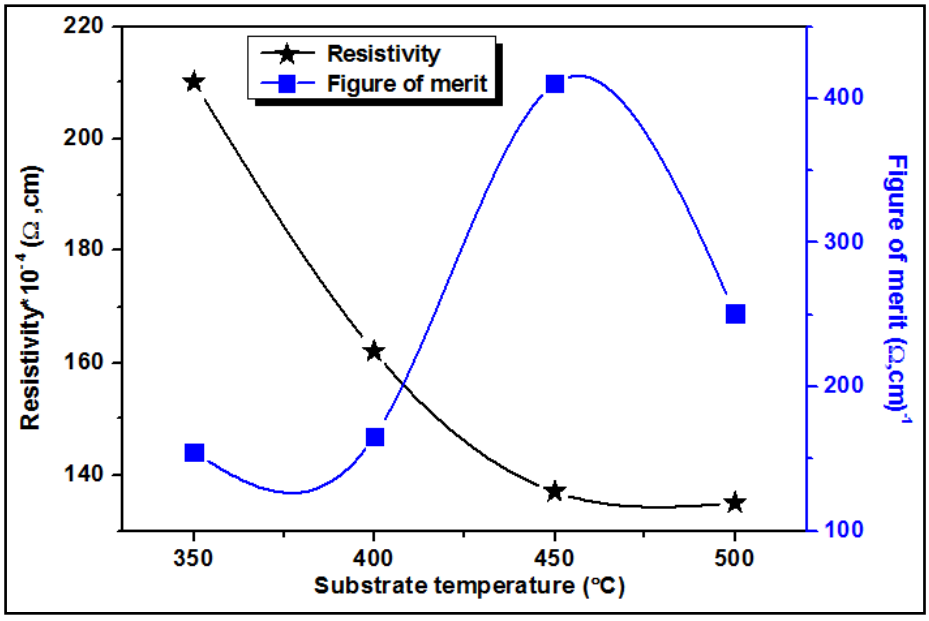

Fig. III.27. Variation of electrical resistivity and figure of merit with substrate temperature.

The variation of films resistivity and figure of merit with substrate temperature are depicted in Fig. III.27. It is clear that the electrical resistivity decreases with the increasing of temperature. The lowest resistivity obtained for the temperature equals 500°C is attributed to a higher crystallite size and formation of oxygen vacancies. The highest figure of merit is found for the sample deposited at 450°C

Conclusion:

The effect of different experimental parameters such as molarity, deposition time and substrate temperature on structural, optical and electrical characteristics of SnO_2 films was studied. The aim of this study is to determine the optimal deposition conditions. It was located that a maximum value of figure of merit for the films deposited at 450°C and 0.1 mol/l concentration whereas the optimum deposition time was found to be 5 min. These conditions are fixed for the rest work.

References

[1] D.R. Deepu, C.S. Kartha, K.P. Vijayakumar, AIP Proc, 58 (2014) 58–59.

[2] K. Muhamed Sajeer and N. Muhammed Rafi, International Journal of Innovative Researchin Science, Engineering and Technology , 4 (5) (2015).

[3] N. Memarian and S.M. Rozati, Can. J. Phys. 90 (2012) 277–281.

[4] C. Agashe, M.G. Takwle, V.G. Bhide, S. Mahamuni, S.K. Kulkarni, J. Appl. Phys. 70 (1991) 7382–7386.

[5] V. Consonni, G.Rey, H.Roussel, D.Bellet, Journal of Applied Physics, 111 (2012) 033523.

[6] N. F. Habubi, Z. M. Abood, A. N. Algamel, International Letters of Chemistry Physics and Astronomy, 65 (2016) 80-90.

[7] S. Belhamri, N. E Hamdadou, Journal of Physics: Conference Series, 758(2016) 012007.

[8] A.K.S. Aqili, N.A. Shah, A. Ali, A. Maqsood, Sci. Int. (Lahre), 18(1) (2006) 1-3.

[9] F. Moharrami, M. M. Bagheri-Mohagheghi, and H. Azimi-Juybari, Thin Solid Films, 520 (21) (2012) 6503–6509.

[10] E. Burstein, Phys. Rev.93, 632 (1954).

[11] T.S. Moss, Proc. Phys. Soc. Lond. B67, 775 (1954).

[12] Ki Hyun Yoon, Dong Jin Nam, Journal of Materials Science, 30 (13) (1995) 3415–3420.

[13] T P Rao, M C S Kumar, Appl Surf Sci, 255 (8) (2009)4579-4584.

[14] A. Bouhdjer., A. Attaf, H. Saidi, H. Bendjedidi, Y. Benkhetta, I. Bouhaf, J. Semicond. 36 (8) (2015), 082002.

[15] H. Kaneko, K. Miyame, J.Appl. Phys, 53 (1982) 3629-3634.

[16] H. De Wall, F. Simonis, Thin Solid Films, 77 (1981) 253-258.

[17] Yu Shihui, Linghong Ding, Chuang Xue, Li Chen, W.F. Zhang, J. Non-Cryst. Solids, 358 (2012) 3137-3140.

[18] S.A. Knickerbocker, A.K. Kulkarni, J. Vac. Sci. Technol, A 13 (3) (1995) 1048.

[19] K.Y. Rajpure, M.N. Kusumade, M. Neumann-Spallart, C.H. Bhosale, Mater.Chem. Phys, 64 (2000) 184.

[20] A.A. Yadav, E.U. Masumdar, A.V. Moholkar, M. Neumann-Spallart, K.Y. Rajpure, C.H. Bhosale, Journal of Alloys and Compounds, 488 (2009) 350–355.

[21] S. Chacko, N. Sajeeth-Philip et V. K. Vaidyan,Phys. Stat. Sol, (a) 204 (10) (2007) 3305–3315.

[22] V.M. Nikale, N.S. Gaikwad, K.Y. Rajpure, C.H. Bhosale, J. Mater. Chem. Phys, 78 (2003) 363.

[23] Kazuhiro Kato, Hideo Omoto, Takao Tomioka, Thin Solid Films 520 (2011)110–116

[24] J.I. Shadia, N.A. Riyad, Phys. Scr, 84 (2011) 055801–055807.

CHAPTER IV

Effect of Indium Doping on the Properties of Tin Dioxide (SnO_2) Thin Films

In this chapter, we study the influence of indium doping on the crystalline structure, optical and electrical properties of sprayed SnO_2:In thin films.

IV.1. Influence of Indium doping on properties of SnO2 thin films: Study of low concentrations (≤ 8 wt%)

The precursor used was $SnCl_4.5H_2O$ (0.1 mol/l), and the doping source was indium chloride ($InCl_3$), the concentration of Indium was varied from 0 to 8 wt%. The precursor solution was sprayed into hot substrates (T_S = 450 °C) for 5 min as a growth time.

IV.1.1.Thickness of the film

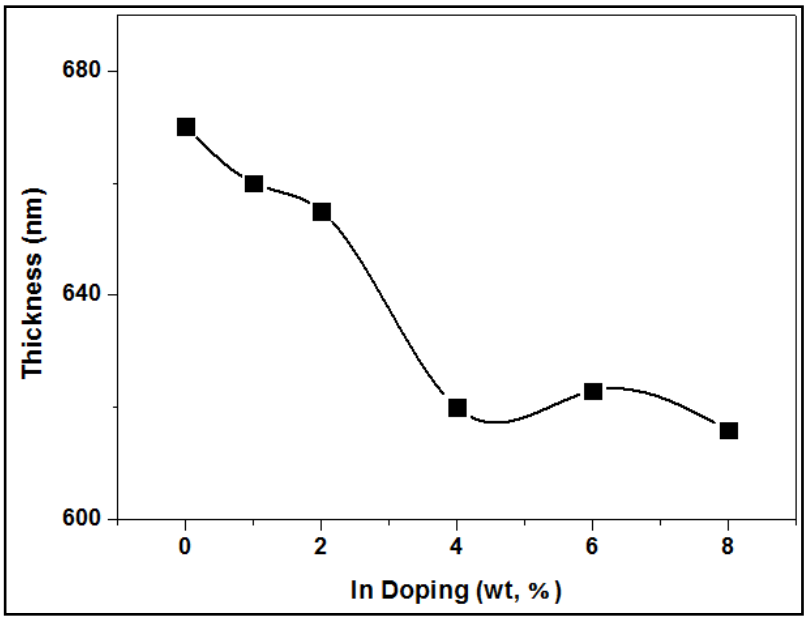

Fig. IV.1. Variation of In doped SnO_2 thin films thickness.

A small decrease of film thickness was observed with increasing the doping concentration (0–2 wt%) and then it was decreased rapidly with an increase in In content (4 wt%). But, when the doping concentration increased to 8 wt%, the thickness remained almost constant (see figure. IV.1). From Fig. IV.2, when indium content is (0–2 wt%), the (200) peak intensity decreases as well as the films thickness. While the doping rate was increasing (4- 8 wt%), the orientation of the films changed from (200) reflection peak to (301) peak. So, the decrement in the films thickness probably attributed to the reorientation effect. All these indicate that the changes in the thickness are due to the structural changes which are caused by the doping [1].

IV.1.2. Structural and morphological properties

The crystalline quality of In doped SnO_2 thin films was carried out by analyzing the X-ray diffraction as it is shown in Fig. IV.2.

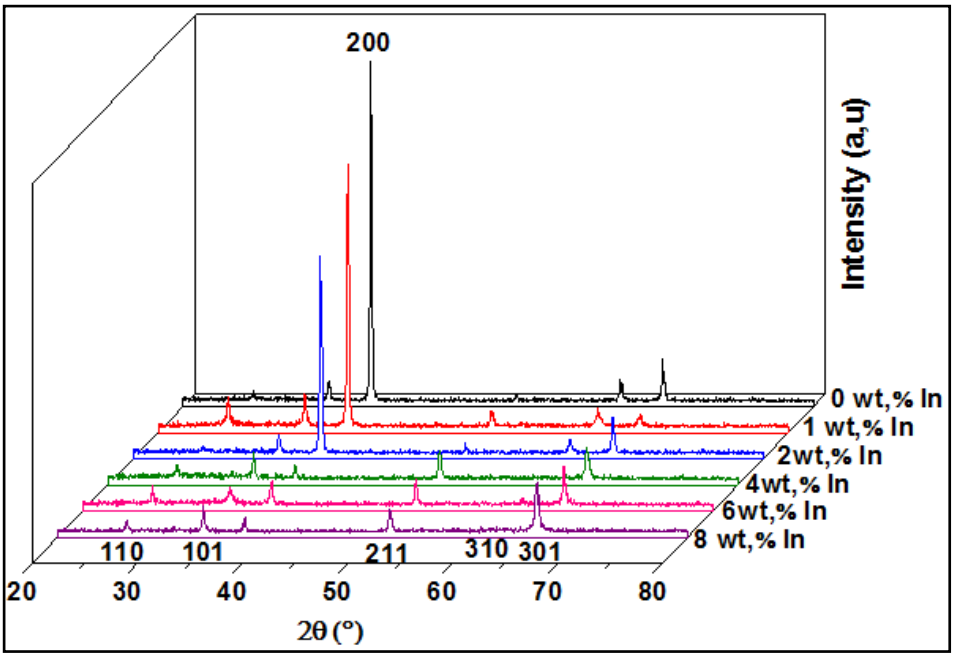

Fig. IV.2. X-ray diffraction spectra of the undoped and In-doped SnO_2 thin films

Overall, several growth directions are observed: (110), (101), (200), (211), (310), (301). These peaks indicate that films are characterized by cassiterite tetragonal crystalline phase (JCPDS card No. 041-1445). It is clear from the XRD spectra there is no secondary phases, this affirms the presence of only single phase of SnO_2 in films. As seen in Fig. IV.2, undoped SnO_2 film prefers orientation along (200) and has a good crystalline structure. The highest increases in In doping lead to the emergence of a new preferred orientation which is (301). We observed that with increasing indium content, the intensity of (200) peak decreased and a significant deterioration was observed in the crystallinity of the films, which possibly due to the stress by the difference in ion size between indium and tin or segregation of dopant in grain boundaries. They [2-4] found that SnO_2: F and SnO_2: In films prepared either by the spray or CVD, it have the dominant plane (200) and also the presence of (301) plane. This agrees with our results for SnO2: In by ultrasonic spray pyrolysis.

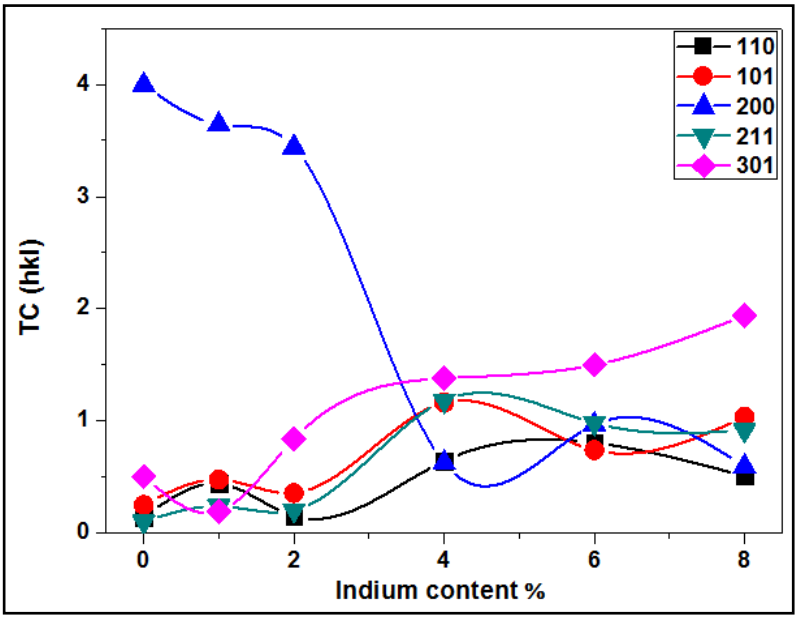

Fig. IV.3. Variation of texture coefficient (TC) with indium content.

Fig. IV.3. shows the variation of the texture coefficient with indium content for each peak of SnO_2 thin films. At lower doping concentration, the texture coefficient of (200) reflection is greater than 1 which indicates that the preferential orientation is (200). At higher doping concentration, the preferential orientation is changed to (301). However, the texture coefficient value of (200) peak is higher than the (301) peak. The variation in TC indicated the change of growth orientation. This possibly attributed to the existence of stress produced by the doping of In.

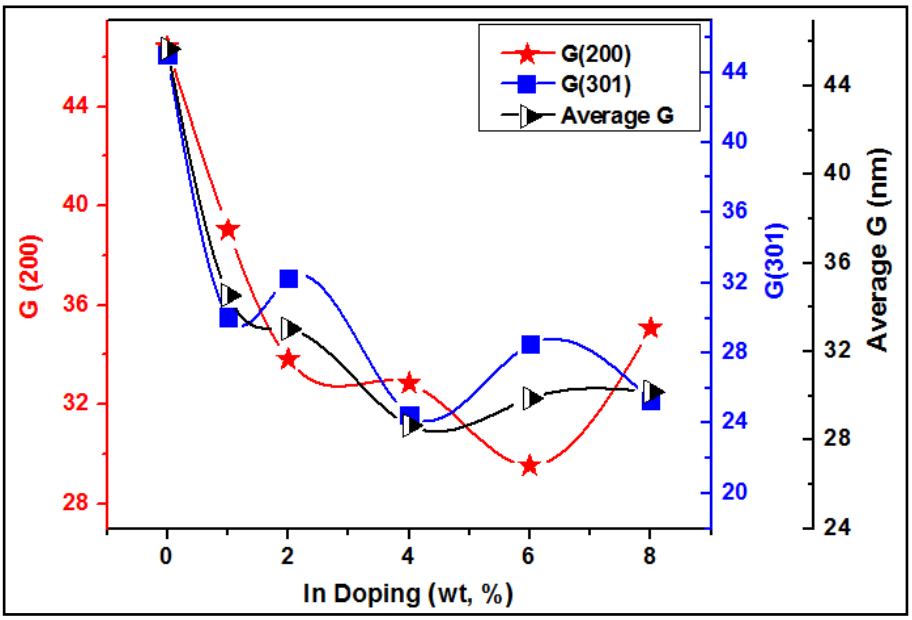

Fig. IV.4. The variation of crystallite size G of the undoped and In doped SnO_2 thin films.

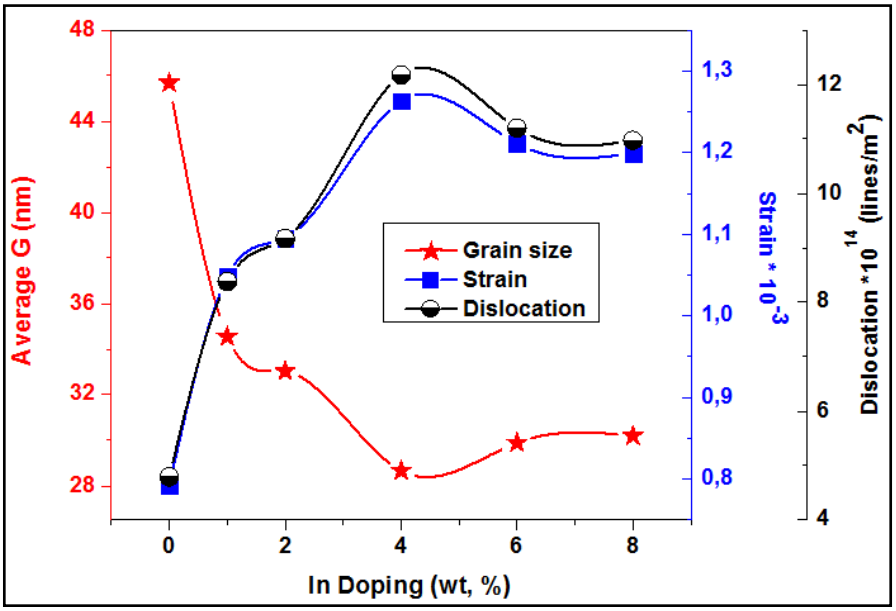

Fig. IV. 5. The variation of average grain size, strain and dislocation density of the undoped and In doped SnO_2 thin films.

The average crystallite size (G) of the films was calculated from preferential orientation (200) and (301) peaks (Fig. IV.4.). The variation average of grain size, strain and dislocation density of the undoped and Indium doped SnO_2 thin films as a function of Indium concentration which is shown in Fig. IV.5.The crystallite size decreased while In content increased. The decrease in the grain size is caused by nucleation centers enhancement when indium ratio increases. It can be seen that the strain and dislocation have an opposite trends to the variation of crystallite size. The change in the crystallite size is mainly related to strain of the crystal, because the existence of internal strain in the film network cause a minimization in the grain growth driving forces [5-6].

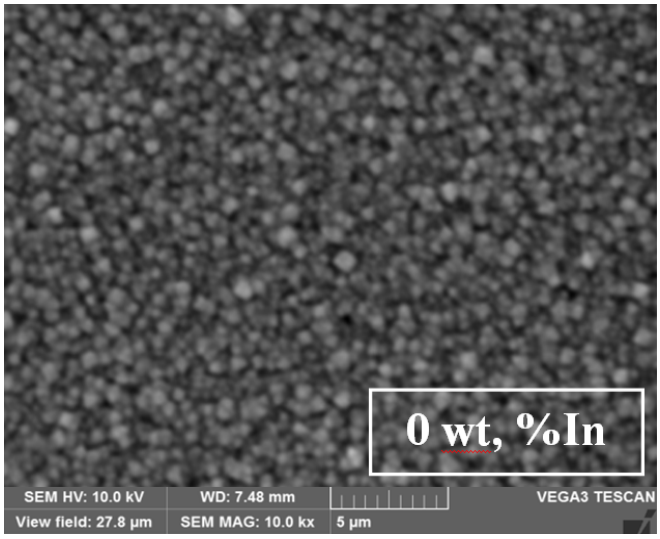

(a)

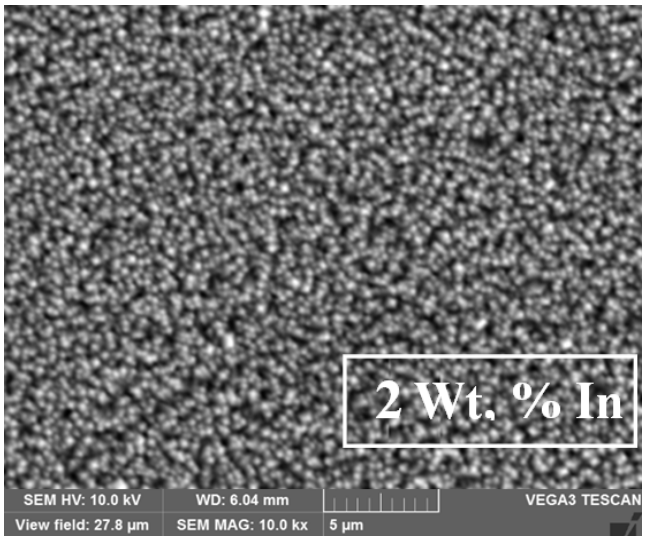

(b)

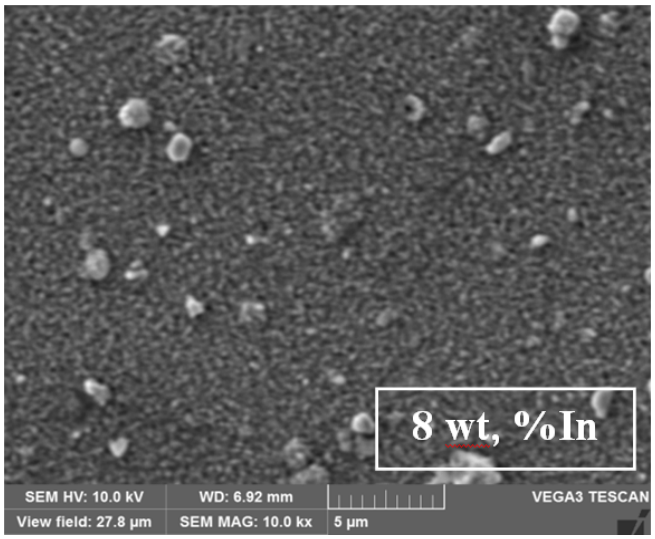

(c)

Fig. IV. 6.SEM micrographs of SnO_2 films obtained for different indium doping levels (a) 0, (b) 2 and (c) 8 Wt. % In

Scanning electron micrographs of SnO_2 films containing 0, 2 and 8 Wt.% of indium are shown in Fig. IV. 6. It is clearly shown that the films consist of uniform distribution of spherical grains (distinct grain boundaries). As seen in Figs. IV. 6.(a-c) that the grain size decreases as the incorporation of indium increases which is consistent with the XRD results. The undoped film has bigger grains than the doped ones. Thus, it can be said that indium doping has a remarkable effect on the morphological properties of our films. It is clear from Fig. IV. 6.(c) that the surface are rough with agglomeration of grains on the smooth local.

IV.1.3. Optical properties

The Optical properties of the undoped and Indium doped SnO_2 thin films deposited at different Indium concentrations were performed by measuring the transmittance in the wavelength region 300 to 800 nm. Fig. IV.7. shows the optical transmission spectrum of undoped and Indium doped SnO_2 thin films.

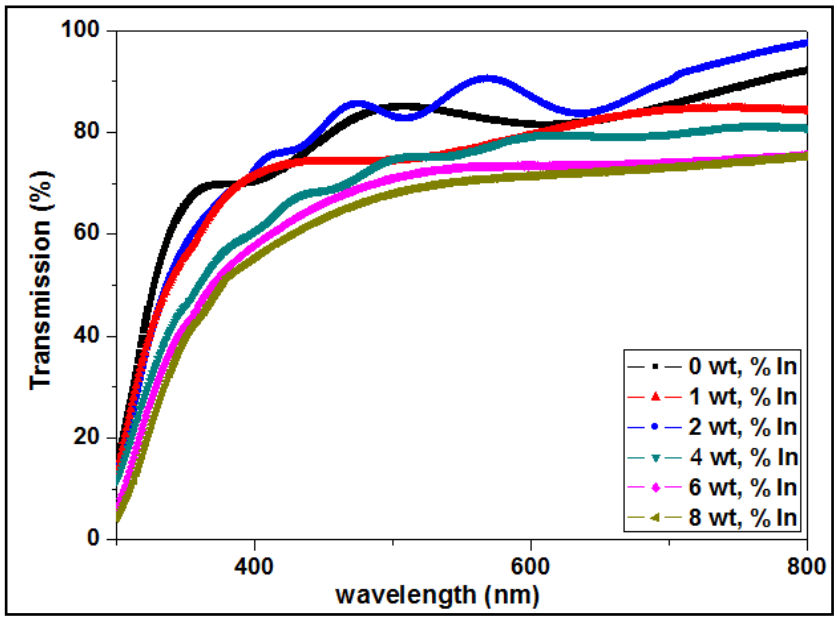

Fig. IV.7. Optical transmission spectra of the undoped and In doped SnO2 thin layer prepared at different indium concentrations.

The transmission augments up to 2 Wt.% doped film, then decreases. This reduction can be attributed to the presence of dopant atoms through grain boundaries and which causes decrease of the crystallinity growth. Undoped and doped films with 2 % display interference fringes which mean that the resulting films are homogeneous with smooth surface (see Fig. IV.6) [7]. The highest transmission in the longer wavelengths (>400 nm) is approximately 97% for 2% In. It was also observed that the undoped film exhibits high optical transmittance. This is attributed to the smooth surface of these films (see SEM images), which generate the least light scattering. At high doping level (for 8 wt.%), the decrease of transmittance may be attributed to the roughness in the surface and defects produced by doping which causes scattering of photons [8]

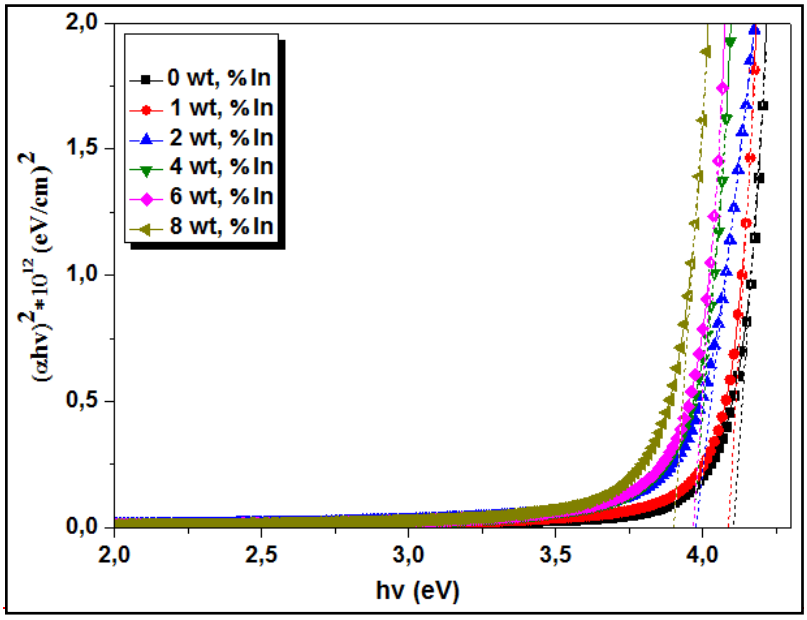

Fig. IV. 8. The plot of $(\alpha h\upsilon)^2$ vs. $(h\upsilon)$ for SnO_2:In film

The values of the optical band gap are obtained by extrapolating the tangential line of the data to the abscissa axis in the plot of αhv^2 as a function of hv as shown in Fig. IV.8.

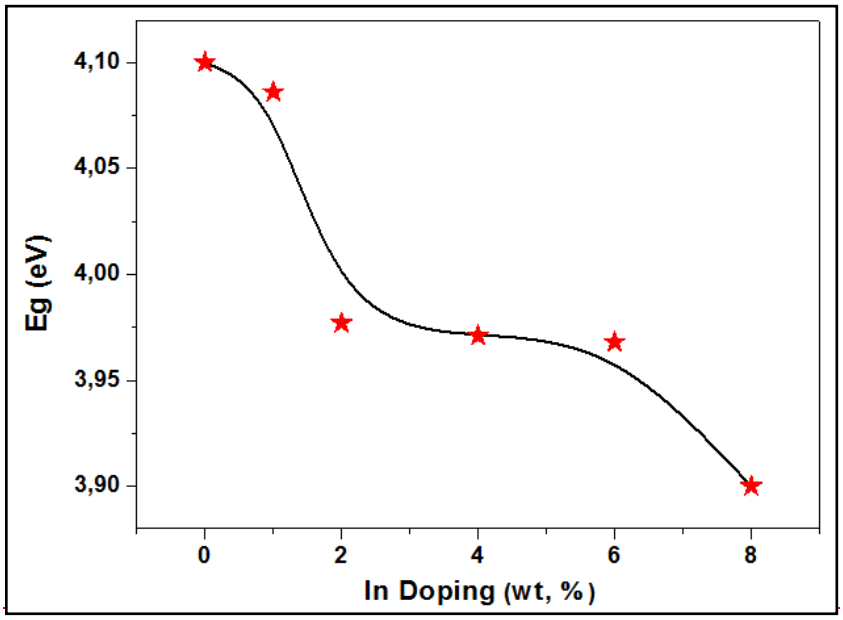

Fig. IV.9. The variation of optical band gap of the undoped and In doped SnO_2thin films with indium doping.

Fig. IV.9. shows the variation of the optical gap depending on the concentration of indium doped SnO_2 thin films. It can be observed that the band gap decreases with the increasing of Indium content. This lowering of the band gap is possibly due to the presence of Indium impurities in the SnO_2 structure, which induces the deterioration in crystallinity.

IV.1.4. Electrical properties

Fig. IV.10. shows the variation of resistivity of indium doped SnO_2 thin films as a function of indium doping. The resistivity of these films increases with the increase of In content. It is clear that the 2 Wt% In doped SnO_2 has a minimum resistivity, in comparison with the other doping values. In our work, undoped and doped films reveal n-type conductivity. Substitution of Sn^{4+} by In^{3+} ions maybe lead to the increase in the number of holes or deficiency of electrons, which in turn increases the resistivity. On the other hand, the increase in resistivity of SnO_2:In films can be due to the low doping of indium in the lattice, which are insufficient to change the films from n to p type. On the other hand, the increase of grains boundaries are attributed to the development of small size grains as result of In incorporation. The boundaries act as charge carriers traps causing then an increase in films resistivity [9].

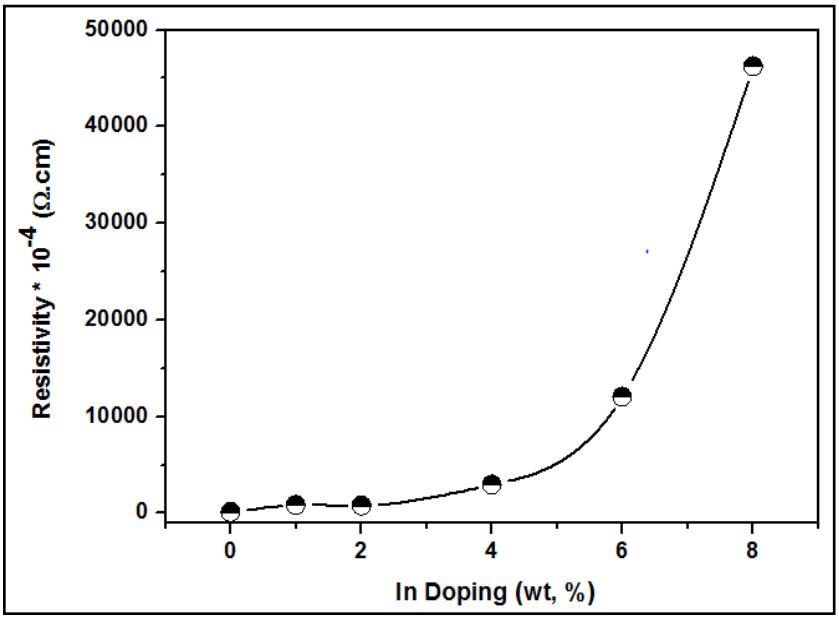

Fig. IV.10. The variation of the resistivity with deposition In content of SnO_2 films

IV.2. Effect of Indium doping on properties of SnO_2 thin films: Study of high concentrations (10, 20 wt%)

The precursor used was $SnCl_4.5H_2O$ (0.1 mol/l), and the doping source was indium chloride ($InCl_3$), the concentration of indium was varied from 0 to 20 wt% in steps of 5 wt%. The precursor solution was sprayed into hot substrates (T_S = 450 °C) for 5 min as a growth time. The films were annealed in air at 600°C for 1h.

IV.2.1. Structural properties

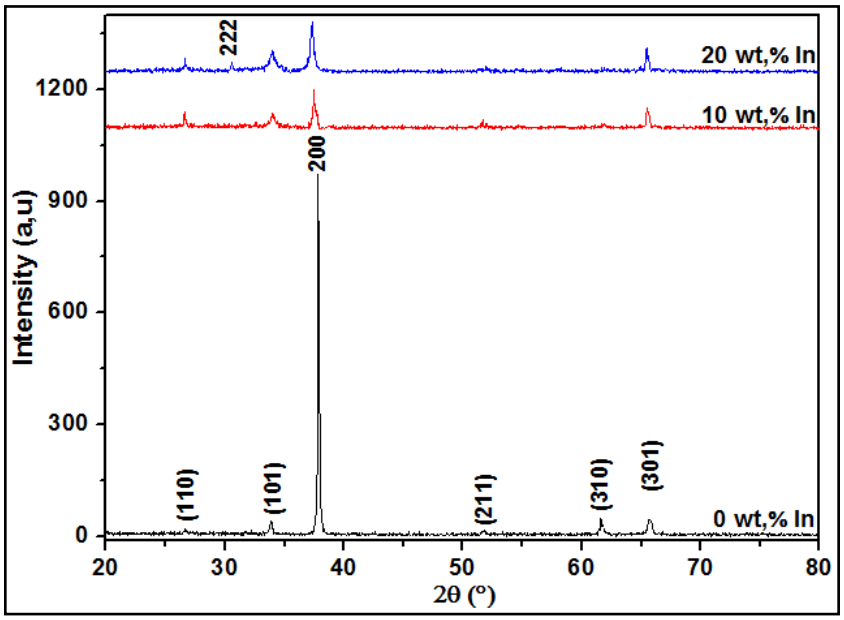

Fig. IV.11.X-ray diffraction spectra of the undoped and In-doped SnO2 films for different indium concentrations.

XRD spectra of undoped and indium doped SnO_2 films for various doping concentrations of indium are shown in Fig. IV.11.All films are polycrystalline in nature with a preferred orientation along the (200) plane. The samples show other peaks (110), (101), (211) and (301), these peaks correspond to SnO_2 phase. i.e. that films are characterized by cassiterite tetragonal crystalline phase (JCPDS card No. 041-1445).

It is observed that the decrease of (200) peak intensity, accompanied by its widening, and could be attributed to deteriorate the crystallinity due to decreasing crystallites size and increasing number of defects. For doped film with 20 Wt.% shows other peak that has low intense correspond to (222) plane of indium oxide (JCPDS card No. 06-0416). Metallic tin and high intensity indium peaks are not observed in the prepared samples.

By increasing the doping ratio, the diffraction peak positions shifts to lower angles (Fig. IV.12). This attributed to substitution of In^{3+} ions with ionic radius = 0.84 Å to Sn^{4+} ions with ionic radius = 0.71 Å which in turn will lead to the increase of the lattice constants.

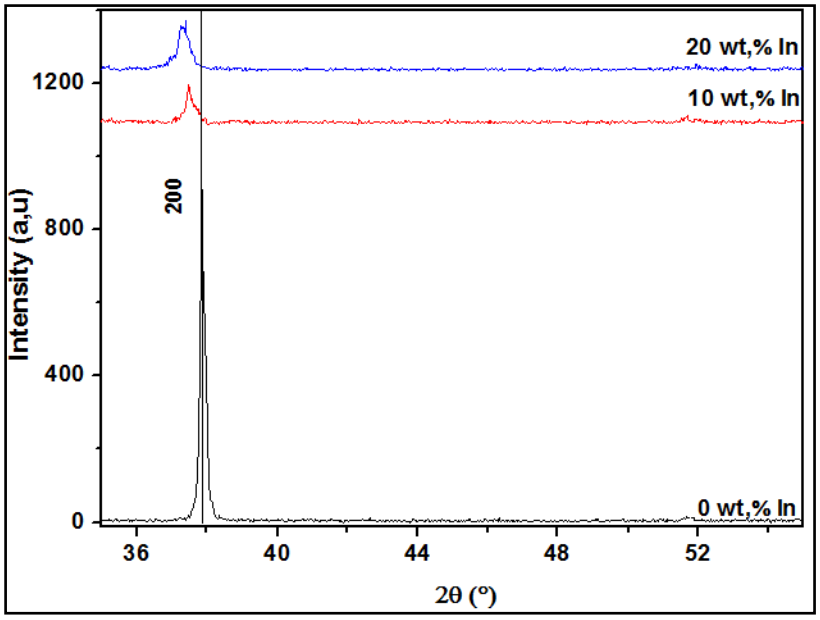

Fig. IV.12. Enlarged pictures for X-ray diffractograms of SnO2:In films with different indium content.

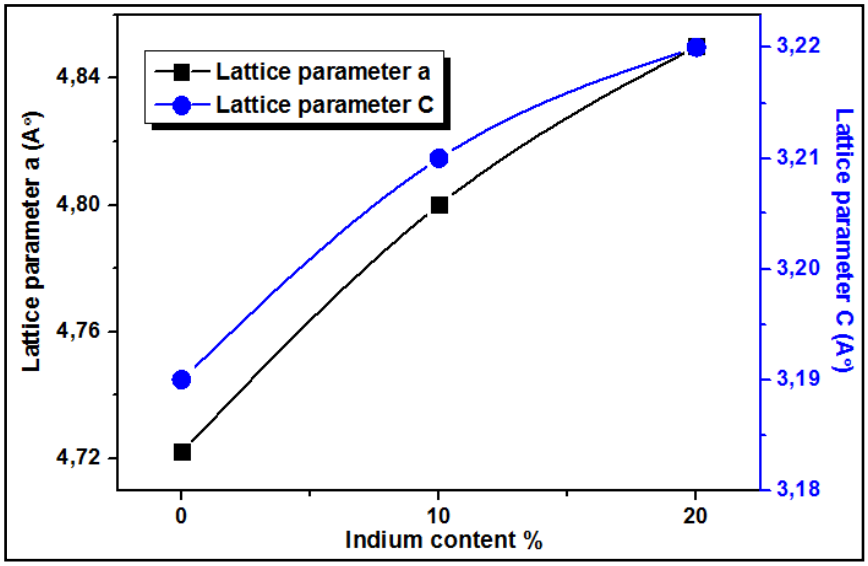

Fig. IV.13. The variation of lattice parameters with amount of doping SnO2:In thin films.

The calculated lattice parameters of undoped and doped SnO_2 thin films are higher than the standard lattice parameters of SnO_2 (according to JCPDS data: a = b = 4.737 Å and c = 3.185 Å). Furthermore, the lattices parameters ‘a’ and ‘c’ are increasing with increasing doping which make the strain of the films increase. This variation in the values of lattice parameters may be related to the substitution of Sn^{4+} ions by In^{3+} ions that have less ion radius (Fig.IV.13.).

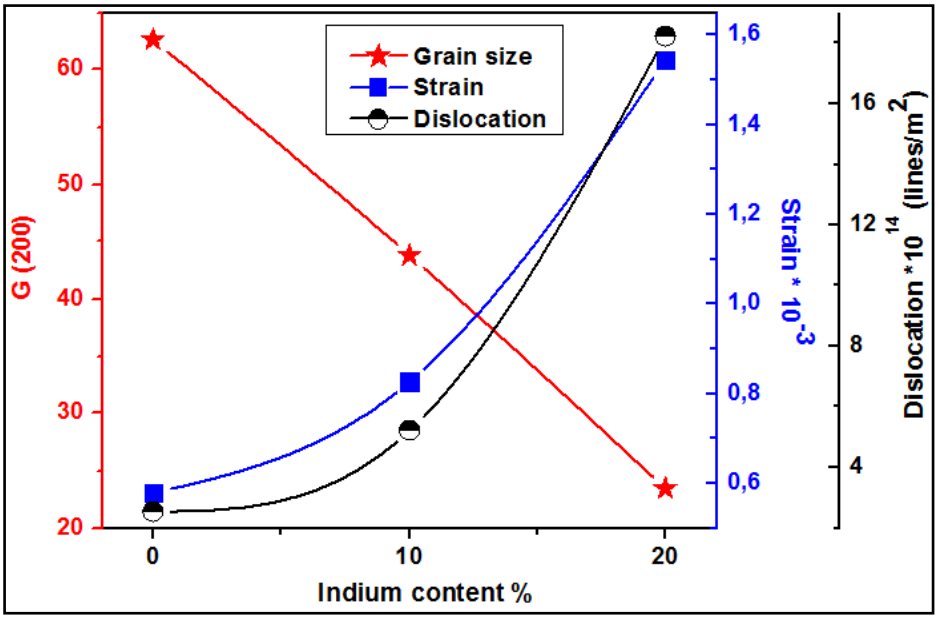

Fig. IV.14. The variation of average grain size, strain and dislocation density of the undoped and In doped SnO_2 thin films.

Fig. IV.14. shows the variation of the crystallite size, strain and dislocation density of SnO_2 and SnO_2:In films. The crystallite size is decreasing with increasing of In concentration.

Furthermore, this confirms the deterioration in the crystallinity of the films. On the other hand, an increase in the doping concentration produces the increase in the strain and dislocation, because of the increase in disorders and crystal defects in network.

Several authors report that whatever the element of the doping: Gallium [10], Indium [11-12], fluorine [13] ... etc., the dimensions of the particles are influenced by the addition of doping atoms.

IV.2.2. Optical properties

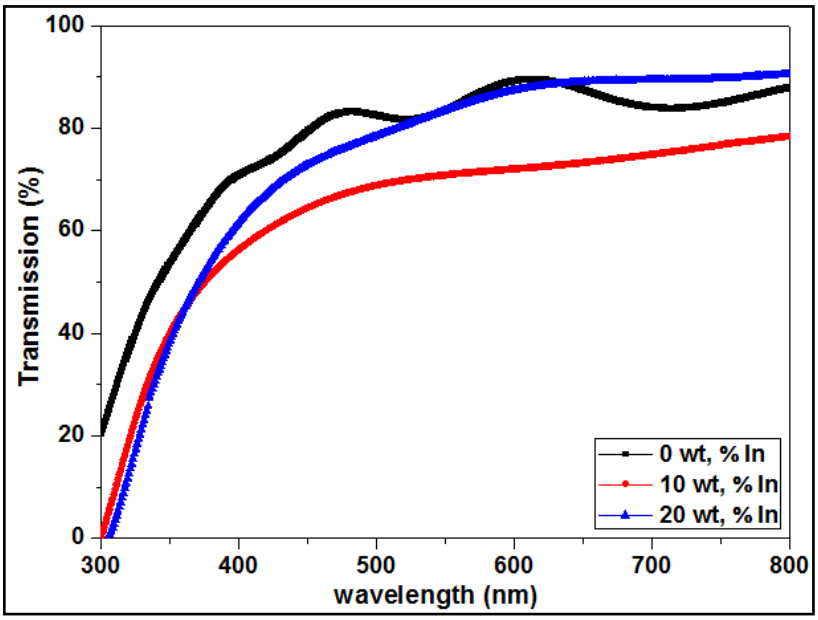

Fig. IV.15. Optical transmission spectra of the undoped and In doped SnO_2 films with different indium concentrations.

Fig. IV.15. shows the optical transmission spectra as a function of wavelength of SnO_2 and SnO_2:In thin films. It is clearly noticed that films are completely transparent in the visible region. We observe that the transmittances values are decreasing while indium concentration is increasing, then they increase. They [12] found that the transmission of SnO_2:In films which was obtained by spray pyrolysis increased with the increasing of indium concentration. The absorption edge shifts to the higher wavelength with an increase of indium content, as shown in Fig. IV.15. This indicate a narrowing of the optical band gap of SnO_2:In films.

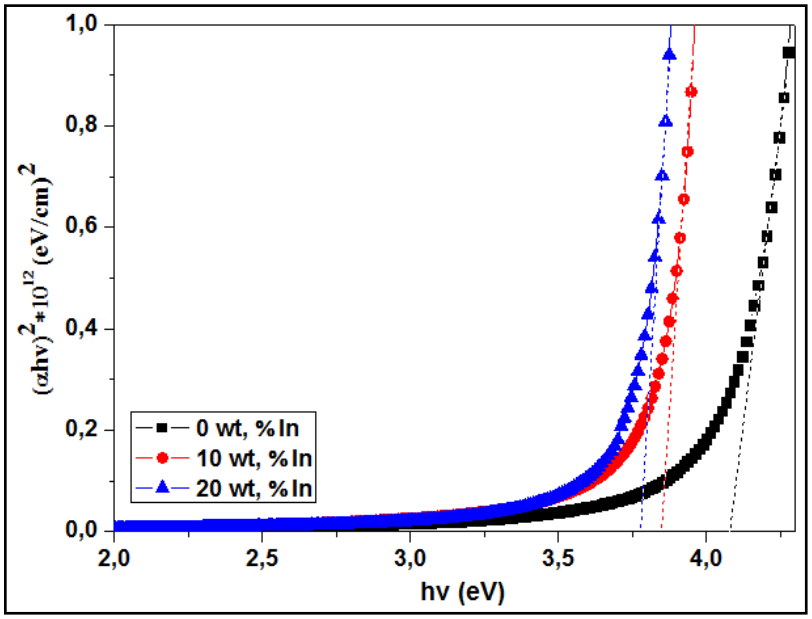

Fig. IV. 16. The plot of $(\alpha h\upsilon)^2$ vs. $(h\upsilon)$ for SnO_2:In film

The optical band gap of our films has been determined on the basis of UV–VIS transmission measurements by plotting $(\alpha h\nu)^2$ as function of $h\nu$ (Fig. IV.16).

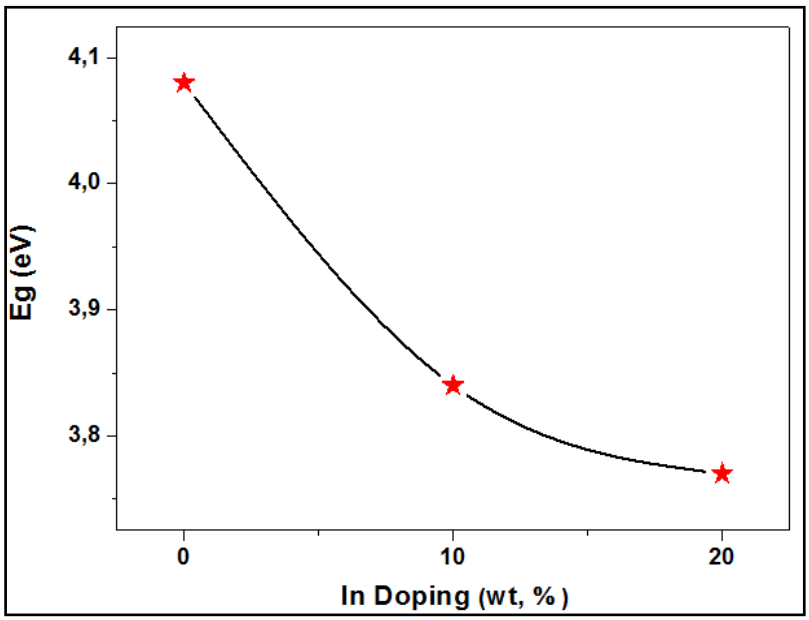

Fig. IV.17. The variation of optical band gap of the undoped and In doped SnO2 thin films with indium doping

The variation of band gap as function of indium content is shown in Fig. IV.17. The optical band gap of SnO_2 films decrease with the increasing of indium concentration**.** The shrinking in band gap energy is due to the increase of lattice spacing d (see Fig. IV.12.) and this shows that there is a good agreement with XRD patterns. On the other hand, this narrowing could be attributed to increase the density of states of dopant which is shaped as band. In literature, SnO_2:In films displayed similar behavior [14]. Also, the same values of gap were obtained for SnO_2 films. Casey et al. [15] found 4.1 eV and Stjerna et al [16] 4.06 eV.

IV.2.3. Electrical properties

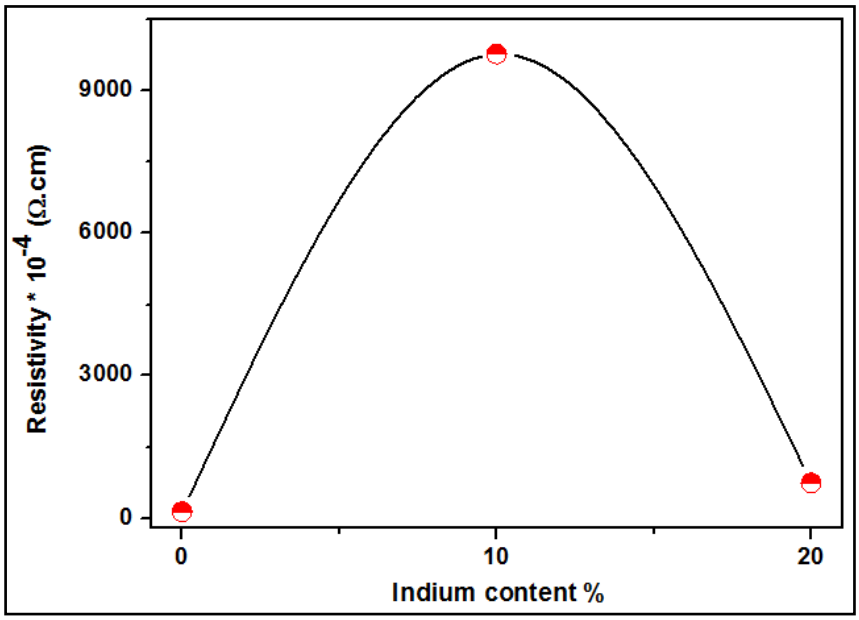

Fig. IV.18. The variation of the resistivity with deposition In content of SnO_2 films

Fig.IV.18. illustrates the variation of the electrical resistivity (ρ) with indium content. We observed that the resistivity increased with the increasing of indium concentration, then decreased. Hall Effect measurement revealed that the undoped and doped films with 10% In had n-type electrical conductivity, and when it was at 20%, In-doped SnO_2 thin films showed a p-type. For undoped SnO_2 films, it is well known that these films displays n-type conductivity because of the existence of native defects i.e., non-stoichiometry (interstitial tin atoms and oxygen vacancies) [17]. At higher doping levels (20 Wt.% In), indium is like an acceptor which compensate firstly the existent of native defects, as donors, and then switch films from n to p type, participates in films resistance decrease [10]. At 10 Wt.% In, we had observed that the resistivity increased, because the indium atoms that incorporate to SnO_2 lattice were insufficient to change them from n to p type film. It is the same idea which explains the resistivity increase in the first part of the chapter. On the other hand, high temperature makes the indium atoms more active as acceptors by the substitution of Sn atoms by In and, as a consequence, the annealed films at 600 ° C are more conductive.

The resistivity decrease is mentioned and explained by salehi et al [18] in terms of the valence state of the tin. It is known that Sn has +2 and +4 oxidation states. At higher indium concentration, In^{+3} can substitute Sn^{+2} and gives one extra charge carrier, subsequently increase the conduction. Also, they [11, 12] reported that if the amount of Indium is very

high, the tin dioxide will behave as an ITO (Indium Tin Oxide: tin doped indium oxide) than Tin Indium Oxide (Indium doped tin oxide). They proved that films become more conductive.

Conclusion:

The study of low and high concentrations of Indium doping on SnO_2 thin films have been investigated. Several methods were adapted for characterizations of the properties were done to the preparation of samples such as XRD, UV-visible and Four-point.

In undoped and doped SnO_2 with low concentrations (1-8 Wt% In), X-ray diffraction shows that the films have a tetragonal structure. The preferential plane is (200), which changed to (301) starting from 4 %. The crystallite size ranged between 24,49- 46,39 nm. While UV-Vis spectrophotometer shows that the transmittance rises up to 2 % doped film, then decreases. Highest transmission in the longer wavelengths (>400 nm) is around 97 %. The direct band gap value is ranged in 3.9 – 4.1eV. The electrical resistivity was influenced remarkably by the doping.

In undoped and doped SnO_2 with high concentrations (10, 20 Wt% In), X-ray diffraction shows a polycrystalline structure. The favorable growth orientation was (200) and the grain size reduced with increasing In concentration. The crystallite size ranged between 23,42- 62,63 nm. The optical and electrical measurements indicated that films transmittance and conductivity are much improved at 20% Wt. Furthermore, the optical band gap is narrowed with increasing In content. The undoped and doped films with 10% showed n-type electrical conductivity and the film showed p-type conducting at high doping level 20% In.

References

[1] M. Ajili, N. Jebbari, N. Kamoun Turki and M. Castagné, EPJconf, 29 (00002) (2012) 1-9.

[2] D. Belanger, J.P. Dodelet, B.A. Lombos and J L Dickson, J. Electrochem. Soc, 132 (1985) 1398.

[3] A. Chitra, B. R. Marathe, M G. Takewale and V G. Bhide, Thin Solid Films. 164 (1988) 261.

[4] H. H. Afify, F. S. Terra, J. Mat. Sci. Materials inElectronics. 7(1996) 149-153.

[5] P. Prathap, G. Gowri Devi, Y. P. V Subbaiah, and al, Curr Appl Phys, 8 (2008) 120.

[6] B. G. Jeyaprakash, R. Ashok Kumar, K. Kesavan, and al, J Am Sci, 6(3) (2010) 22.

[7] B.D. Ann, S.H. Oh, D.U. Hong, D.H. Shin, A. Moujoud, H.J. Kim, Cryst. Growth ,310 (2008) 3303.

[8] S.S. Lekshmy and K. Joy, J. Sol–Gel Sci. Technol. 67(2013) 29–38.

[9] K.-Mu Lee, K.-Liang Shih, C.-Hung Chiang, V. Suryanarayanan, C.-Guey Wu, Thin Solid Films, 570 (2014) 7-15.

[10] C.Y.Tsay, S.C.Liang, J. Alloys and Compounds, 622 (2015) 644-650.

[11] Z. Ji, Z. He, Y. Song, K. Liu et Z. Ye, J. Crystal Growth, 259(2003) 282–285.

[12] Z. Ji, L. Zhao, Z. He, Q. Zhou et C. Chen, Materials Letters, 60(2006) 1387–1389.

[13] H.L. Ma, D.H. Zhang,Y.P.Chen, S.Y. Li, J. Ma et F.J. Zong, Thin Solid Films, 298(1997) 151-155

[14] S. Laghrib, Synthèse des films minces de : SnO2, SnO2: In par deux procédés physique et chimique et étude de leur caractérisation, PhD thesis, University Ferhat Abbas, Setif, 2010.

[15] V. Casey, et M. Stephenson, J. of Physics D: Applied Physics, 23(1990) 1212.

[16] B. Stjerna, E. Olsson, C.G. Granqvist, Journal Applied physics, 76 (6) (1992) 3797.

[17]P. Ravikumar, K. Ravichandran, B.Sakthivel,J. Mater. Sci. Technol, 28(11) (2012) 999–1003.

[18] A. Salehi, M. Gholizade, Sensors and Actuators B, 89(2003) 173-179.

CHAPTER V

Effect of Precursor and Annealing Temperature on the Properties of SnO_2:In Thin Films

For the present investigation, SnO_2:In films were grown on glass substrates by ultrasonic spray pyrolysis technique using two inorganic tin compounds as precursor solutions, stannic chloride pentahydrate $SnCl_4.5H_2O$ and stannous chloride dihydrate $SnCl_2 \cdot 2H_2O$, and $InCl_3$ as the source of the doping impurities. The precursors play important key roles in dominant the structure of thin films. The advantages of $SnCl_2$ are cheaper than $SnCl_4$ and can be generated easily in the laboratory.

In this chapter we have discussed the effect of precursor and annealing temperature on structural, optical and electrical properties of SnO_2:In films.

V.1. Effect of precursor on the properties of SnO_2:In thin films

The samples discussed in this part were grown under similar conditions (Solution flow rate 50 ml/h,distance spray nozzle-substrate 5 cm, temperature substrate 450°C, molarity 0.1 mol/l, deposition time 5 min and the concentration of indium is varied from 0 to 4 wt% in steps of 1wt%.)

V.1.1. Structural properties

X-ray diffraction spectra recorded on SnO2.In films prepared from $SnCl_4$ and $SnCl_2$ precursor solutions as a function of the In^{+3} concentration are shown in Fig.V.1.

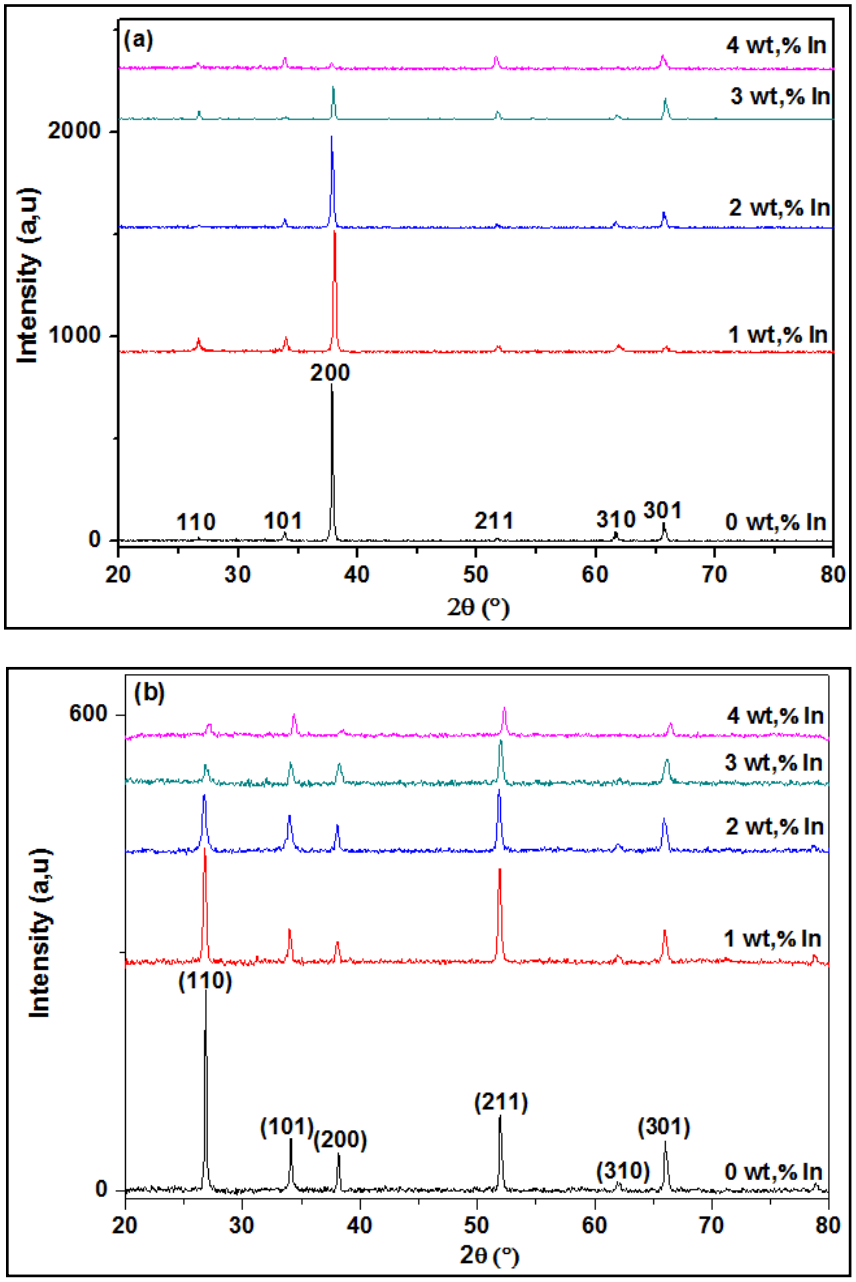

Fig V.1. Typical XRD spectra of SnO_2:In films deposited from (a) $SnCl_4$ and (b) $SnCl_2$ as precursor solutions, doped with $InCl_3$.

As seen in Fig. V.1.a, several peaks along (110), (101), (200), (211), (301) and (310) planes are clearly observed which indicate that the films are polycrystalline in nature. These peaks clarify that the films have a cassiterite tetragonal crystalline phase (JCPDS card No. 041-1445). It is clear from the XRD spectra there are no indium oxide phases are detected in the prepared samples. As shown in Fig. V.1.a, intensity of peak for (200) plane decreases with the increasing of In content and this may be attributed to deteriorated crystal quality. However, the diffraction peaks of the undoped film are more intense and sharper. In the high

doping level (4 Wt.%, In), the preferential orientation is altered to (301). A similar behavior has been found by another researcher [1].

In Fig. V.1.b, all the major peaks in the patterns correspond to the rutile structure of SnO_2 and are indexed on the basis of JCPDS file no. 41-1445.It is evident from the XRD spectra there are no indium or indium oxide phases are observed in the prepared samples. As seen in Fig. V.1.b, with increasing In content the intensity of the (110) peak decreases gradually. At high doping level (4 Wt.%, In), the preferential orientation is changed to (211).We should mention here that the preferential orientation can be influenced by the deposition conditions (precursors, substrate, annealing temperature, etc.) and also by the doping element and its percentage[2].

Comparing the X-ray spectra of Fig. V.1.a and b, we conclude that SnO2:In films deposited using $SnCl_4$ present a preferential orientation along the (200) while the samples prepared from $SnCl_2$ present a disordered growth, with a inclination to grow along the (110), (211), (301) and (101) orientations. Also, the diffraction peaks of the SnO_2 films deposited using the $SnCl_4$ solutions were more intense than those prepared from $SnCl_2$.In the $SnCl_2$ solution the Sn and Cl atoms are held together by ionic bonds while in the $SnCl_4$ solution a larger part of the Sn and Cl species are covalently bonded. As far as the forces which held together the atoms in ionic compounds seem to be stronger than those in covalently bonded ones, the formation of SnO_2 films from a $SnCl_4$ precursor needs a smaller amount of energy than in the case where $SnCl_2$ is used [3].

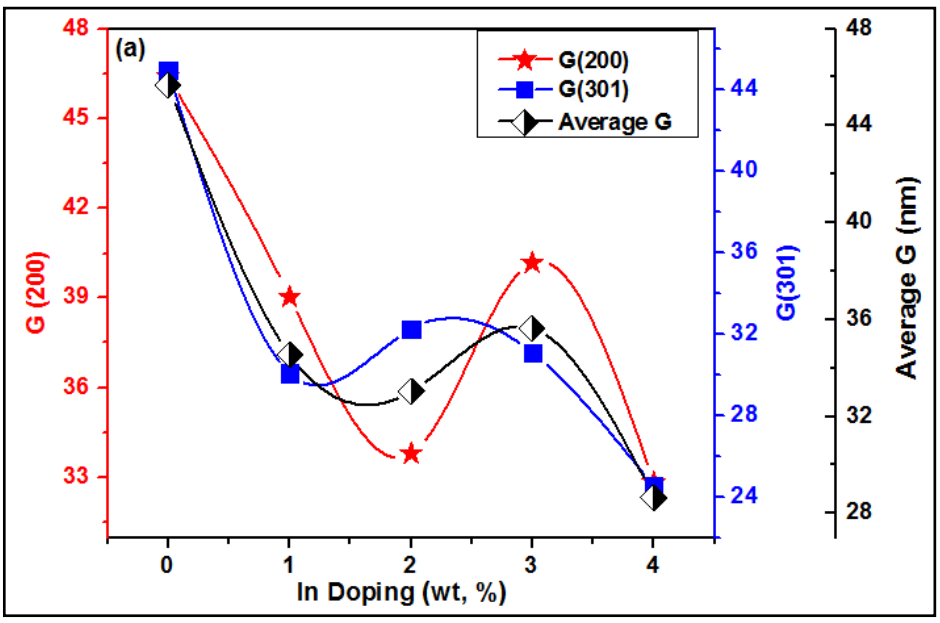

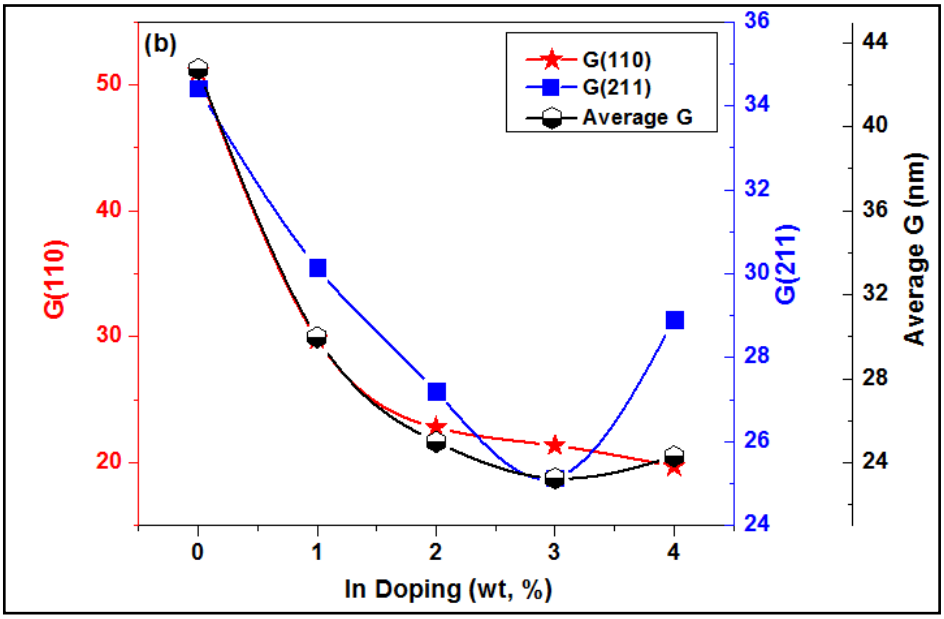

Fig. V.2. The variation of the crystallite size with In content of SnO_2 films (a) SnCl4.5H2O and (b) SnCl2.2H2O as precursor solution.

Figure.V.2.a and b show the variation of grain size as a function of indium content with the two types of precursor solutions $SnCl_4.5H_2O$ and $SnCl_2.2H_2O$, respectively.

Generally, in both cases, the crystallite sizes for all planes decrease with the increasing of In content.

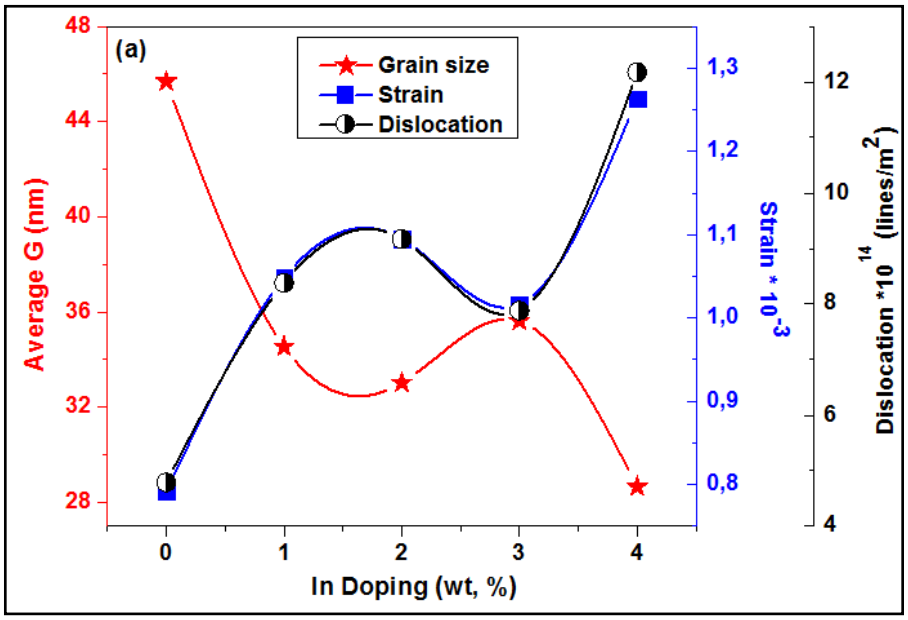

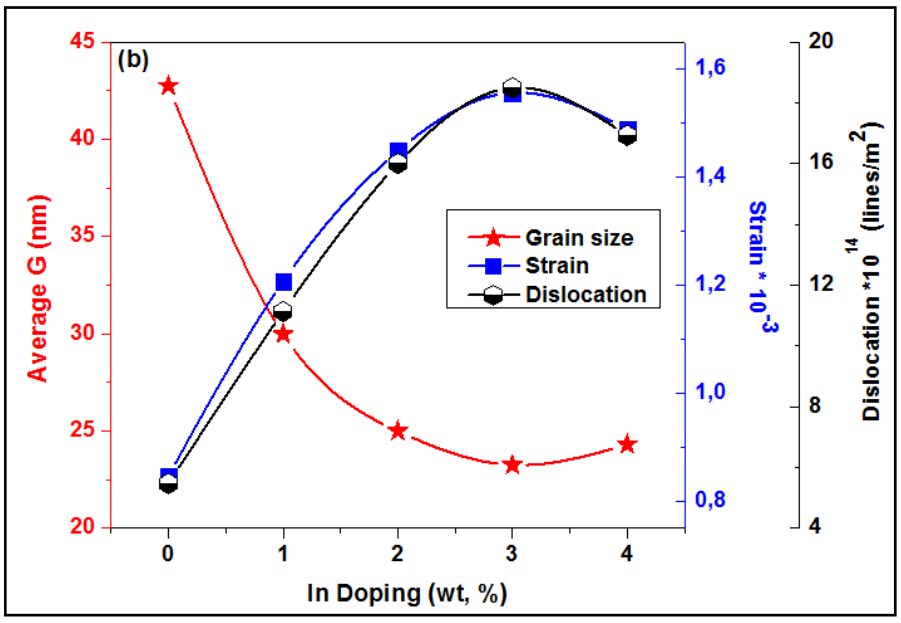

Fig. V.3. The variation of the crystallite size, strain and dislocation density with In content of SnO_2 films (a) $SnCl_4.5H_2O$ and (b) $SnCl_2.2H_2O$ as precursor solution.

Figure. V.3.a and b show the variation average of grain size, strain and dislocation density as a function of indium content with the two types of precursor solutions $SnCl_4.5H_2O$, and $SnCl_2.2H_2O$, respectively.

The value of grain size is in the range of 28,661-45,68 nm and 23,256- 42,7405nm for both Figs. V.3.a and b, respectively. There is no significant difference in the grain size in both cases. As clearly seen in the previous figures, the crystallite size diminishes with the increasing of In content which possibly due to the formation of stresses, because of the difference in ion size between tin and the dopant. The increment in the strain and dislocations emphasize this hypothesis. Smaller G, larger δ and ε values indicate a deteriorated crystallization of the films.

V.1.2. Optical properties

Fig. V.4.a and b show the variation of transmittance of the SnO_2:In films as a function of the wavelength prepared from $SnCl_4.5H_2O$ and $SnCl_2.2H_2O$ as precursor solutions, respectively.

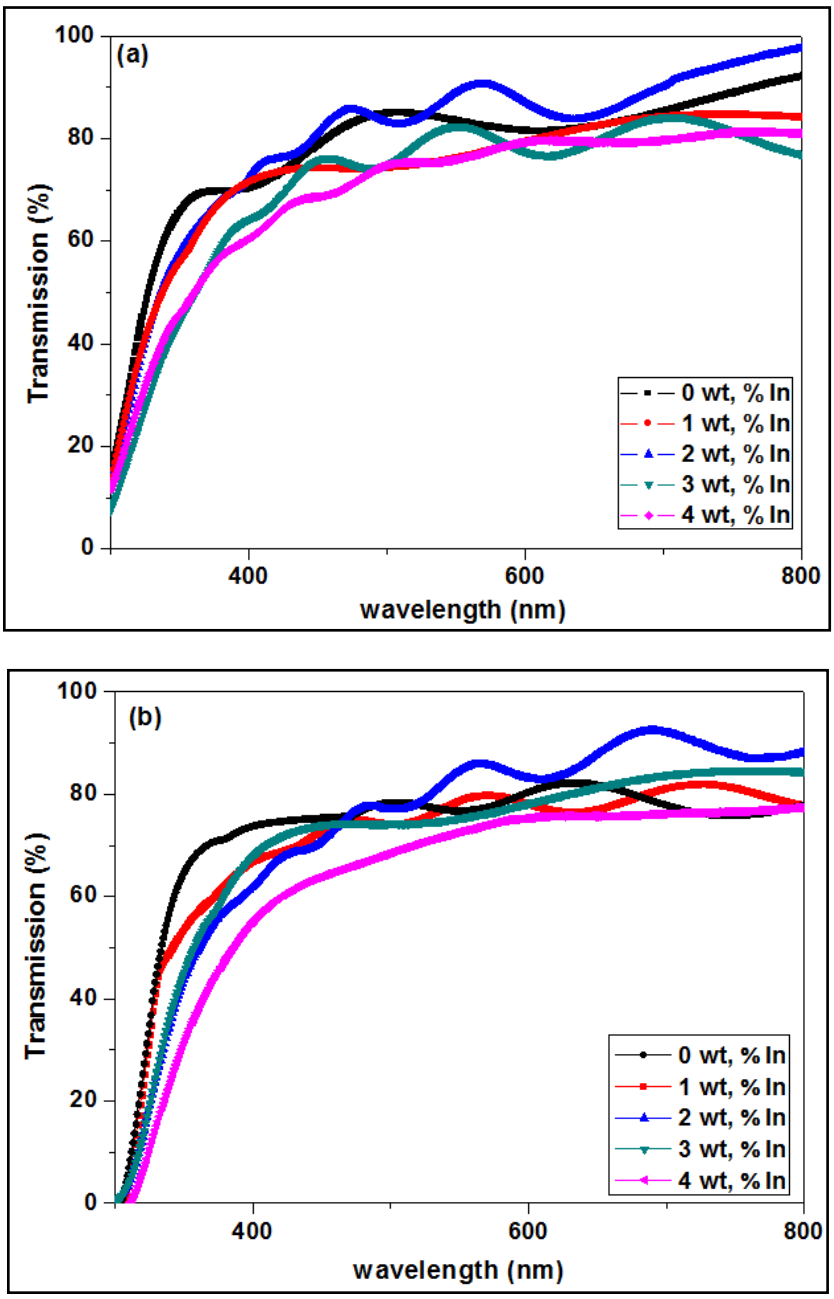

Fig. V.4. Optical transmittance T (%) versus wavelength λ of SnO_2:In films at various indium amounts(a) $SnCl_4.5H_2O$ and (b) $SnCl_2.2H_2O$ as precursor solution.

.

Fig. V.4.a and b show that the prepared films are fully transparent in the visible region and a minimum transmittance in the UV for all films which means that strong absorbance for all films in the interval where λ< 400 nm due to the excitation and the migration of the electrons from the valence band to the conduction band. However, the films prepared from $SnCl_4.5H_2O$ have higher transmittance than those produced in SnO_2 films deposited from $SnCl_2.2H_2O$. As we said previously that, the formation of SnO_2 films from a $SnCl_4$ precursor needs a smaller amount of energy than in the case where $SnCl_2$ is used. So, the films prepared from $SnCl_2$ maybe have undesirable compounds due to insufficient energy. The latter cause a

decrease in the homogeneity of the layers which in turn reduces the transmittance of the films. Also, the absorption edges for the films prepared from $SnCl_4.5H_2O$ shifted to shorter wavelength compared to those films deposited from $SnCl_2.2H_2O$. In both cases, the introduction of In^{+3} impurities to the SnO_2 films are affected significantly the transmittance of the samples. So that the optical transmittance is reduced with the increasing of In doping. Furthermore, 0% In and 2% In exhibit higher transmittance.

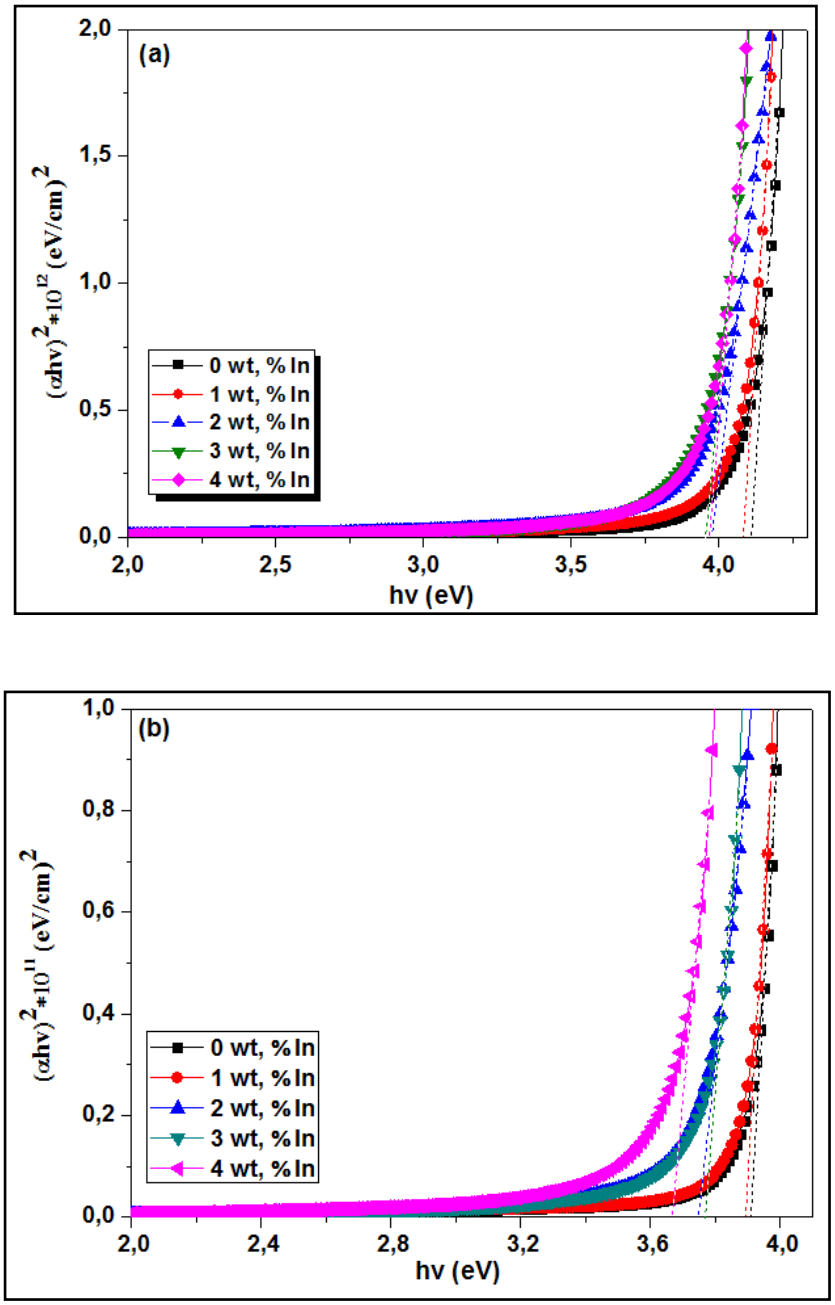

Fig. V.5. The plot of $(\alpha h\upsilon)^2$ vs. $(h\upsilon)$ for SnO_2:In film(a) $SnCl_4.5H_2O$ and (b) $SnCl_2.2H_2O$ as precursor solution.

The fundamental absorption edge can be used to determinate films optical band gap (see chapter II), as shown in Fig. V.5.a and b.

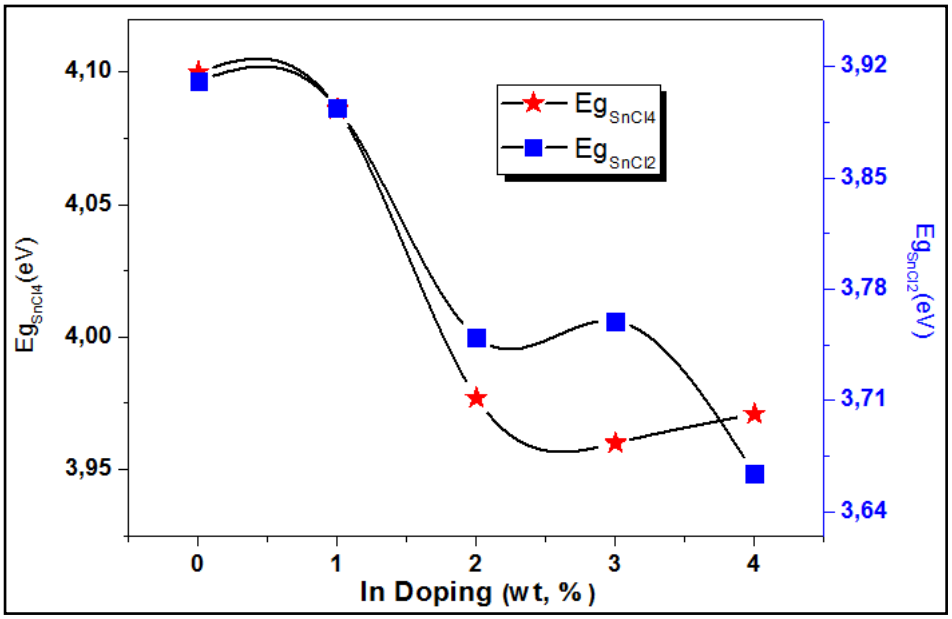

Fig. V.6. The variation of optical band gap of SnO_2:In films at various indium amounts,$SnCl_4.5H_2O$ and $SnCl_2.2H_2O$ as precursor solutions.

Figure. V.6. shows the variation of the optical band gap energy as a function of indium content with the two types of precursor solutions $SnCl_4.5H_2O$ and $SnCl_2.2H_2O$, respectively.

The value of Eg is in the range of 3,96 to 4,1 eV for sample from $SnCl_4$ and 3,664 to 3,911 eV for samples from $SnCl_2$ precursor. It is noticed that the band gap has the same variation in both cases. However, the band gap energy values are higher for the samples prepared from $SnCl_4$ precursor. These high values of band gap energy can be attributed to the crystalline structure in these samples.

V.1.3. Electrical properties

The plots of resistivity versus indium content for SnO_2 films prepared from $SnCl_4$ and $SnCl_2$ are shown in Fig. V.7.

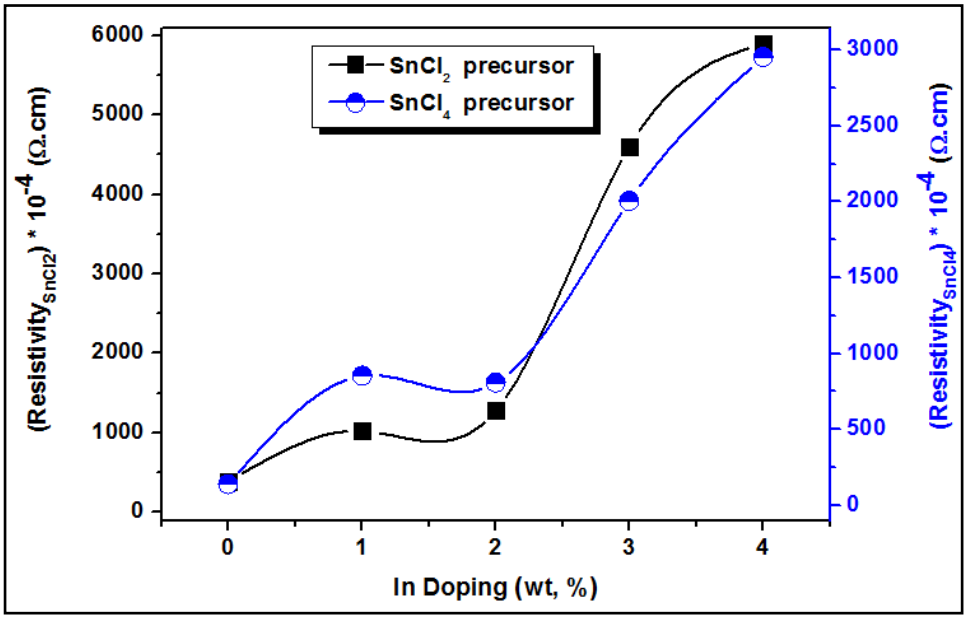

Fig. V.7. variation of resistivity with Indium content of SnO2 films, $SnCl_4.5H_2O$ and $SnCl_2.2H_2O$ as precursor solutions.

The resistivity increases with the increasing of In content in both cases and reaches the maximum at high doping level. This is may be attributed to the deterioration in the crystalline nature of these samples which is consistent with XRD data.

In the previous XRD patterns, we found that SnO_2 films deposited using $SnCl_4$ have an identified preferential orientation while the samples prepared from $SnCl_2$ have a disordered growth. This could be the answer to the question: why the SnO_2:In films deposited using the $SnCl_2$ solutions are more resistive than those prepared from $SnCl_4$.

So, it is noticed that the films prepared from $SnCl_4$ have better crystallinity and conductivity than the other prepared from $SnCl_2$. This agreed with the fact that even an improved crystallinity favors have low resistance.

V.2. Effect of annealing temperature on the properties of SnO_2:In thin films

0.1 mol/l tin chloride penta-hydrate ($SnCl_4.5H_2O$) was used as tin source and indium chloride ($InCl_3$) as indium dopant source. The concentration of indium is varied from 1 wt% to 8 wt%. The precursor solution was sprayed into hot substrates (T_S = 400 °C) for 5 min as a growth time. After successful completion of deposition, the films were annealed at annealing temperature at 600°C for 1h in air.

V.2.1. Structural properties

The XRD patterns for the SnO_2:In thin films before and after annealing are represented in Fig. V.8.

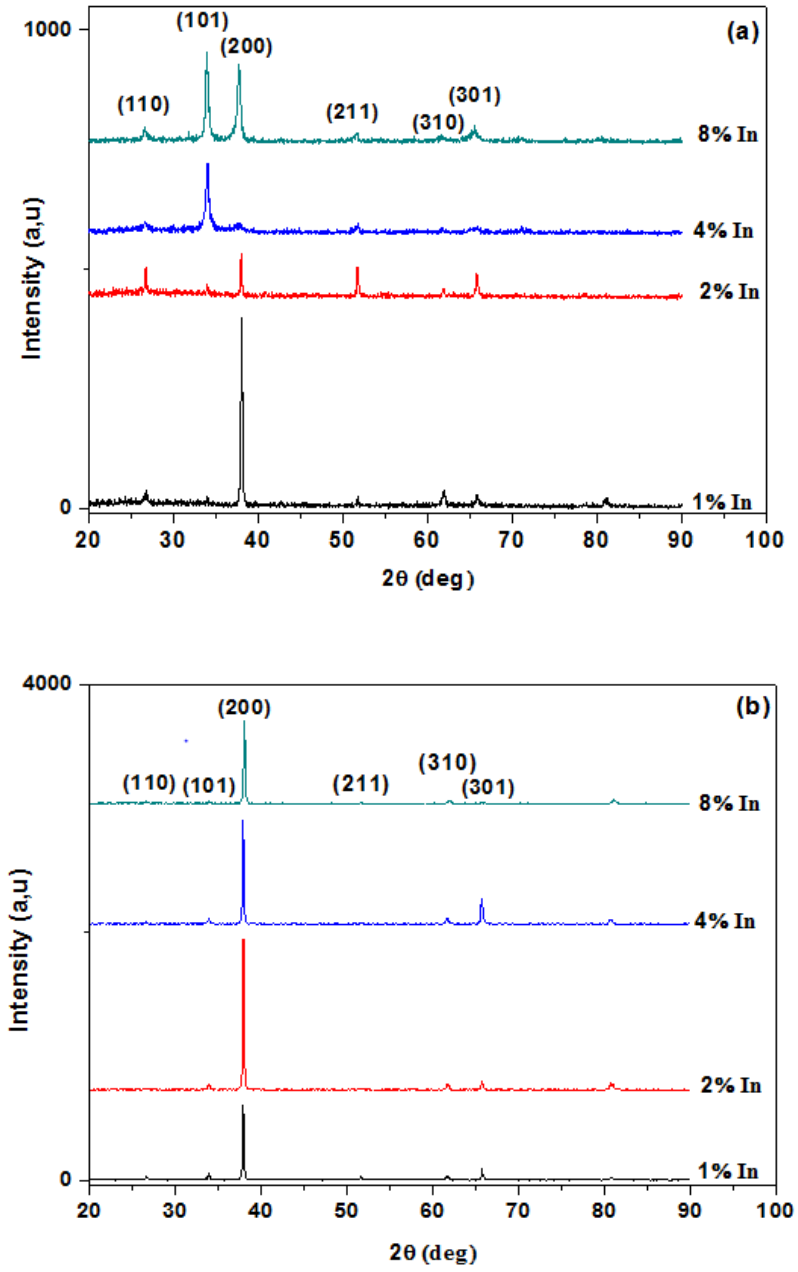

Fig. V.8. X-ray diffractograms of indium-doped tin dioxide films with different indium concentration: (a) before annealing. (b) after annealing.

The XRD patterns for the as-deposited SnO_2:In thin films are represented in Fig. V.8.a. In the present study, all the major peaks in the pattern correspond to the rutile structure of $SnO_2$are indexed on the basis of JCPDS file no. 41-1445. As exhibited in Fig.V. 8.a, the intensity of (200) peak reduces with the increasing of In content till4 %, then increases. For the heavily Indium doped SnO_2 thin films (4 and 8 wt.%) the preferential orientation is altered to (101). The presence of other orientations like (110), (211), (310) and (301) have also been

revealed. There are no indium oxide phases appeared from the XRD patterns that is to say In substitutes Sn in the tetragonal lattice

Fig.V.8.b. shows the diffraction patterns of SnO_2: In thin films annealed at 600°C. The XRD results illustrate that all films are tetragonal rutile structure with a preferential orientation along (200) crystal plane. Film annealed at 600°C displays intense XRD peaks, indicating film crystallinity amelioration in comparison to the as-deposited films. This refers to that annealing at 600°C for 60 min is sufficient to regulate the crystalline structure of the films and enforces the enhancement of the crystal quality of SnO_2 films [4].

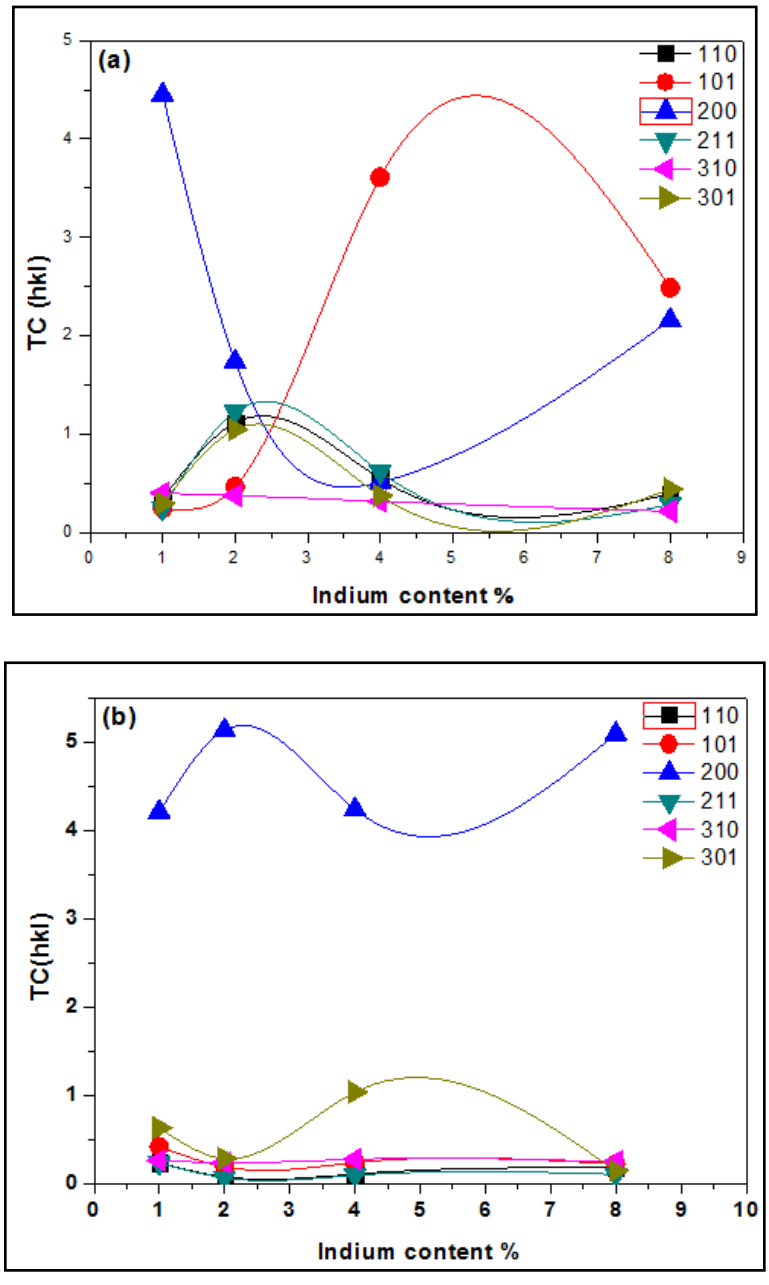

Fig. V.9. The variation of TC values with deposition Indium content: (a) before annealing (b) after annealing of (110), (101), (200) and (211) planes.

From the TC in Fig.V.9.a it seems that at 1 wt.% and 2 wt.% the preferential (200) orientation is improved while the (101) orientation repressed. However, at 4 wt.% and 8 wt.% the preferential (200) orientation is suppressed while the (101) orientation is improved. The variation of the TCs with Indium content after annealing as shown in Fig.V.9.b The highest TC value for each film belongs to (200), this implies that there is a significant growth along (200).

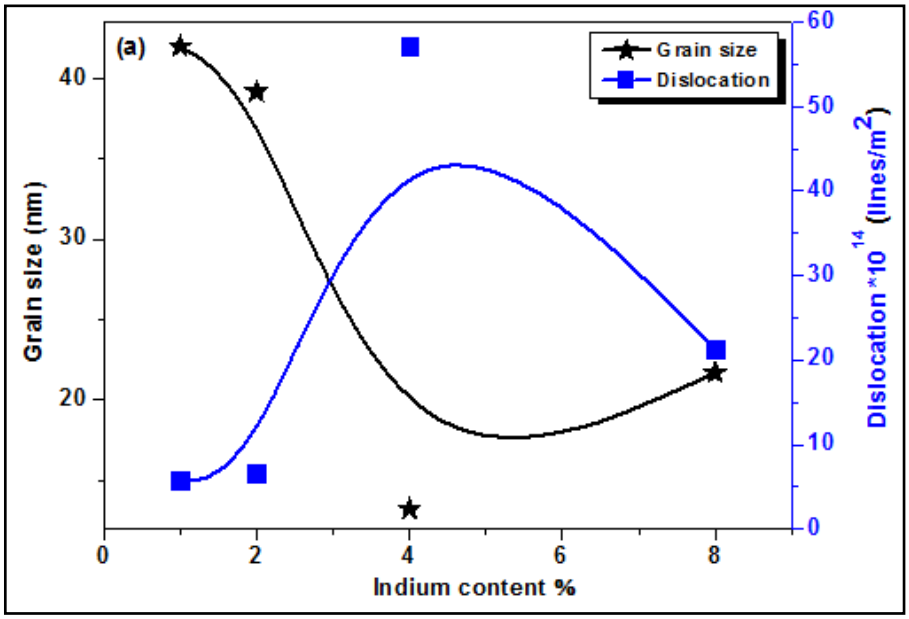

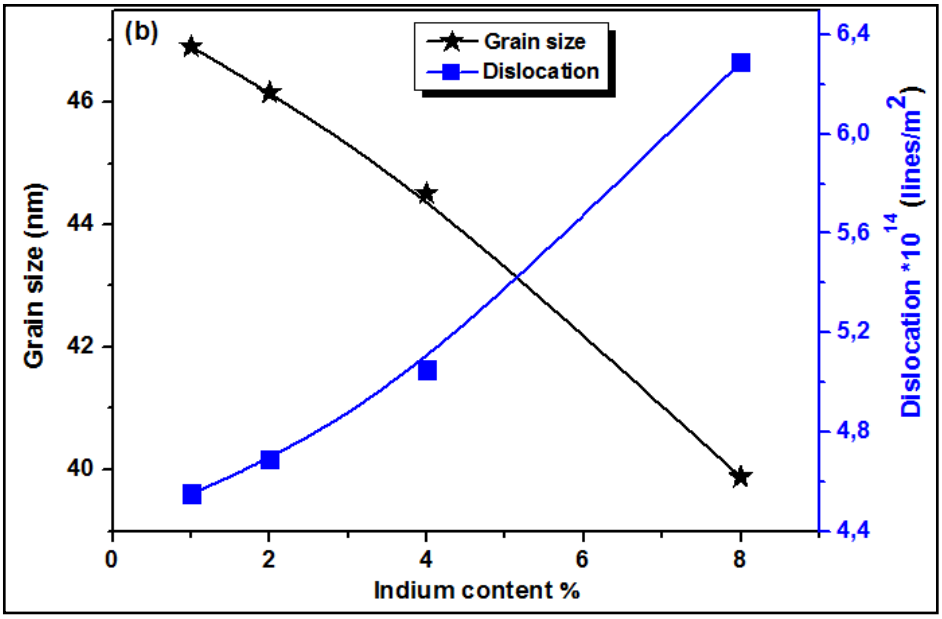

Fig. V.10. The variation of the crystallite size and dislocation density with deposition In content of SnO_2 films before and after annealing temperature at 600°C.

Fig. V.10.a and b show the plot of crystallite size and dislocation density as a function of deposition In content before and after annealing. We found that the crystallite size reduced with indium concentration increase (before and after annealing). This indicates that indium incorporation in the SnO_2 lattice results in a decrease in crystallite size [5].

As can be seen, the crystallite sizes were changed in the range of 13,234-41,986 nm for the as deposited films while it became in the range 39.879-46.895 nm after annealing. The crystallite sizes of the as deposited films are tinier than the annealed ones. The rise in the crystallites size and the crystallinity amelioration after annealing temperature can be due to the improvement of kinetic energy of atoms at high temperature that helps more atoms to move to more stable states in the lattice points [6]. Similar results were reported for F-doped [7] Ga-doped [8] and Mn-doped [9] SnO_2 thin films. The dislocation density values of the films are increasing with the increasing of the In content and change inversely with *G* of the films.

V.2.2.Optical properties

Fig. V.11. shows the transmittance spectra of Indium doped SnO_2 thin films for both as-deposited and annealed, where in longer wavelengths (λ>400 nm) all films become transparent. The films show significant oscillations in all wavelength average. Those oscillations are due to the multiple reflections at two film edges, i.e. at the film/air and the film/substrate interfaces [10].

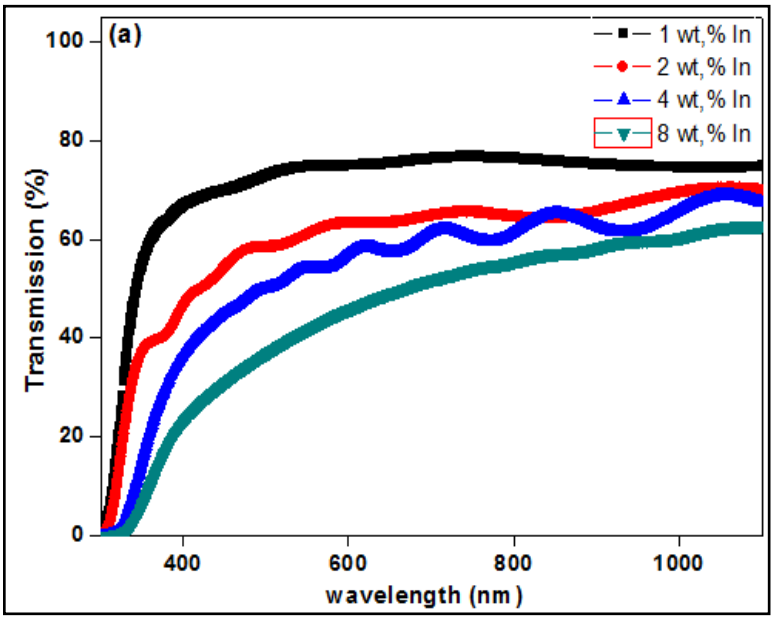

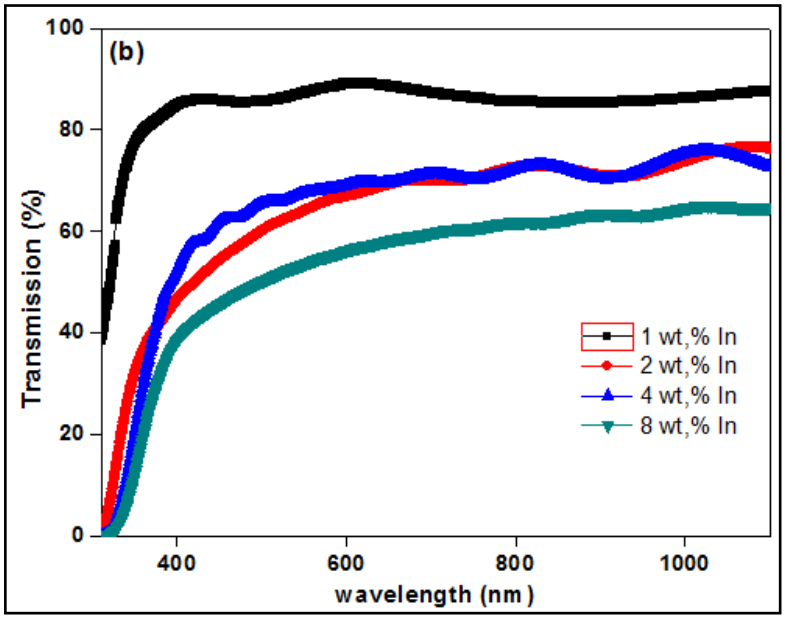

Fig. V.11. Optical transmittance T (%) versus wavelength λ of TO:In films at various indium amounts (a) before annealing. (b) after annealing.

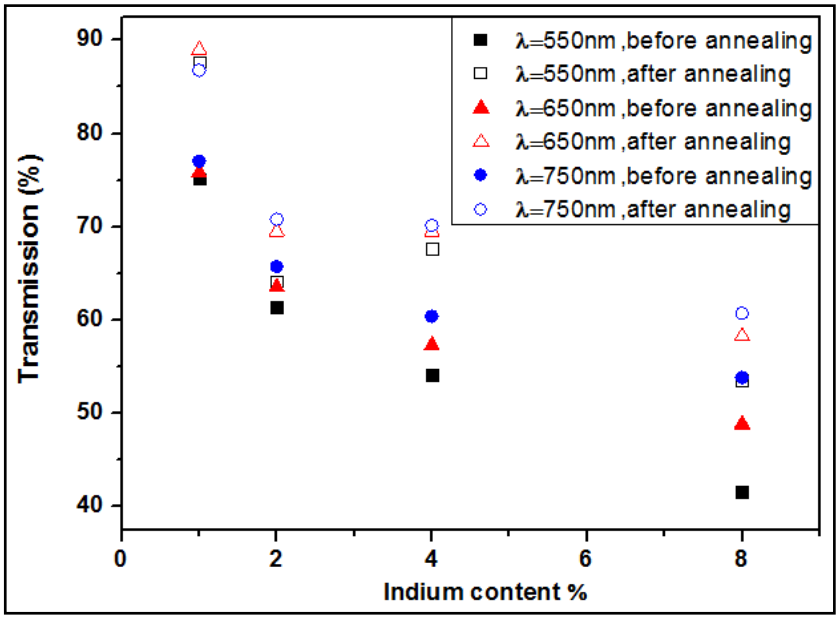

Fig. V.12. Variation of transmittance versus different indium concentrations at different values of wavelengths, before and after annealing.

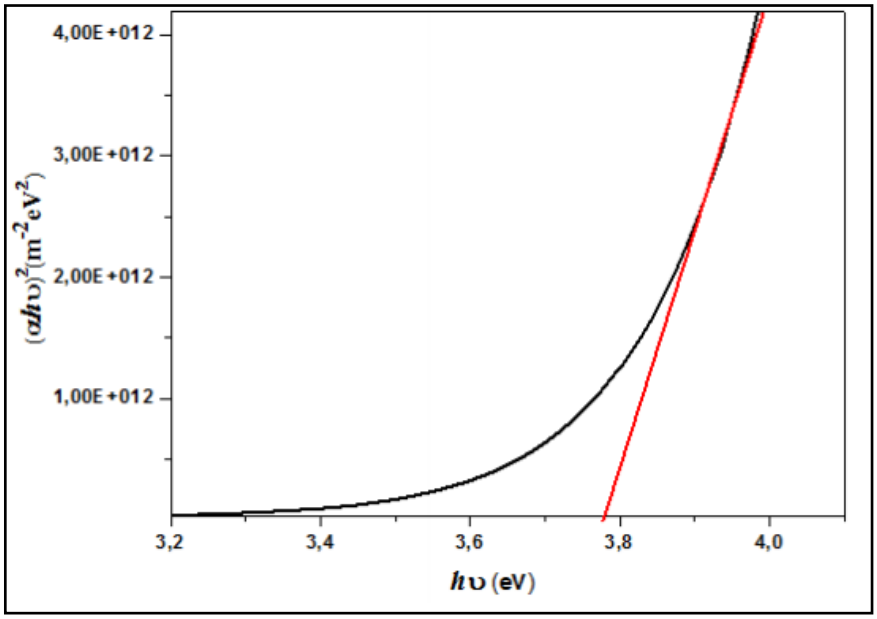

Fig.V.13. The plot of $(\alpha h\upsilon)^2$ vs. $(h\upsilon)$ for SnO_2:In film

The transmittance values of films at 550 nm, 650 nm and 750 nm are shown in Fig. V.12. Before annealing, the highest value of transmittance is reached 77.022 % at 750 nm. While after annealing, it reaches 88.904 % at 650 nm. It is noticed that the transmittance is higher in annealed films than that of as-deposited films over the entire wavelengths. This is due to the improvement in the crystal quality of the films which leading to decrease of scattering effect.

From Fig. V.12, it can be seen that optical transmittance reduces with the increasing of In doping. The absorption edges for the annealed films shifted to shorter wavelength compared with that of as-deposited films which is attributed to Burstein–Moss effect [11,12] as shown in Fig. V.11. The fundamental absorption edge can be used to determinate films optical band gap, E_g. It was calculated by plotting $(\alpha h\upsilon)^2$ against the photon energy $(h\upsilon)$ as shown in Fig. V.13. The linear nature of the plot refers to the presence of direct transition.

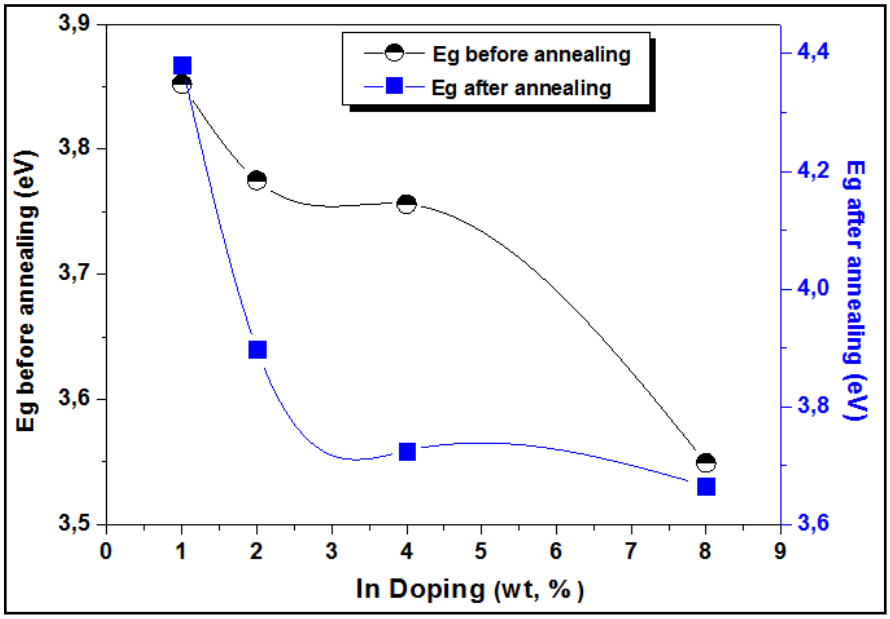

Fig. V.14. The variation of optical band gap of TO:In films at various indium amounts, before and after annealing.

The variation of band gap before and after annealing is shown in Fig. V.14.The value of E_g is in the range of 3,54-3,85 eV which is in good agreement with the previously reported values [13,14], and 3,66-4,38 eV for both as-deposited and annealed films, respectively. As shown in Fig. V.14, in both cases, the band gap energy diminishes with increasing In content. On the other hand, the dislocation density increases with the increasing of In doping ratio (see Fig. V.10).This increase of δ leads to disorders and crystal defects in the SnO_2 lattice and may cause a decline of the Eg values with In doping. Many authors have reported the red shift of Eg by different dopant in the SnO_2 [15-17]. However, the band gap energy is lower for as-deposited films than that of annealed films (see Fig. V.14).This is attributed to the decrease of disorder in the film due to the improvement in crystalline quality of this latter [18]. El Sayed et al. [19] also reported the narrowing of E_g of SnO_2:Co.

V.2.3.Electrical properties

The effect of In content and annealing on resistivity of SnO2:In films were studied. Films resistivity ρ is plotted in Fig. V.15. From this figure, it is noted that ρ value increases with the increasing of In concentration for both as-deposited and annealed films. The rising of grain boundaries is caused by the development of small size grains as consequence of In incorporation and also by the incomplete bonding between the layers of the atoms. The

boundaries act as sinks to catch charge carriers and so increase the resistance [20]. Comparable behavior has been reported in the literature [21].

Furthermore, Dobler et al. [22] clarified that doping with elements having lower than 4 valency (such In) give rise electron density reducing, causing after that, the material resistivity improvement. However, the ρ values for annealed films are lower than ρ of those as-deposited films. The process of annealing improves the crystal structure and grain boundaries reduction, this leads to the decrease in films resistance [23]. In literature, SnO_2:In films annealed displayed similar behaviors [1, 24]. Also N. D. Papadopoulos et al [25] and M.A. Yıldırım et al [26] found that the electrical resistivity of SnO_2 films decrease after annealing in air. All these researchers agreed that the improvement in crystallinity could be accountable for low resistivity of annealed films.

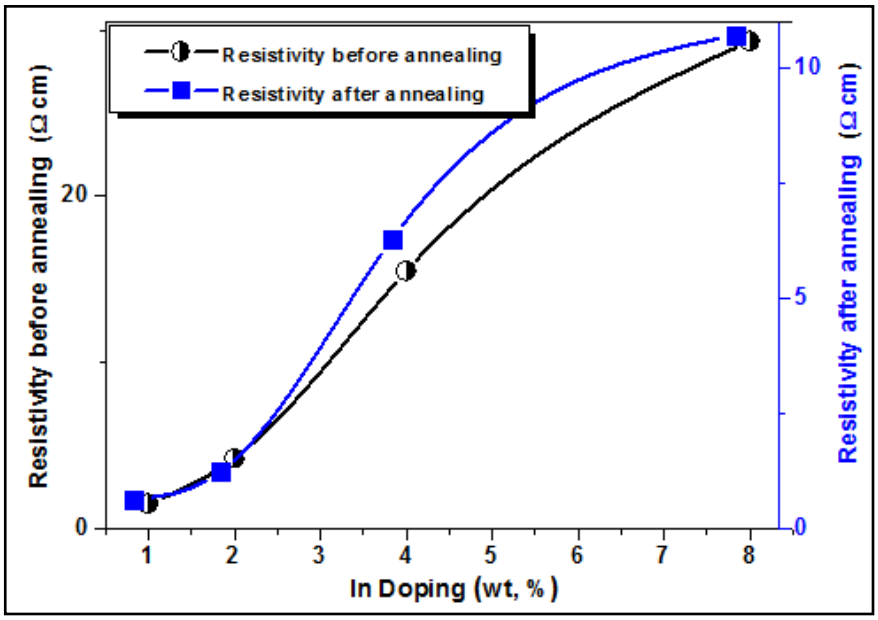

Fig. V.15. Variation of resistivity with In content for SnO_2 films, before and after annealing.

Conclusion

In-doped SnO_2 films were deposited by ultrasonic spray technique into glass substrates. In the first section, we have studied the influence of precursor solutions ($SnCl_4 \cdot 5H_2O$, $SnCl_2 \cdot 2H_2O$) and In content on SnO_2 thin films deposition while in the second section, we investigated the effect of annealing and In content on SnO_2 films properties.

In the first part, X-ray diffraction measurements indicated that all films have a tetragonal structure. The SnO_2:In films deposited using $SnCl_4$ present a preferential orientation along the (200) while the samples prepared from $SnCl_2$presented a disordered growth with a inclination to grow along the (110), (211), (301) and (101) orientations. A

lowest resistivity (0.08 Ω.cm) and highest optical transmittance (97%) are obtained for the film prepared from $SnCl_4.5H_2O$.

In the second part, as the evidence of X-ray diffraction analysis stated, films crystallite size increased with annealing while it is reduced with the increasing of In content. The crystal quality is improved by annealing unlike In doping which do not yield to an improvement in crystal quality. The optical measurements indicated that films transmittance were improved with annealing but decreased with indium concentrations. Moreover the optical band gap was narrowed with the increasing of In content and shifted to a shorter wavelength with annealing. The films resistivity was found to increase with In content, but decreased with annealing temperature.

References

[1] P.K.Manoj, Benny Joseph, V.K. Vaidyan,D. Sumangala Devi Amma, Ceram.Int. 33(2007) 273–278.

[2] S. Laghrib, Synthèse des films minces de : SnO2, SnO2: In par deux procédés physique et chimique et étude de leur caractérisation,PhD thesis, University Ferhat Abbas, Setif, 2010.

[3] G. Gordillo, L. C. Moreno, W. de la Cruz, P. Teheran, Thin Solid Films, 252 (1994) 61-66

[4] J. Henry, K. Mohanraj, G. Sivakumar, S. Umamaheswari, Spectrochim. Acta A 143 (2015) 172-178.

[5] J. Kaur, R. Kumar, M.C. Bhatnagar, Sensors and Actuators B 126 (2007) 478–484.

[6] R. Lotfi Orimi, M. Maghouli, Optik 127 (2016) 263–266.

[7] Sh. J. Ikhmayies, international journal of hydrogen energy xxx, (2016) 1-8.

[8] C.Y. Tsay, S.C. Liang, J. Alloy. Compd, 622 (2015) 644-650.

[9] F. Ghodsi, J. Mazloom, Appl. Phys. A Mater. 108 (2012) 693-700.

[10] J.J. Berry, D.S. Ginley, P.E. Burrows, Appl. Phys. Lett. 92 (2008) 193304.

[11] E. Burstein, Phys. Rev. 93 (1954) 632–633.

[12] T.S. Moss, Section B 57 (1954) 775.

[13] E. Çetinörgü, Optics Communications 280 (2007) 114–119.

[14] M.-M. Bagheri-Mohagheghi, N. Shahtahmasebi, M.R. Alinejad, A. Youssefi, M.Shokooh-Saremi, Solid State Sciences 11 (2009) 233–239.

[15] S. S. Lekshmy and K. Joy , J. Mater. Sci.: Mater. Electron, 25 (2014) 1664.

[16] S.S. Pan, Y.X. Zhang, X.M. Teng, G.H. Li, L. Li, Journal of Applied Physiology 103(2008) 093103.

[17] L.M. Fang, X.T. Zu, Z.J. Li, S. Zhu, C.M. Liu, L.M. Wang, F. Gao, Journal of Material Science Materials in Electronics 19 (2008) 868–874.

[18] N. Lehraki, M.S. Aida, S. Abed, N. Attaf, A. Attaf, M. Poulain, Current Applied Physics 12 (2012) 1283-1287.

[19] A.M. El Sayed, S. Taha, M. Shaban, G. Said, Superlattices and Microstructures,95 (2016) 1-13.

[20] K.-Mu Lee, K.-Liang Shih, C.-Hung Chiang, V. Suryanarayanan, C.-Guey Wu, Thin Solid Films 570 (2014) 7-15.

[21] M. E. White, O. Bierwagen, M. Ying Tsai, S. James. Speck, Appl. Phys. Expr. 3 (2010) 051101–51103.

[22] D. Dobler, S. Oswald, G. Behr, J. Werner, K. Wetzig, Cryst. Res. Technol. 38 (2003) 956–961.

[23] W. Mao, B. Xiong, Q. Li, Y. Zhou, C. Yin, Y. Liu, C. He, Phys. Lett. A 379 (2015) 1946-1950.

[24] S. S. Lekshmy and K. Joy, J. Sol-Gel. Sci. Technol, 67 (2013) 29–38

[25] N. D. Papadopoulos, P. E. Tsakiridis, E. Hristoforou, Journal of Optoelectronics and Advanced Materials, 7 (5) (2005) 2693-2706.

[26] M.A. Yıldırım, S. T. Yıldırım, E. F. Sakar , A. Ates, Spectrochimica Acta Part A: Molecular and Biomolecular Spectroscopy 133 (2014) 60–65

General conclusion and perspectives

In this study we have deposited and characterized thin films of undoped and doped tin dioxide using ultrasonic spray technique on glass substrates. The effect of different parameters on the structural, optical and electrical properties had been investigated to give good quality films.

In the first part of our work, we have prepared series of films SnO_2 deposited with different parameters (substrate temperature, molarity and deposition time). In the second, we have studied the influence of low and high concentrations of indium doping. In the third one, the effect of annealing temperature and type of precursor on the physical properties of the SnO_2 doped samples.

The effect of the substrate temperature (from 350 to 500 ° C), the molarity (0.05- 0.2 mol /l) and the deposition time (from 2 to 5 minutes) on optical, structural and electrical properties of undoped SnO_2 films were investigated (by using $SnCl_4$ as precursor). It was located that a maximum value of figure of merit for the films deposited at 450 °C and 0.1 mol/l concentration whereas the optimum deposition time was found to be 5 min.

We have made a study of the influence of indium doping rate on the structural, optical and electrical properties of SnO_2 thin films. The X-ray diffraction analysis of the undoped and doped samples (with low or high concentrations of indium) showed that the thin films crystallize in the tetragonal structure. Therefore, we observed an evolution of the intensities of the diffraction peaks as a function of the deposition parameters. However, we found that the intensity of diffraction peaks decreased versus doping. This result clearly indicates that In^{+3} can be incorporated into the SnO_2 network. We concluded that Indium doping did not exhibit an improvement in crystal quality. Furthermore, the optical band gap was narrowed with the increasing of In content. The value of Eg was in the range of 3,9- 4,1 eV and 3,77- 4.08 eV for low and high concentrations of indium, respectively. The optical and electrical measurements indicated that films transmittance and conductivity were much improved at 2% and 20% In. The highest value of transmittance was reached 97% for 2% In (for low concentrations) and 95% for 20% In (for high concentrations). The SnO_2:In films revealed the minimum resistivity about 0,075 (Ωcm) at 20%. Also, Hall Effect measurement revealed that the undoped and doped films with 10% In had n-type electrical conductivity and when it was at 20%, In-doped SnO_2 thin films would show a p-type.

In the third part, we have discussed the difference in structural, optical and electrical properties of doped SnO_2 films obtained from two precursors. The SnO_2:In films deposited using $SnCl_4$ showed a good crystallization compared to $SnCl_2$. Also, the lowest resistivity (0.08 Ωcm) and highest optical transmittance (97%) were obtained for the film prepared from $SnCl_4$.

From the study of annealing temperature, for $SnCl_4$ as a precursor, X-ray diffraction analysis appears an improvement in crystal quality. The optical measurements indicated that films transmittance improved, the optical band gap was widening with annealing. Also, the films resistivity was decreased with annealing temperature.

In conclusion, we can say that doping enhance the properties of SnO_2 thin films, which make them very suitable for optoelectronic applications. It would be interesting to continue the investigations on the SnO_2 solid notably by its use in the photovoltaic field. In particular, one could look at whether the increase in the Indium content can improve their conductivity and their transmission.

Elaboration and characterization of SnO_2:In thin films deposited by spray pyrolysis technique

Abstract

In this work, we have used the ultrasonic spray technique to deposit thin films of undoped and doped SnO_2 on glass substrates. To optimize the quality of SnO_2 thin films, we have studied the influence of molarity, deposition time and substrate temperature on film's physical properties.

The other aim of this work is to optimize the quality of these films by studying the influence of the dopants, the annealing temperature and the type of precursor of the starting solution on the structural, optical and electrical properties in order to obtain transparent and conductive films. For this reason, we used indium as a dopant and two types of the precursor of the starting solution ($SnCl_2.2H_2O$, $SnCl_4.5H_2O$).

We used several characterization techniques, such as X-ray diffraction, UV-visible spectroscopy, scanning electron microscopy, Hall Effect and the four-point technique. We have shown that undoped and doped SnO_2 films are transparent in the visible range and their structure is of tetragonal type. In our work, we found that the undoped SnO_2 film deposited at 450° C for 5 minutes of deposition at a concentration of 0.1 mol / l has good properties. Also, indium-doped SnO_2 thin films with the best properties can be prepared using $SnCl_4$ as a precursor and at the 2% and 20% doping rate. Also, Hall Effect measurement revealed that the undoped and doped films with 10% In had n-type electrical conductivity, and when it was at 20%, In-doped SnO_2 thin films showed a p-type conductivity.

The results showed that the process of annealing leads to the improvement of the crystallinity, the optical and electrical properties of SnO_2.In films.

Keywords: Tin dioxide, Indium, Thin film, Ultrasonic spray.

تحضير و توصيف الشرائح الرقيقة لثنائي أكسيد القصدير المطعم بالإنديوم المودعة بتقنية الرش فوق الصوتي

ملخص

في هذا العمل، استخدمنا تقنية الرش فوق الصوتي لإيداع شرائح رقيقة من SnO_2 غير المطعم والمطعم على ركائز الزجاج. لتحسين جودة الأغشية الرقيقة SnO_2 ،قمنا أولا بدراسة تأثير المولارية ، وقت الترسب ودرجة حرارة الركيزة على خصائصها الفيزيائية.

من ناحية ثانية و لنفس الغرض تحسين جودة هذه الأفلام درسنا تأثير التطعيم ودرجة حرارة التلدين ونوع السلائف لمحلول البدء على الخواص البنيوية والبصرية والكهربائية للحصول على أفلام شفافة وموصلة .لهذا السبب ، استخدمنا الإنديوم كمطعم ونوعين من المركبات لمحلول البدء ($SnCl_2.2H_2O$, $SnCl_4.5H_2O$).

استخدمنا العديد من تقنيات التشخيص مثل انعراج الأشعة السينية ، مطيافية الأشعة فوق البنفسجية والمرئية ، المجهر الالكتروني الماسح، مفعول هول وتقنية أربعة مسابير . لقد بينا أن أفلام SnO_2 غير المطعمة و المطعمة شفافة في المدى المرئي و بنيتها من نوع رباعي الزوايا . في عملنا، وجدنا أن غشاء SnO_2 غير المطعم المودع عند 450 درجة مئوية لمدة 5 دقائق من الترسب بتركيز 0.1 مول / لتر له خصائص جيدة .أيضا ، يمكن تحضير أغشية رقيقة SnO_2 مطعمة بالأنديوم مع خصائص أفضل باستخدام $SnCl_4$ كمركب بدء وعند معدل تطعيم 2٪ و 20٪. أيضا، أظهرت قياسات مفعول هول ان الافلام الغيرمطعمة و المطعمة بنسبة 10٪ إنديوم تظهر الناقلية الكهربائية من نوع n بينما المطعمة بنسبة 20٪ تظهر الناقلية من النوع p .

أظهرت النتائج أن عملية التلدين تؤدي إلى تحسين التبلور ، والخصائص البصرية والكهربائية للأغشية.SnO_2.In

الكلمات المفتاحية: ثنائي أكسيد القصدير، أنديوم، طبقة رقيقة، الرش فوق الصوتي.